USGS
science for a changing world

Prepared in cooperation with the Albuquerque Bernalillo County Water Utility Authority and the U.S. Air Force

Hydrogeologic Framework and Delineation of Transient Areas Contributing Recharge and Zones of Contribution to Selected Wells in the Upper Santa Fe Group Aquifer, Southeastern Albuquerque, New Mexico, 1900–2050

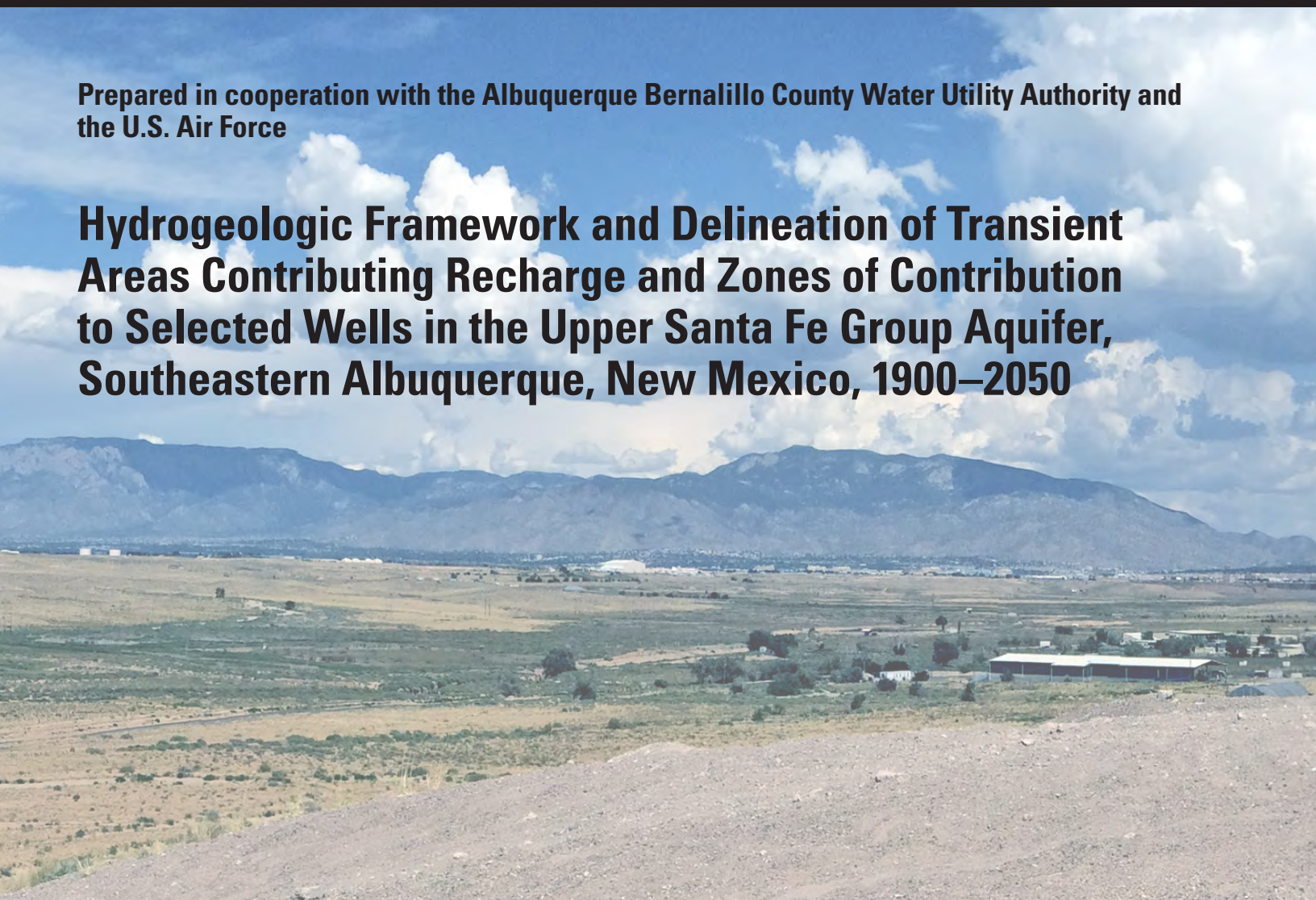

Scientific Investigations Report 2019–5052

U.S. Department of the Interior
U.S. Geological Survey

Cover. Photograph showing view looking northeast towards the Sandia Mountains from the southwest corner of the study area in southeastern Albuquerque, New Mexico. Foreground shows axial-fluvial sediments of the Sierra Ladrones Formation on a bluff overlooking Tijeras Arroyo. Photograph by Nathan Myers, U.S. Geological Survey, August 28, 2015.

Hydrogeologic Framework and Delineation of Transient Areas Contributing Recharge and Zones of Contribution to Selected Wells in the Upper Santa Fe Group Aquifer, Southeastern Albuquerque, New Mexico, 1900–2050

By Nathan C. Myers and Paul J. Friesz

Prepared in cooperation with the Albuquerque Bernalillo County Water Utility Authority and the U.S. Air Force

Scientific Investigations Report 2019–5052

U.S. Department of the Interior
U.S. Geological Survey

U.S. Department of the Interior
DAVID BERNHARDT, Secretary

U.S. Geological Survey
James F. Reilly II, Director

U.S. Geological Survey, Reston, Virginia: 2019

For more information on the USGS—the Federal source for science about the Earth, its natural and living resources, natural hazards, and the environment—visit https://www.usgs.gov or call 1–888–ASK–USGS.

For an overview of USGS information products, including maps, imagery, and publications, visit https://store.usgs.gov.

Suggested citation:
Myers, N.C., and Friesz, P.J., 2019, Hydrogeologic framework and delineation of transient areas contributing recharge and zones of contribution to selected wells in the upper Santa Fe Group aquifer, southeastern Albuquerque, New Mexico, 1900–2050: U.S. Geological Survey Scientific Investigations Report 2019–5052, 73 p., https://doi.org/10.3133/sir20195052.

ISSN 2328-0328 (online)

Acknowledgments

The authors would like to acknowledge the many investigators who laid the geologic and hydrologic foundations upon which this report rests. In particular, the works of John Hawley, Hawley Geomatters, and Sean Connell, New Mexico Bureau of Geology and Mineral Resources, provided much of the conceptual and physical basis for development of the local-scale model described in this report. We wish to thank the U.S. Department of Veterans Affairs employees who kindly provided access to well data and records.

Jerry and JoAnne Landry kindly provided access to and granted permission for installation of monitoring wells in the Interfaith Bible Center parking lot. The City of Albuquerque granted permission for the installation of monitoring wells in Phil Chacon Park and near the Cesar Chavez Community Center. Installation of the Phil Chacon Park and Cesar Chavez Community Center wells was greatly facilitated by personnel of the Albuquerque Parks and Recreation Department and the Albuquerque Public Schools Real Estate Office.

Contents

Acknowledgments iii
Abstract 1
Introduction 2
Purpose and Scope 5
Description of the Study Area 5
Previous Investigations 5
Hydrogeologic Framework 6
Geologic Framework 6
Hydrologic Framework 9
External Basin Boundaries 9
Internal Basin Hydrogeologic Characteristics 12
Groundwater Recharge and Discharge 17
Recharge 17
Discharge 19
Hydrochemical Zones 19
Water-Level and Groundwater-Flow Changes 21
Aquifer Properties 22
Formation of the EDB Plume 22
Numerical Groundwater-Flow Model Development and Calibration 22
Description and Modification of the Updated Regional Model 22
Local-Scale Model Design 28
Spatial and Temporal Discretization 28
Local-Scale Model Inflow and Outflow 31
Model Inflow 31
Mountain-Front and Tributary Recharge 31
Leakage From Water-Distribution and Sewage-Collection Systems 31
Irrigated Agriculture Seepage 33
Septic-Field Seepage 33
Aquifer Storage and Subsurface Inflow 33
Model Outflow 33
Hydraulic Parameters 33
Local-Scale Model Calibration 35
Observations 35
Estimation of Parameters 37
Comparison of Observations and Simulated Equivalents 39
Local-Scale and Updated Regional Model Modifications for a Future Pumping Scenario 40
Limitations of Analysis 44
Delineation of Transient Areas Contributing Recharge and Zones of Contribution to Selected Water-Supply Wells 47
Historical Pumping Conditions 48
Future Pumping Scenario 59
Summary 67
References Cited 69

Figures

1. Map showing locations of Middle Rio Grande Basin, Middle Rio Grande Basin model, local-scale model, Albuquerque-Rio Rancho metropolitan area, and Kirtland Air Force Base, New Mexico....3
2. Map showing locations of the local-scale model, Kirtland Air Force Base Bulk Fuels Facility, ethylene dibromide plume, faults, trace of hydrogeologic section shown in figure 3, and locations of wells and well clusters....4
3. Hydrogeologic section *A*–*A*' showing axial-fluvial sediments above, between, and below the A1 and A2 units of the Sierra Ladrones Formation in the local-scale model area, southeastern Albuquerque, New Mexico....7
4. Maps showing surfaces representing the tops of the A1 and A2 units within the local-scale model area....8
5. Map showing hydraulic conductivity of Sierra Ladrones Formation sediments in relation to the ethylene dibromide plume, locations of faults, and approximate east and west limits of axial-fluvial sediments....13
6. Graphs showing groundwater-level hydrographs for Trumbull wells TR-1A, TR-1B, and TR-1C, January 2014 through December 2016....18
7. Map showing hydrochemical zones, potentiometric contours and areas of water-level drawdown in 2008, and ethylene dibromide plume in the local-scale model area....20
8. Graph showing daily mean and annual depth to groundwater in the deep and shallow Jerry Cline wells, January 1, 2005–December 31, 2016, an example of water-level rise in southeastern Albuquerque after the Albuquerque Bernalillo County Water Utility Authority began using surface water for part of the municipal supply....21
9. Diagrams showing layer thicknesses in *A*, the updated regional model and *B*, the local-scale model....25
10. Diagram showing three-dimensional perspective of *A*, east-west hydraulic conductivity and *B*, the distribution of hydraulic parameters for local-scale model rows 1–88, columns 1–80, and layers 1–21....29
11. Maps showing spatial and temporal distribution of simulated recharge sources from *A*, mountain-front and tributary recharge and water-distribution and sewage-collection systems leakage; *B*, irrigated agriculture seepage; and *C* and *D*, septic-field seepage in the local-scale model....32
12. Map showing locations of water-supply wells and observation wells and simulated water-level contours for October 2013 in layer 12 of the local-scale model....34
13. Map showing plume source location and advective-transport observation for the ethylene dibromide plume....38
14. Graph showing composite scaled sensitivities of the hydraulic parameters for the local-scale model....39
15. Graphs showing relations of *A*, observed to simulated groundwater levels and *B*, residual to simulated groundwater levels....41
16. Graphs showing observed and simulated groundwater levels for observation wells *A*, SD-2; *B*, SC-1; *C*, SC-2; *D*, JC-1; *E*, JC-2; and *F*, JC-3....42
17. Map showing locations of existing and simulated extraction, water-supply, and injection wells that were included in the historical and future pumping model scenarios....45

18. Diagram showing area contributing recharge and zone of contribution to a single discharging well in a hypothetical groundwater system 48
19. Maps and cross section showing simulated particle pathlines to water-supply well RC-4 for particles released on October 31, 2013 in *A*, map view, *B*, simulated particle pathlines and predevelopment steady-state water-level contours in layer 3 of the local-scale model and updated regional models, and *C*, cross-section view....49
20. Map showing areas contributing recharge to selected water-supply wells within the local-scale model area 51
21. Maps showing sensitivity analysis of effective porosities of *A*, 0.15 and *B*, 0.35 on the areas contributing recharge to selected water-supply wells 53
22. Maps showing zones of contribution to selected water-supply wells in the local-scale model area 55
23. Maps showing sensitivity analysis of the effects of effective porosity of *A*, 0.15 and *B*, 0.35 on the zone of contribution to well RC-5 for particles released on October 31, 2013, in the local-scale model area....60
24. Graph showing projected groundwater table elevation in local-scale model layer 3 near the Trumbull well cluster and at the Bulk Fuels Facility simulated by using the "medium demand, medium supply" future pumping scenario....61
25. Map showing areas contributing recharge to selected water-supply wells in the local-scale model area 62
26. Maps showing zones of contribution to water-supply wells in the local-scale model area 63

Tables

1. Depths to and elevations of the tops and bases of the A1 and A2 units of the Sierra Ladrones Formation for selected wells in the local-scale model area 10
2. Elevations of tops and bases of A1 and A2 units from digital elevation models and difference as compared to geophysical-log- and lithologic-based elevations 12
3. Transmissivity and hydraulic conductivity values determined from aquifer tests at wells in the local-scale model area 14
4. Ranges of aquifer properties in the Middle Rio Grande Basin, New Mexico 23
5. Net water budget values for the regional and local-scale models....27
6. Vertical refinement of local-scale model layers with respect to the updated regional model....28
7. Descriptions of hydraulic parameters, optimal or specified parameter values, and parameter-estimation statistics in the local-scale model and comparison to updated regional model parameter values 36
8. Simulated water withdrawals from selected wells in the local-scale model 47

Conversion Factors

U.S. customary units to International System of Units

Multiply	By	To obtain
	Length	
inch (in.)	25.4	millimeter (mm)
foot (ft)	0.3048	meter (m)
mile (mi)	1.609	kilometer (km)
	Area	
square mile (mi^2)	2.590	square kilometer (km^2)
	Volume	
gallon (gal)	3.785	liter (L)
gallon (gal)	0.003785	cubic meter (m^3)
cubic foot (ft^3)	0.02832	cubic meter (m^3)
acre-foot (acre-ft)	1,233	cubic meter (m^3)
	Flow rate	
acre-foot per year (acre-ft/yr)	1,233	cubic meter per year (m^3/yr)
acre-foot per year (acre-ft/yr)	0.001233	cubic hectometer per year (hm^3/yr)
cubic foot per second (ft^3/s)	0.02832	cubic meter per second (m^3/s)
gallon per minute (gal/min)	0.06309	liter per second (L/s)
gallon per day (gal/d)	0.003785	cubic meter per day (m^3/d)
million gallons per day (Mgal/d)	0.04381	cubic meter per second (m^3/s)
inch per year (in/yr)	25.4	millimeter per year (mm/yr)
	Hydraulic conductivity	
foot per day (ft/d)	0.3048	meter per day (m/d)
	Hydraulic gradient	
foot per mile (ft/mi)	0.1894	meter per kilometer (m/km)
	Transmissivity	
foot squared per day (ft^2/d)	0.09290	meter squared per day (m^2/d)
	Leakance	
foot per day per foot ([ft/d]/ft)	1	meter per day per meter ([m/d]/m)

International System of Units to U.S. customary units

Multiply	By	To obtain
	Length	
meter (m)	3.281	foot (ft)
kilometer (km)	0.6214	mile (mi)
kilometer (km)	0.5400	mile, nautical (nmi)
meter (m)	1.094	yard (yd)
	Area	
square kilometer (km^2)	247.1	acre
square kilometer (km^2)	0.3861	square mile (mi^2)

Temperature in degrees Celsius (°C) may be converted to degrees Fahrenheit (°F) as follows:

$$°F = (1.8 \times °C) + 32$$

Datum

Unless otherwise indicated, vertical coordinate information is referenced to the North American Vertical Datum of 1988 (NAVD 88).

Horizontal coordinate information is referenced to the North American Datum of 1983 (NAD 83).

Elevation, as used in this report, refers to distance above the vertical datum.

Supplemental Information

Concentrations of chemical constituents in water are given in micrograms per liter (µg/L).

Abbreviations

ACR	area contributing recharge
BFF	Bulk Fuels Facility
DEM	digital elevation model
EDB	ethylene dibromide (also known as 1,2-dibromoethane)
KAFB	Kirtland Air Force Base
MNW1	Multi-Node Well package, version 1
MNW2	Multi-Node Well package, version 2
SJC	San Juan-Chama
USGS	U.S. Geological Survey
VAH	U.S. Department of Veterans Affairs hospital
Water Authority	Albuquerque Bernalillo County Water Utility Authority
ZOC	zone of contribution

Hydrogeologic Framework and Delineation of Transient Areas Contributing Recharge and Zones of Contribution to Selected Wells in the Upper Santa Fe Group Aquifer, Southeastern Albuquerque, New Mexico, 1900–2050

By Nathan C. Myers and Paul J. Friesz

Abstract

The Santa Fe Group aquifer is an important source of water to communities within the Middle Rio Grande Basin, including the Albuquerque-Rio Rancho metropolitan area and Kirtland Air Force Base, New Mexico. In November 1999, Kirtland Air Force Base personnel observed fuel-stained soils at the Bulk Fuels Facility on the base. Subsequent pressure tests identified pipeline leaks. Fuels stored at the Bulk Fuels Facility have included aviation gasoline, jet propellant 4, and jet propellant 8. The fuels migrated about 480 feet down to the water table. Ethylene dibromide, the constituent making up the most extensive part of the plume and a component of leaded aviation gasoline, has formed a plume that, in December 2016, was 400 to 1,300 feet wide, extended about 5,800 feet northeast from the Bulk Fuels Facility, and was about 3,700 feet from the nearest downgradient water-supply well.

Prior to widespread development of groundwater resources in southeastern Albuquerque, groundwater near the present-day location of the Bulk Fuels Facility flowed to the southwest. Groundwater began flowing northeast in about 1980 towards a large area of lowered water levels caused by groundwater pumping.

In 2013 and 2014 the Albuquerque Bernalillo County Water Utility Authority, the U.S. Air Force, and the U.S. Geological Survey began a cooperative study to characterize the geology and hydrology of the Santa Fe Group aquifer in the vicinity of the ethylene dibromide plume and to develop a local-scale groundwater flow model to delineate areas contributing recharge and zones of contribution to selected water-supply wells.

For this study, a previously developed Middle Rio Grande Basin regional groundwater-flow model was updated, and a smaller local-scale model was developed. Advective groundwater-flow paths were delineated and visualized with the MODPATH particle-tracking program.

Of 11 wells included in the historical pumping analysis of areas contributing recharge, only wells K-3, K-7, and RC-4 derived a portion of their water from simulated recharge sources within the local-scale model. None of the areas contributing recharge overlap the Bulk Fuels Facility area or the ethylene dibromide plume footprint as delineated using December 2016 ethylene dibromide data.

For the historical pumping analysis of zones of contribution, particles for the 11 selected wells generally moved southwest from the north and east boundaries of the local-scale model, moved past their target well, but reversed direction and moved back towards their target well after 1980 when groundwater flow changed to the northeast. Of the 11 wells, only BR-5, RC-5, and VH-2 had 1980–2013 particle pathlines that overlap the December 2016 ethylene dibromide plume footprint, and wells BR-5 and VH-2 have 1980–2013 particle pathlines that overlap the Bulk Fuels Facility area. Particles that were north of the Bulk Fuels Facility when groundwater flow reversed direction would not have the opportunity to interact with the ethylene dibromide plume. Wells BR-5, K-15, and VH-2 did have particles southwest of the Bulk Fuels Facility in 1980. Particles traveling to BR-5 and K-15 passed under or very near the Bulk Fuels Facility area in the 1980–2013 period, but none of the pathlines were shallow enough to interact with ethylene dibromide at the Bulk Fuels Facility. A few particles traveling to VH-2 passed through the Bulk Fuels Facility area at shallow enough depths to interact with ethylene dibromide at the Bulk Fuels Facility in the 1980–2013 period. Ethylene dibromide has not been detected in water samples collected in 2012 through 2015 from the VH-2 well.

Of 10 water-supply wells near the ethylene dibromide plume included in the future pumping analysis of areas contributing recharge, only wells K-3, RC-3, and RC-4 had areas contributing recharge within the local-scale model. The areas contributing recharge for wells RC-3 and RC-4 do not overlap the Bulk Fuels Facility area or the December 2016 ethylene

dibromide plume footprint, but K-3 derives part of its recharge prior to 1980 and during 1980–2015 from within the area of the December 2016 plume footprint.

The analysis of the future pumping scenarios indicated that wells BR-5, K-3, K-16, RC-5, and VH-2 have pathlines for 1980–2015 and wells K-16 and VH-2 have pathlines for 2015–50 that when projected in plan view pass through the December 2016 plume footprint. Of these five wells, only K-3 and RC-5 have pathlines for 1980–2015 that are above an elevation of 4,800 feet and could interact with the ethylene dibromide plume if ethylene dibromide was present when the particles were present.

Introduction

The Santa Fe Group aquifer is an important source of water to communities within the Middle Rio Grande Basin, including the Albuquerque-Rio Rancho metropolitan area and Kirtland Air Force Base (KAFB), New Mexico (fig. 1). In the arid climate of the southwestern United States, maintaining the quality of limited groundwater supplies is particularly important to the health and economic well-being of communities in the Middle Rio Grande Basin. The Albuquerque Bernalillo County Water Utility Authority (Water Authority), KAFB, and the U.S. Department of Veteran's Affairs hospital complex (VAH) operate production wells located in and near southeast Albuquerque, New Mexico, that supply drinking water to the Water Authority distribution system, KAFB facilities, and VAH facilities, respectively (U.S. Air Force Civil Engineer Center, 2014).

In November 1999, KAFB personnel observed fuel-stained soils at the Bulk Fuels Facility (BFF) on the base (fig. 2). Subsequent pressure tests identified leaks in underground fuel pipes used to transfer aviation fuels from an offloading terminal to storage tanks at the BFF (U.S. Air Force, 2011). Various types of fuels have been stored at the BFF including aviation gasoline from 1953 to 1975, jet propellant 4 (JP-4) from 1975 to 1993, and jet propellant 8 (JP-8) from 1993 to present (U.S. Army Corps of Engineers, 2017a). The BFF has been used for fuel transfer and storage since 1953, but the exact date when the pipes began leaking and the amounts of fuels that leaked are unknown (U.S. Army Corps of Engineers, 2017a).

After leaking from the pipes, the fuels migrated about 480 feet (ft) down to the water table, where the fuels and fuel components formed a plume at the water table with nonaqueous and aqueous phases. The fuel component that makes up the most extensive part of the plume is ethylene dibromide (EDB; also known as 1,2-dibromoethane). EDB was a component of leaded aviation gasoline but not of JP-4 or JP-8 (U.S. Army Corps of Engineers, 2017a). Monitoring wells have been installed to delineate the extent of the EDB plume. As monitoring wells were installed, the extent of contamination became better known. The EDB plume may not yet be fully characterized, but as of December 2016 the EDB plume, delineated by EDB concentrations in groundwater that equal or exceed the regulatory limit of 0.05 microgram per liter (U.S. Army Corps of Engineers, 2017b), ranged from 400 to 1,300 ft wide and extended about 5,800 ft northeast from the BFF (fig. 2). At its deepest, the EDB plume is about 85 ft below the water table (U.S. Army Corps of Engineers, 2017a). As shown in figure 2, in December 2016 the leading edge of the EDB plume was about 3,700 ft from the nearest downgradient water-supply well (RC-5).

Prior to widespread development of groundwater resources (1960s to 1980s) in southeastern Albuquerque, groundwater near the present-day location of the BFF flowed to the southwest (Bexfield and Anderholm, 2000). After widespread development of groundwater resources, groundwater levels began falling, and directions of groundwater flow in some areas have changed. Near the BFF, groundwater began flowing to the northeast in about 1980 towards a large area of lowered water levels caused by groundwater pumping from Water Authority water-supply wells (Powell and McKean, 2014; Rice and others, 2014). But, since the Water Authority began diverting San Juan-Chama (SJC) surface water from the Rio Grande in late 2008 to supplement its groundwater supply, groundwater levels in southeastern Albuquerque have been rising (Powell and McKean, 2014). Because of the complex history of groundwater flow and the proximity of the EDB plume to water-supply wells, a detailed hydrogeologic study and groundwater-flow modeling were undertaken to determine the origin and flow paths of water being produced by Water Authority and KAFB water-supply wells.

In 2013 the Water Authority and the U.S. Geological Survey (USGS) began a cooperative study to characterize the geology and hydrology of the Santa Fe Group aquifer in the vicinity of the EDB plume and to use the Middle Rio Grande Basin groundwater-flow model (fig. 1) developed by McAda and Barroll (2002) and refined by Bexfield and others (2011) and a local-scale model as the basis to delineate areas contributing recharge and zones of contribution to selected Water Authority water-supply wells. In 2014, the U.S. Air Force and the USGS began a cooperative project to characterize aquifer properties, water quality, and directions of groundwater flow in the vicinity of the EDB plume and to delineate directions of groundwater flow under historical pumping conditions and future pumping scenarios for water-supply wells.

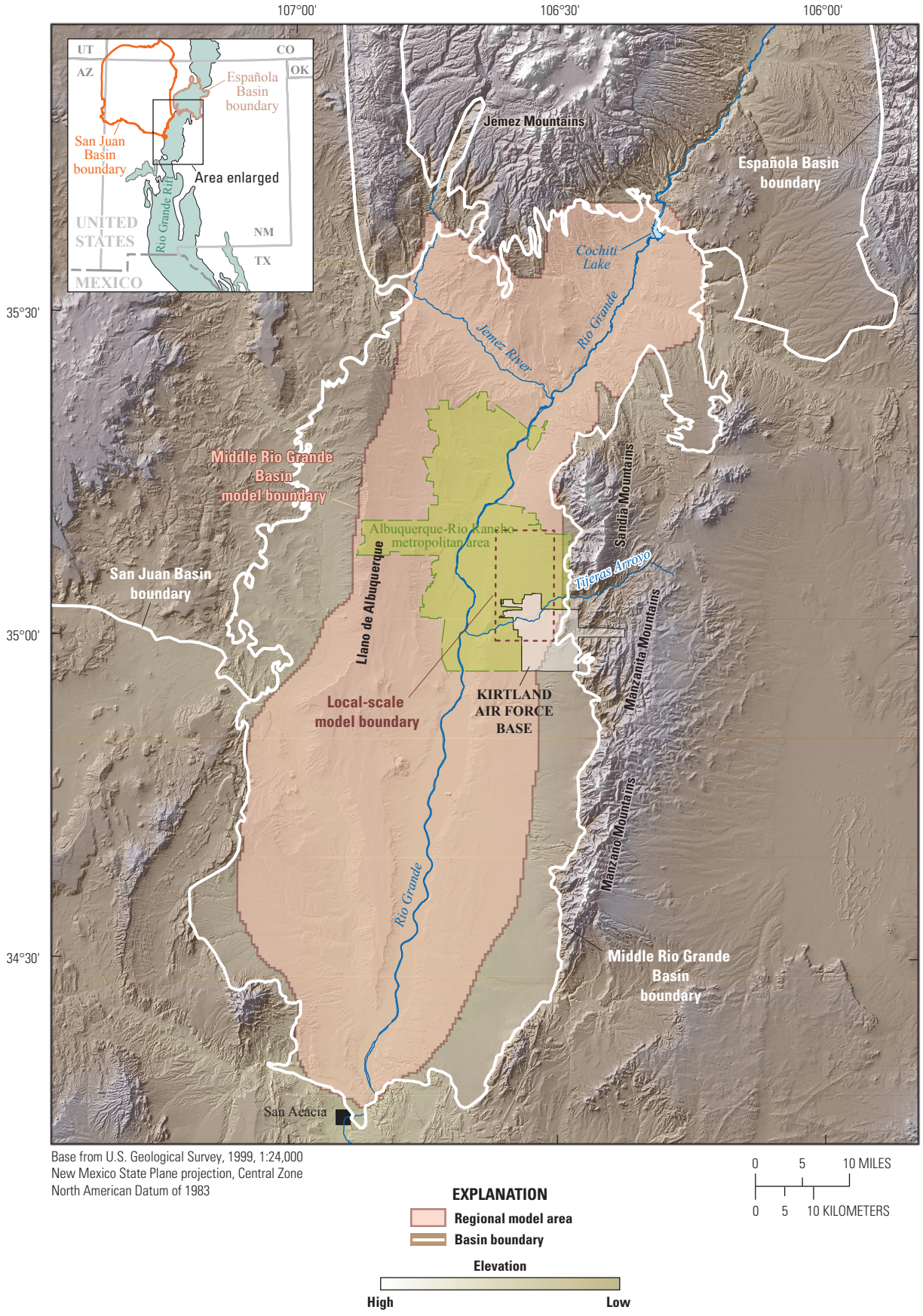

Figure 1. Locations of Middle Rio Grande Basin, Middle Rio Grande Basin model, local-scale model, Albuquerque-Rio Rancho metropolitan area, and Kirtland Air Force Base, New Mexico. Middle Rio Grande Basin boundary from Plummer and others (2004). Middle Rio Grande model boundary modified from Bexfield and others (2011). Rio Grande Rift boundary modified from Hudson and Grauch (2013). Española Basin boundary modified from Grauch and others (2009). San Juan Basin boundary modified from Kernodle (1996).

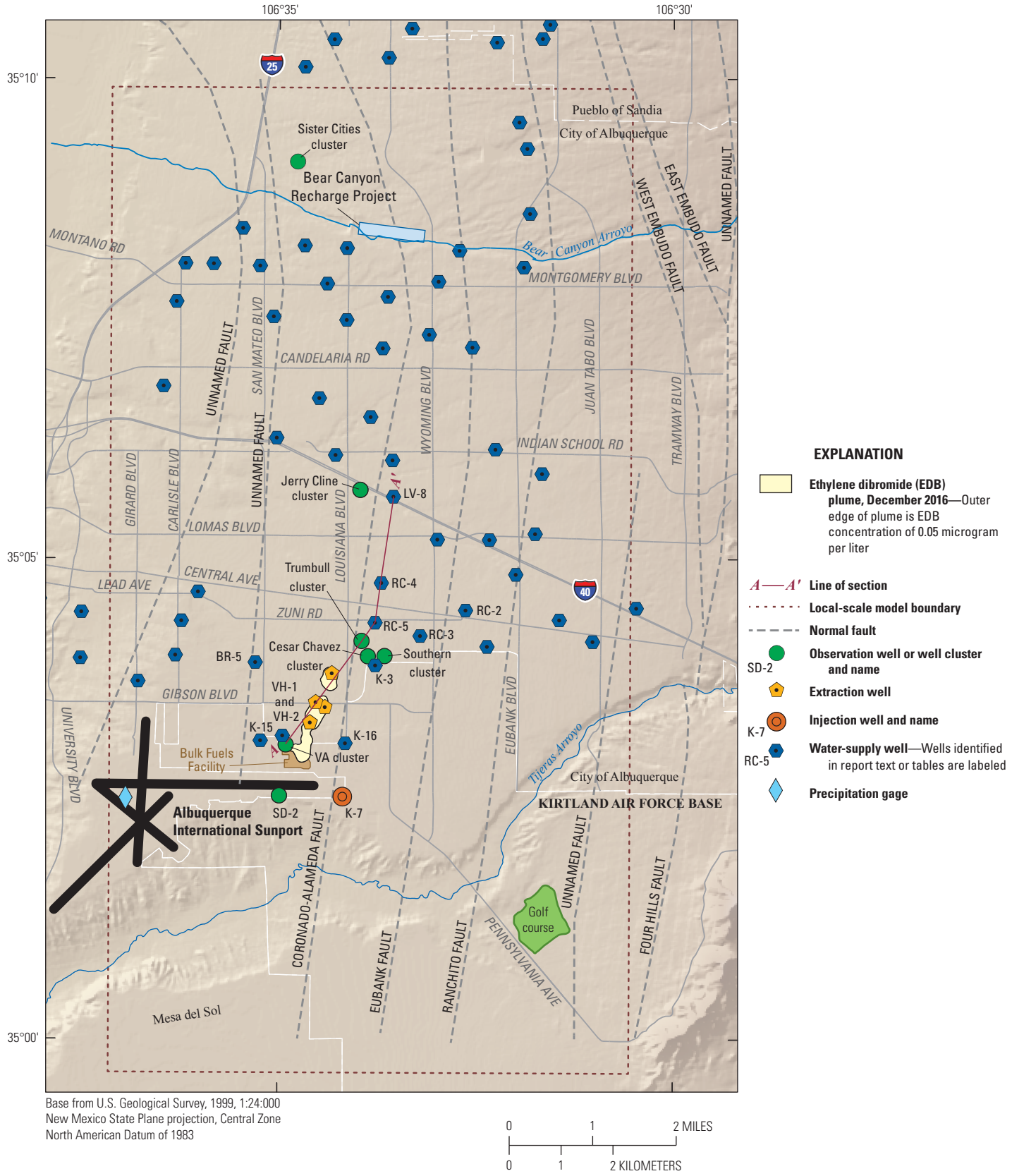

Figure 2. Locations of the local-scale model, Kirtland Air Force Base Bulk Fuels Facility, ethylene dibromide plume (U.S. Army Corps of Engineers, 2017b), faults (Connell, 2006), trace of hydrogeologic section shown in figure 3, and locations of wells and well clusters. Extent of the local-scale model within the Middle Rio Grande Basin is shown on figure 1.

Purpose and Scope

This report describes the hydrogeologic framework of the upper Santa Fe Group aquifer in southeastern Albuquerque, New Mexico, and documents the development and calibration of a 73.2-square-mile (mi^2) local-scale model that is used to simulate groundwater flow near the EDB plume. The report also presents results of particle-tracking simulations that delineate transient areas contributing recharge and zones of contribution to 11 water-supply wells near the EDB plume under selected pumping scenarios. Simulations of historical groundwater-flow conditions span the time from 1900 through October 2013. Simulations of projected future groundwater flow span the time from November 2013 through October 2050.

Description of the Study Area

From north to south, the study area (local-scale model area) extends from northeastern Albuquerque to Mesa Del Sol and from east to west extends from near Juan Tabo Boulevard to near Girard Boulevard (fig. 2). The local-scale model boundary encompasses 73.2 mi^2 (fig. 2) and is located in an area of westward sloping, overlapping alluvial fans that emanate from the Sandia and Manzanita Mountains (fig. 1). Albuquerque lies within the Middle Rio Grande Basin, which is one of several sediment-filled structural basins associated with the north-south trending Rio Grande Rift (fig. 1). In the Albuquerque-Rio Rancho metropolitan area, the Sandia and Manzanita Mountains to the east and the Llano de Albuquerque to the west form the boundaries of the rift valley (fig. 1).

The climate in the Albuquerque-Rio Rancho metropolitan area is semiarid. Mean annual precipitation at the Albuquerque International Sunport (airport) for 1981–2010 was 9.45 inches per year (in/yr) (Western Regional Climate Center, 2017). About 55 percent of the mean annual precipitation falls from July through October (Western Regional Climate Center, 2017). Because of the dry climate, potential evapotranspiration can be four or more times greater than precipitation (Bartolino and Cole, 2002).

The principal stream in the Middle Rio Grande Basin is the north-south flowing Rio Grande (fig. 1). Through the Albuquerque-Rio Rancho metropolitan area, the Rio Grande is perennial but generally loses water to the adjacent aquifer (Rankin and others, 2016). Within the local-scale model area Tijeras Arroyo, originating in the Manzanita Mountains, is the primary drainage. Tijeras Arroyo, which is ephemeral within the local-scale model area, conveys water southwest to the Rio Grande in southern Albuquerque (figs. 1 and 2).

Water supplied to Albuquerque residents currently (2019) is obtained from both the Santa Fe Group aquifer below the city and from SJC surface water. Groundwater from the Santa Fe Group aquifer was the sole source of water to Albuquerque until late 2008, when the SJC surface-water diversion and treatment plant began supplying potable water. During 2014 the Water Authority supplied 99,000 acre-feet (acre-ft) of water to its customers, of which about 39 percent was groundwater, 57 percent was surface water, and 4 percent was treated nonpotable water (Albuquerque Bernalillo County Water Utility Authority, 2016). Water use has decreased from 175 gallons per capita per day in 1997 to 135 gallons per capita per day in 2014 (Albuquerque Bernalillo County Water Utility Authority, 2016). The local-scale model encompasses 52 active Water Authority, KAFB, and VAH water-supply wells, one currently inactive well (VH-1) which was replaced by the VH-2 well, and one former water-supply well (K-7) which is now an injection well (fig. 2) that obtain their water from the upper Santa Fe Group aquifer. The KAFB, Water Authority, and VAH water systems are interconnected such that KAFB can purchase supplemental water from the Water Authority if needed (U.S. Air Force Civil Engineer Center, 2014).

Previous Investigations

Bartolino and Cole (2002) provided an extensive overview of the hydrogeology of the Middle Rio Grande Basin and provided references to publications with detailed descriptions of the hydrogeology of the basin. Hawley and Haase (1992) and Hawley and others (1995) described the fundamental hydrogeologic framework of the Middle Rio Grande Basin and developed much of the modern stratigraphic nomenclature for the basin. Connell and others (1998) and Connell (2006, 2008), through detailed analyses of geophysical logs and drill cuttings from wells, developed a comprehensive understanding of both the vertical and horizontal extents of sedimentary facies in the Middle Rio Grande Basin and the influence of faulting on the types and locations of sedimentary deposits. Plummer and others (2004) provided a comprehensive geochemical analysis of Middle Rio Grande Basin groundwater and contributed substantially to the understanding of groundwater recharge sources and flow patterns in the basin. McAda and Barroll (2002) developed the first version of the Middle Rio Grande Basin regional groundwater-flow model and simulated groundwater conditions from 1900 through March 2000. Bexfield and others (2011) refined the McAda and Barroll (2002) model by decreasing the horizontal grid cell size, adding simulated recharge from leaking water-distribution and sewage-collection systems, extending the model simulation period through December 2008, and recalibrating the model. Heywood (2013) developed a local-scale model for an area west of the local-scale model described in this report and used the model to simulate the transport of anthropogenic and natural contaminants near a Water Authority water-supply well.

Hydrogeologic Framework

Geologic Framework

The Rio Grande Rift (fig. 1) is a north-south zone of crustal stretching and thinning that extends from central Colorado through New Mexico and into west Texas and northern Mexico (Hawley and others, 1995). Initiated 25–30 million years ago, the rifting formed a chain of deep, fault-separated structural basins which, collectively, form the Rio Grande Rift (fig. 1). As the basins formed they filled with the Oligocene- to Pleistocene-age sediments of the Santa Fe Group. As much as about 14,500 ft thick in the central Middle Rio Grande Basin (Lozinsky, 1994), the Santa Fe Group has been subdivided into informal lower, middle, and upper lithostratigraphic units on the basis of lithology and age (Hawley and others, 1995; Connell and others, 1998). Units within the upper Santa Fe Group in the Albuquerque area have primarily been assigned to the Ceja and Sierra Ladrones Formations (Connell, 2008). The lower and middle Santa Fe Group units consist primarily of locally derived alluvial, eolian, and lacustrine sediments deposited in closed, internally drained basins (Hawley, 1996).

Of the upper Santa Fe Group, the Ceja Formation, found in the western and east-central parts of the Middle Rio Grande Basin, consists of fluvial sediments carried into the basin from the west (Connell, 2008). The Sierra Ladrones Formation consists of ancestral Rio Grande axial-fluvial sediments and piedmont-slope sediments derived from mountains to the east (Hawley and others, 1995; Connell and others, 1998). The axial-fluvial sediments were deposited on the eastern side of the basin by the ancestral Rio Grande (Connell and others, 1998; Connell, 2006). The axial-fluvial sediments of the Sierra Ladrones Formation interfinger with the Ceja Formation in the central part of the basin and interfinger with piedmont-slope sediments near the eastern edge of the basin (Connell and others, 1998; Connell, 2006). As the channel of the ancestral Rio Grande shifted from the eastern side of the basin towards its present-day position near the center of the basin, piedmont-slope sediments overtopped axial-fluvial sediments and prograded westward as the river retreated (Connell and others, 1998; Connell, 2006). Deposition of Santa Fe Group sediments ended about 1 million years ago when the ancestral Rio Grande began a period of rapid incision (Hawley, 1996). Near the LV-8 well (fig. 2) (formerly Charles-6 [CH-6]), the Sierra Ladrones Formation is about 1,900 ft thick (Connell and others, 1998). Locally within the axial-fluvial sediments of the Sierra Ladrones Formation, two lithologic units characterized by abundant silt and clay layers and identifiable on geophysical logs have informally been named the A1 (lower) and A2 (upper) units (figs. 3 and 4; Connell and others, 1998). Based on observations of grain size, the coarse-grain axial-fluvial sediments represent periods of time when high-energy depositional environments dominated, whereas the fine-grain A1 and A2 units represent low-energy depositional environments.

During deposition of Sierra Ladrones Formation sediments, episodic fault movement and displacement of sediments along listric-normal faults on the east side of the basin caused fault blocks to tilt eastward (Hawley and Haase, 1992; Connell, 2004; cross section *C–C′* in Connell, 2006). The eastward tilting and downward displacement along faults caused the depositional locus (and the ancestral Rio Grande) to shift to the eastern side of the basin (Hawley and others, 1995). As a result, the ancestral Rio Grande deposited a stacked sequence of braided river-channel sediments (the axial-fluvial sediments) in the eastern Middle Rio Grande Basin (Hawley and others, 1995; Hawley, 1996; Connell, 2006). Connell (2006) showed the eastern and western limits of axial-fluvial sediments (fig. 5), but the greatest thickness of axial-fluvial sediments within the local-scale model area lies between the Eubank Fault and the westernmost unnamed fault shown in figure 2 (cross section *C–C′* in Connell, 2006).

Near the present-day Rio Grande in the Albuquerque-Rio Rancho metropolitan area (fig. 1), the uppermost geologic unit consists of Quaternary alluvial sediments that have been deposited on top of upper Santa Fe Group sediments (Connell, 2006). The Rio Grande alluvial sediments are as much as 120 ft thick but on average are about 80 ft thick (Hawley and Haase, 1992). Based on mapping by Connell (2006) Rio Grande alluvial sediments are not present in the local-scale model area; a thin layer of recent alluvium is present in Tijeras Arroyo, and piedmont-slope sediments are mostly above the water table in the local-scale model area but are thicker on the east side of the local-scale model area.

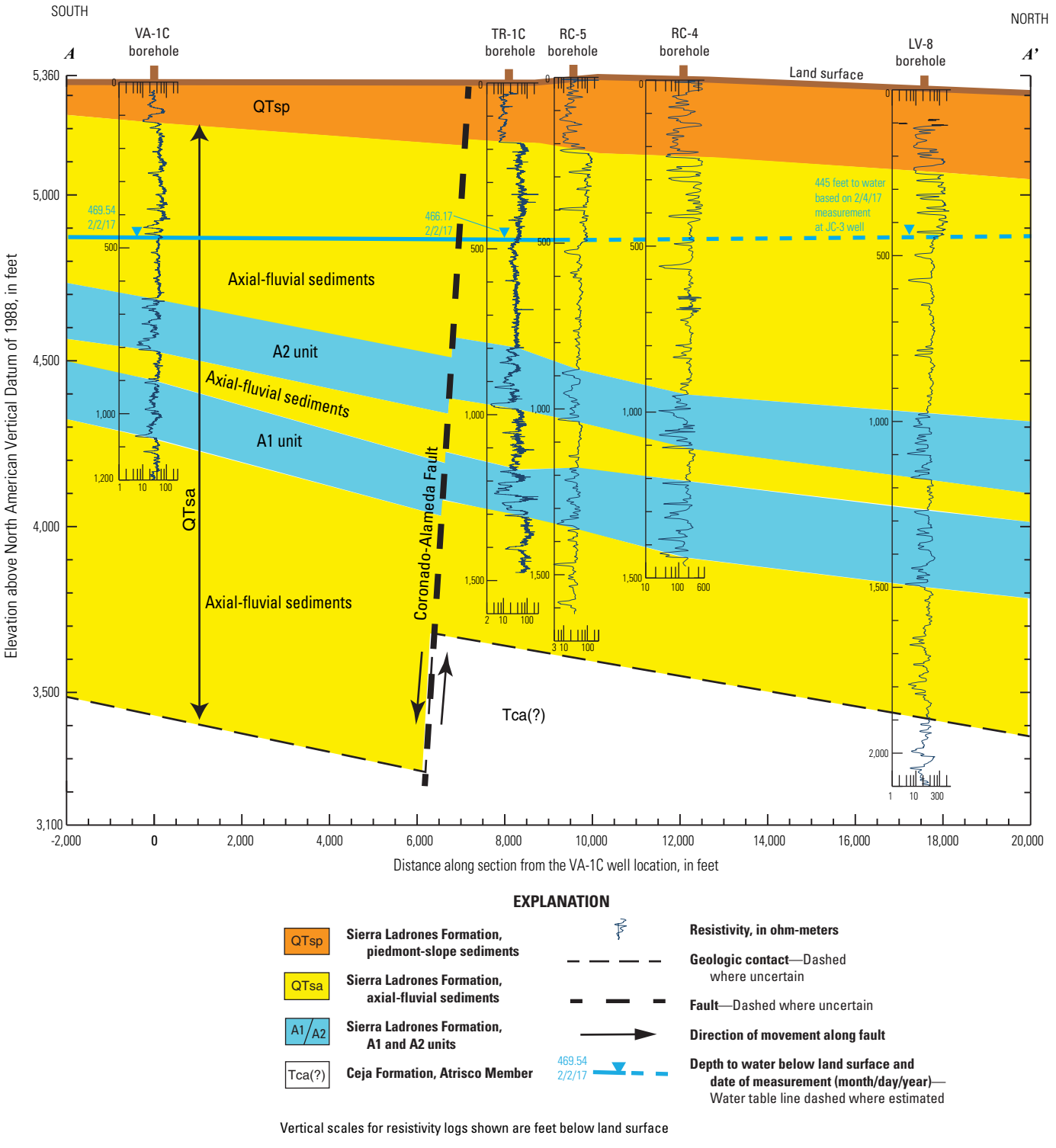

Figure 3. Axial-fluvial sediments above, between, and below the A1 and A2 units of the Sierra Ladrones Formation in the local-scale model area, southeastern Albuquerque, New Mexico. Locations of faults based on Connell (2006). Lithologic tops of the A1 and A2 units for wells RC-5 and LV-8 from Connell and others (1998) and Connell (2006). Other lithologic tops based on geophysical logs used in this study and available online (U.S. Geological Survey, 2018). Line of section shown on figure 2.

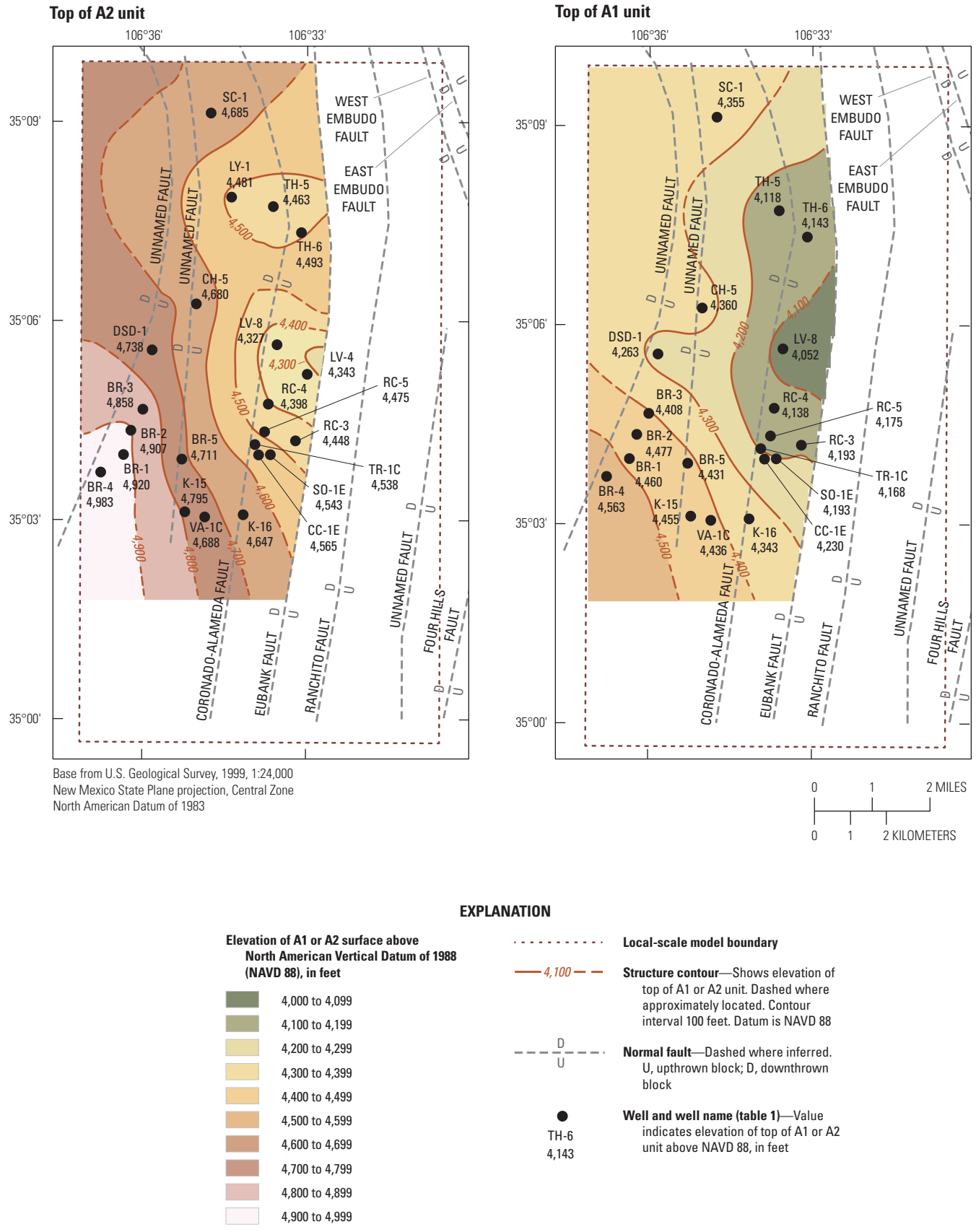

Figure 4. Surfaces representing the tops of the A1 and A2 units within the local-scale model area. Fault traces from Connell (2006). Data and data sources listed in table 1.

For this study, we focus on two types of depositional units that strongly influence groundwater flow: the low-energy, fine-grain A1 and A2 units and the high-energy, coarse-grain axial-fluvial sediments above, between, and below the A1 and A2 units (fig. 3). The A1 and A2 units were identified on the basis of geophysical and lithologic logs (Connell and others, 1998; Connell, 2006) over much of the local-scale model area but appear to be absent approximately east of the Eubank Fault (fig. 2). Tops and bases of the A1 and A2 units were identified by Connell and others (1998) and Connell (2006) on the basis of geophysical log correlations and examination of sediment drill cuttings from wells (table 1). Tops and bases of the A1 and A2 units were identified in this study in additional wells within the local-scale model area on the basis of geophysical log correlations (table 1). Geophysical logs used for this study are available through the USGS GeoLog Locator website (U.S. Geological Survey, 2018).

Digital elevation models (DEMs) were generated for the top and base elevations (table 1) of the A1 and A2 units by using the ArcGIS Topo to Raster tool (Esri, 2017). The Topo to Raster tool uses a thin-plate spline interpolation technique (Wahba, 1990) for which the roughness penalty has been modified to allow the fitted surface to follow abrupt changes in terrain (Esri, 2017). DEM extrapolation was limited to an area within the local-scale model area west of the Eubank Fault roughly north of Tijeras Arroyo (figs. 2 and 4). Faults were not incorporated into the DEM surfaces because of insufficient data specifying fault location and displacement at depth. The resulting DEMs show that the A1 and A2 units generally slope east and, with local variations in slope, toward a low point near the east-central edge of each surface (fig. 4).

The DEMs were generated before the VA-1C well (fig. 4) was drilled, so the A1 and A2 units represented in the local-scale model are as shown in figure 4. Differences between the A2 DEM and the top of A2 unit elevation at VA-1C (tables 1 and 2) may be the result of variations in lithologic thickness, changes in stratigraphy, faulting, or geophysical log quality. Both the A1 and A2 units are thinner in VA-1C than in most other wells in the local-scale model area (table 1). Excluding VA-1C, differences between the DEM elevations and top and base elevations from geophysical logs have root mean square errors of 11.5 and 17.8 ft for the top and base of the A1 unit and 6.9 and 8.9 ft for the top and base of the A2 unit (table 2).

Hydrologic Framework

The hydrologic framework of the Middle Rio Grande Basin is defined by external boundaries, internal hydrogeologic characteristics, recharge to and discharge from the aquifer, and aquifer properties that govern rates of groundwater flow and volumes of groundwater stored in the aquifer. Internally within the basin, the axial-fluvial sediments and A1 and A2 units are of particular importance because the axial-fluvial sediments have relatively high hydraulic conductivities and the A1 and A2 units have lower hydraulic conductivities that inhibit vertical groundwater movement and confine or partially confine water in the underlying axial-fluvial sediments.

External Basin Boundaries

Structural features that define the outer boundaries of the Middle Rio Grande Basin in the Albuquerque area also influence groundwater movement into and out of the basin. The crystalline and consolidated sedimentary rocks of the Sandia and Manzanita Mountain uplifts to the east and the edge of the San Juan Basin to the west (fig. 1) generally are thought to be less permeable than Middle Rio Grande Basin sediments (McAda and Barroll, 2002) and so can be represented as leaky basin boundaries. The northern and southern boundaries of the Middle Rio Grande Basin are defined by convergence of the basin's eastern and western structural boundaries and the presence of associated bedrock highs (McAda and Barroll, 2002). The bottom of the Middle Rio Grande Basin is defined as the interface between the sediments of the Santa Fe Group and the underlying pre-Santa Fe Group volcanic, shale, sandstone, and limestone rocks (Hawley and others, 1995). The Sandia and Manzanita Mountains are composed of fractured Precambrian igneous and metamorphic rocks overlain by Paleozoic sandstone, limestone, and shale (Connell, 2006). The San Juan Basin margin to the west is composed of Paleozoic limestone, sandstone, and shale and Cenozoic basalt flows (Hawley and others, 1995). In general, the lithified rocks surrounding and underlying the Middle Rio Grande Basin are less permeable than are the unconsolidated sediments of the Santa Fe Group (McAda and Barroll, 2002).

Table 1. Depths to and elevations of the tops and bases of the A1 and A2 units of the Sierra Ladrones Formation for selected wells in the local-scale model area.

[Well locations shown on figure 4. Except for land surface, elevations are rounded to the nearest foot. Land surface elevations obtained from National Water Information System (U.S. Geological Survey, 2015). Elevations reported in height above the National Geodetic Vertical Datum of 1929 were converted to height above the North American Vertical Datum of 1988. USGS, U.S. Geological Survey; depth, depth below land surface; elevation, height above the North American Vertical Datum of 1988; –, lithologic unit not present or not evident on log]

Well name	USGS site number	Land surface elevation (feet)	Bottom of borehole		Base of piedmont-slope member (top of axial-fluvial member)		Top of A2 unit	
			Depth (feet)	Elevation (feet)	Depth (feet)	Elevation (feet)	Depth (feet)	Elevation (feet)
BR-1	350401106363201	5,319.74	1,553	3,767	160	5,160	400	4,920
BR-2	350421106361001	5,287.00	900	4,387	120	5,167	380	4,907
BR-3	350440106355801	5,218.00	995	4,223	–	–	360	4,858
BR-4	350343106364401	5,293.00	1,450	3,843	165	5,128	310	4,983
BR-5	350355106351501	5,281.00	1,170	4,111	235	5,046	570	4,711
CC-1E	350359106335205	5,349.95	1,410	3,940	270	5,080	785	4,565
CH-5	350615106345901	5,223.00	3,000	2,223	123	5,100	543	4,680
DSD-1	350534106354701	5,213.00	1,570	3,643	–	–	475	4,738
K-15	350308106351301	5,335.00	1,520	3,815	–	–	540	4,795
K-16	350304106340801	5,367.00	1,511	3,856	–	–	720	4,647
LY-1	350752106342101	5,291.00	996	4,295	–	–	810	4,481
LV-4	350511106325601	5,372.72	1,284	4,089	300	5,073	1,030	4,343
LV-8	350538106333001	5,317.00	3,336	1,981	180	5,137	990	4,327
RC-3	350401106331401	5,387.71	1,475	3,913	350	5,038	940	4,448
RC-4	350445106334001	5,347.72	1,450	3,898	305	5,043	950	4,398
RC-5	350420106334401	5,355.00	1,470	3,885	230	5,125	880	4,475
SC-1	350908106344401	5,243.00	1,308	3,935	235	5,008	558	4,685
SO-1E	350359106333905	5,363.00	1,500	3,863	120	5,243	820	4,543
TH-5	350744106333501	5,358.00	1,450	3,908	225	5,133	895	4,463
TH-6	350720106330401	5,403.00	1,540	3,863	250	5,153	910	4,493
TR-1C	350408106335603	5,337.94	1,477	3,861	180	5,158	800	4,538
VA-1C	350304106345403	5,341.00	1,220	4,121	125	5,216	653	4,688

Base of A2 unit		Top of A1 unit		Base of A1 unit		Base of axial-fluvial member		Source of data
Depth (feet)	Elevation (feet)	Depth (feet)	Elevation (feet)	Depth (feet)	Elevation (feet)	Depth (feet)	Elevation (feet)	
640	4,680	860	4,460	1,125	4,195	–	–	U.S. Geological Survey, 2018.
630	4,657	810	4,477	–	–	–	–	U.S. Geological Survey, 2018.
620	4,598	810	4,408	–	–	–	–	U.S. Geological Survey, 2018.
620	4,673	730	4,563	990	4,303	1,345	3,948	Connell and others, 1998.
770	4,511	850	4,431	1,055	4,226	–	–	U.S. Geological Survey, 2018.
980	4,370	1,120	4,230	1,305	4,045	–	–	U.S. Geological Survey, 2018.
743	4,480	863	4,360	1,103	4,120	2,030	3,193	Connell and others, 1998; Connell, 2006.
740	4,473	950	4,263	1,260	3,953	–	–	U.S. Geological Survey, 2018.
770	4,565	880	4,455	1,150	4,185	–	–	U.S. Geological Survey, 2018.
940	4,427	1,024	4,343	1,230	4,137	–	–	Connell and others, 1998.
1,000	4,291	–	–	–	–	–	–	U.S. Geological Survey, 2018.
–	–	–	–	–	–	–	–	U.S. Geological Survey, 2018.
1,175	4,142	1,265	4,052	1,500	3,817	1,980	3,337	Connell and others, 1998.
1,070	4,318	1,195	4,193	1,390	3,998	–	–	U.S. Geological Survey, 2018.
1,110	4,238	1,210	4,138	1,440	3,908	–	–	U.S. Geological Survey, 2018.
1,040	4,315	1,180	4,175	1,350	4,005	–	–	Connell and others, 1998; top of A1 from U.S. Geological Survey, 2018.
808	4,435	888	4,355	1,108	4,135	–	–	U.S. Geological Survey, 2018; base of piedmont-slope member based on lithologic description in Johnson and others, 1996.
1,030	4,333	1,170	4,193	1,330	4,033	–	–	U.S. Geological Survey, 2018.
1,095	4,263	1,240	4,118	1,415	3,943	1,850	3,508	Connell and others, 1998.
1,085	4,318	1,260	4,143	1,425	3,978	–	–	U.S. Geological Survey, 2018.
980	4,358	1,170	4,168	1,310	4,028	–	–	U.S. Geological Survey, 2018.
810	4,531	905	4,436	1,072	4,269	–	–	U.S. Geological Survey, 2018.

Table 2. Elevations of tops and bases of A1 and A2 units from digital elevation models and difference as compared to geophysical-log- and lithologic-based elevations.

[Well locations shown on figure 4. Geophysical-log- and lithologic-based elevations are shown in table 1. Positive differences indicate that the digital elevation model (DEM) elevation is higher than the elevation from the geophysical log in table 1, and negative differences indicate that the DEM elevation is lower than the elevation from the geophysical log in table 1. USGS, U.S. Geological Survey; NAVD 88, North American Vertical Datum of 1988; –, lithologic unit not present]

Well name	USGS site number	DEM elevation at selected wells (feet above NAVD 88)				Difference between DEM elevation and geophysical-log- and lithologic-based elevations (table 1) (feet)			
		Top of A2	Base of A2	Top of A1	Base of A1	Top of A2	Base of A2	Top of A1	Base of A1
BR-1	350401106363201	4,921	4,674	4,477	4,214	1	–6	17	19
BR-2	350421106361001	4,901	4,650	4,466	4,182	–6	–7	–11	–
BR-3	350440106355801	4,853	4,594	4,407	4,130	–5	–4	–1	–
BR-4	350343106364401	4,977	4,678	4,553	4,294	–6	5	–10	–9
BR-5	350355106351501	4,723	4,522	4,422	4,274	12	11	–9	48
CC-1E	350359106335205	4,562	4,364	4,218	4,050	–3	–6	–12	5
CH-5	350615106345901	4,671	4,463	4,343	4,102	–9	–17	–17	–18
DSD-1	350534106354701	4,740	4,481	4,275	3,969	2	8	12	16
K-15	350308106351301	4,791	4,561	4,453	4,192	–4	–4	–2	7
K-16	350304106340801	4,650	4,434	4,345	4,137	3	7	2	0
LY-1	350752106342101	4,487	4,296	4,220	4,033	6	5	–	–
LV-4	350511106325601	4,326	4,177	4,079	3,850	–17	–	–	–
LV-8	350538106333001	4,339	4,164	4,067	3,830	12	22	15	13
RC-3	350401106331401	4,452	4,309	4,188	3,992	4	–9	–5	–6
RC-4	350445106334001	4,406	4,249	4,140	3,920	8	11	2	12
RC-5	350420106334401	4,480	4,315	4,172	3,999	5	0	–3	–6
SC-1	350908106344401	4,679	4,432	4,351	4,132	–6	–3	–4	–3
SO-1E	350359106333905	4,539	4,342	4,203	4,034	–4	9	10	1
TH-5	350744106333501	4,465	4,268	4,129	3,950	2	5	11	7
TH-6	350720106330401	4,494	4,312	4,141	3,940	1	–6	–2	–38
TR-1C	350408106335603	4,540	4,356	4,197	4,038	2	–2	29	10
VA-1C	350304106345403	4,738	4,515	4,415	4,174	50	–16	–21	–95
		Root mean square error excluding USGS VA-1C				6.9	8.9	11.5	17.8

Internal Basin Hydrogeologic Characteristics

Internal hydrogeologic characteristics that influence the direction and rate of groundwater flow primarily are the hydraulic properties of geologic units, the three-dimensional stratigraphic and structural arrangement of the geologic units, and faults. Within the upper Santa Fe Group, the coarse-grain axial-fluvial sediments form an important geologic feature that greatly influences groundwater flow. The axial-fluvial sediments, deposited by the ancestral Rio Grande, form a north-northeast to south-southwest trending corridor of deposits (between the western and eastern limits of axial-fluvial sediments) with relatively higher hydraulic conductivities (table 3, fig. 5). Given the same hydraulic gradients and effective porosities, groundwater within this corridor of higher hydraulic conductivity will flow at a faster volumetric rate than groundwater outside the corridor where hydraulic conductivities are lower. The axial-fluvial sediments, then, form a preferred corridor of flow, within which groundwater near the EDB plume flowed to the northeast towards a large area of groundwater-level drawdown (Powell and McKean, 2014).

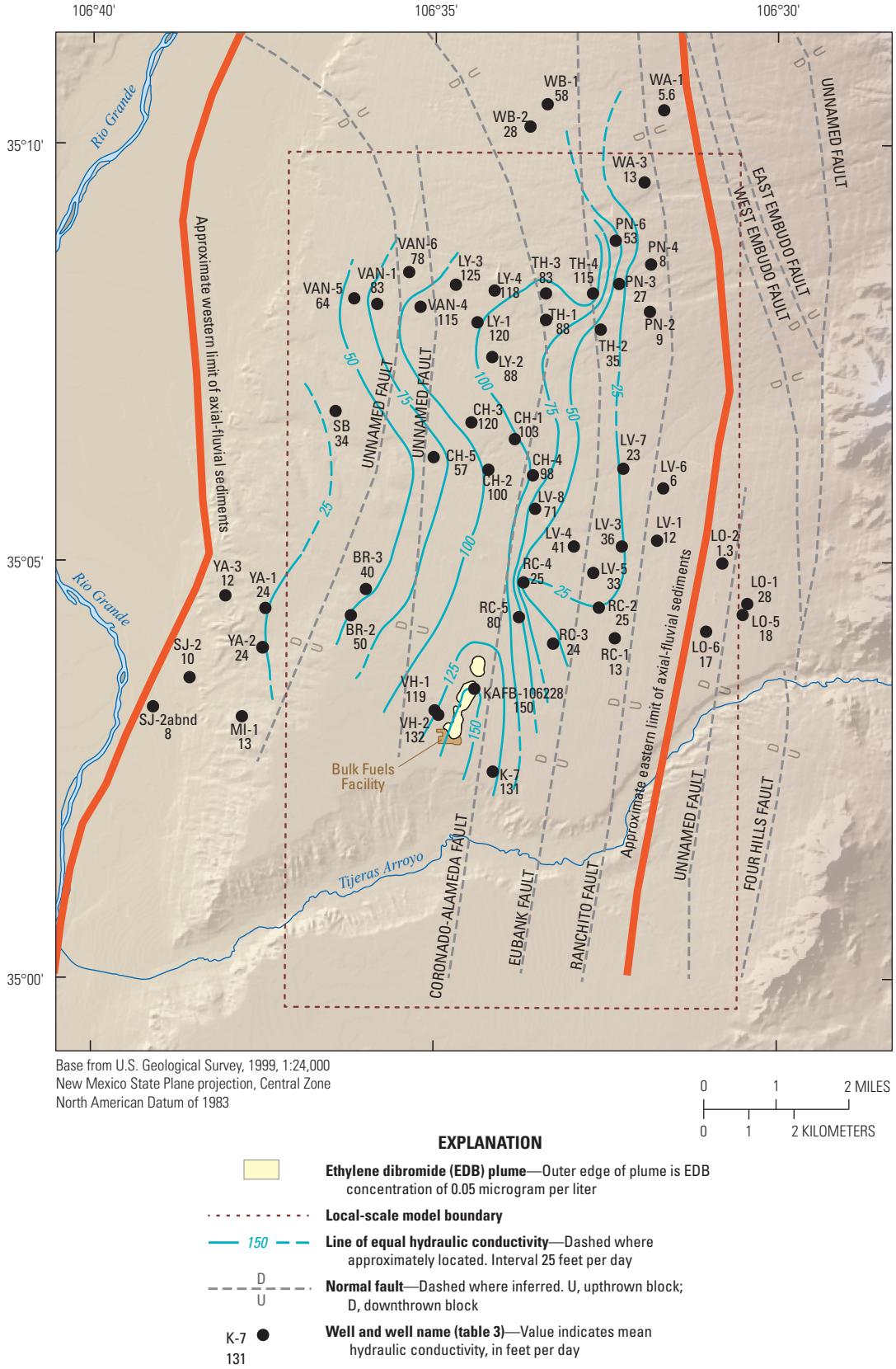

Figure 5. Hydraulic conductivity of Sierra Ladrones Formation sediments in relation to the ethylene dibromide plume (U.S. Army Corps of Engineers, 2017b), locations of faults, and approximate east and west limits of axial-fluvial sediments (Connell, 2006). See table 3 for well identification and sources of hydraulic conductivity data.

Table 3. Transmissivity and hydraulic conductivity values determined from aquifer tests at wells in and near the local-scale model area.

[Well locations shown on figure 5. USGS, U.S. Geological Survey; –, not reported]

Well name	USGS site number	Transmissivity (feet squared per day)	Length of well screen (feet)	Hydraulic conductivity (feet per day)	Additional reported transmissivity (feet squared per day)	Additional hydraulic conductivity (feet per day)	Hydraulic conductivity for well or mean hydraulic conductivity if more than one value reported (feet per day)	Source of data	Comment
BR-2	350421106361001	21,040	420	50	–	–	50	Thorn and others, 1993	
BR-3	350440106355801	25,320	636	40	–	–	40	Thorn and others, 1993	
CH-1	350628106334801	59,500	576	103	–	–	103	Thorn and others, 1993	
CH-2	350606106341101	56,280	564	100	–	–	100	Thorn and others, 1993	
CH-3	350640106342601	67,000	576	120	–	–	120	Thorn and others, 1993	
CH-4	350602106333201	56,280	576	98	–	–	98	Thorn and others, 1993	
CH-5	350615106345901	–	–	57	–	–	57	Ellinger, 2013	
K-7	350235106340801	–	–	131	–	–	131	Ellinger, 2013	Also known as KAFB-ST105-EX1.
KAFB-106228	350328106342701	–	–	150	–	–	150	U.S. Army Corps of Engineers, 2016a	Hydraulic conductivity is the reported geometric mean of results from the pumping well and eight observation wells.
LO-1	350430106302401	17,020	600	28	–	–	28	Thorn and others, 1993	
LO-2	350459106304601	1,070	796	1.3	–	–	1.3	Thorn and others, 1993	
LO-5	350422106312601	14,740	828	18	–	–	18	Thorn and others, 1993	Formerly named Lomas-7.
LO-6	350410106310001	13,400	812	17	–	–	17	Thorn and others, 1993	Formerly named Lomas-8.
LV-1	350517106314401	6,030	500	12	–	–	12	Thorn and others, 1993	
LV-3	350511106321401	15,000	600	25	28,140	47	36	Thorn and others, 1993	
LV-4	350511106325601	23,720	684	35	32,000	47	41	Thorn and others, 1993	
LV-5	350452106323901	14,740	588	25	24,000	41	33	Thorn and others, 1993	
LV-6	350553106313801	4,690	759	6	–	–	7	Thorn and others, 1993	
LV-7	350607106321301	18,760	831	23	–	–	23	Thorn and others, 1993	
LV-8	350538106333001	56,940	800	71	–	–	71	Thorn and others, 1993	Formerly named Charles-6.

Table 3. Transmissivity and hydraulic conductivity values determined from aquifer tests at wells in and near the local-scale model area.—Continued

[Well locations shown on figure 5. USGS, U.S. Geological Survey; –, not reported]

Well name	USGS site number	Transmissivity (feet squared per day)	Length of well screen (feet)	Hydraulic conductivity (feet per day)	Additional reported transmissivity (feet squared per day)	Additional hydraulic conductivity (feet per day)	Hydraulic conductivity for well or mean hydraulic conductivity if more than one value reported (feet per day)	Source of data	Comment
LY-1	350752106342101	55,210	528	105	71,000	134	120	Thorn and others, 1993	
LY-2	350727106340801	40,600	528	77	54,000	100	88	Thorn and others, 1993	
LY-3	350819106344001	56,010	540	100	80,000	150	125	Thorn and others, 1993	
LY-4	350815106340601	49,040	516	95	71,000	140	118	Thorn and others, 1993	
MI-1	350308106374601	9,650	750	13	–	–	13	Thorn and others, 1993	
PN-2	350800106315001	7,240	768	9	–	–	9	Thorn and others, 1993	
PN-3	350820106321701	19,160	720	27	–	–	27	Thorn and others, 1993	
PN-4	350834106314901	4,820	613	8	–	–	8	Thorn and others, 1993	
PN-6	350851106322001	42,610	810	53	–	–	53	Thorn and others, 1993	
RC-1	350405106322001	--	--	13	–	–	13	Ellinger, 2013	
RC-2	350427106323401	--	--	25	–	–	25	Ellinger, 2013	
RC-3	350401106331401	--	--	24	–	–	24	Ellinger, 2013	
RC-4	350445106334001	--	--	25	–	–	25	Ellinger, 2013	
RC-5	350420106334401	--	--	80	–	–	80	Ellinger, 2013	
SB	350648106362501	22,910	672	34	–	–	34	Thorn and others, 1993	
SJ-2	350336106383201	7,000	732	10	–	–	10	Thorn and others, 1993	Formerly named San Jose-7.
SJ-2-abnd	350315106390401	6,030	732	8	–	–	8	Thorn and others, 1993	Well abandoned.
TH-1	350754106332101	28,940	468	62	54,000	115 (see comment)	88	Thorn and others, 1993	Additional hydraulic conductivity value is reported by Thorn and others (1993) as 112, but division of additional reported transmissivity by well screen length gives hydraulic conductivity of 115.
TH-2	350747106323301	18,220	528	35	–	–	35	Thorn and others, 1993	
TH-3	350813106332101	43,680	528	83	–	–	83	Thorn and others, 1993	

Table 3. Transmissivity and hydraulic conductivity values determined from aquifer tests at wells in and near the local-scale model area.—Continued

[Well locations shown on figure 5. USGS, U.S. Geological Survey; –, not reported]

Well name	USGS site number	Transmissivity (feet squared per day)	Length of well screen (feet)	Hydraulic conductivity (feet per day)	Additional reported transmissivity (feet squared per day)	Additional hydraulic conductivity (feet per day)	Hydraulic conductivity for well or mean hydraulic conductivity if more than one value reported (feet per day)	Source of data	Comment
TH-4	350813106324001	40,070	348	115	40,000	115 (see comment)	115	Thorn and others, 1993	Additional hydraulic conductivity value is reported by Thorn and others (1993) as 110 but division of additional reported transmissivity by well screen length gives hydraulic conductivity of 115.
VAN-1	350805106354901	55,610	672	83	–	–	83	Thorn and others, 1993	
VAN-4	350803106351101	58,020	504	115	–	–	115	Thorn and others, 1993	
VAN-5	350809106360901	40,470	636	64	–	–	64	Thorn and others, 1993	
VAN-6	350828106352101	51,320	660	78	–	–	78	Thorn and others, 1993	
VH-1	350313106345701	43,000	600 (360; see comment)	72			72 (119; see comment)	Thorn and others, 1993	Assuming water-producing intervals in this well are similar to those of the nearby VH-2 well, the hydraulic condicitvity for this well would be about 119 feet per day.
VH-2	350310106345601	44,117	360	123	50,935	141	132	U.S. Department of Veterans Affairs, 1997	
WA-1	351027106314001	4,020	721 (see comment)	5.6	–	–	5.6	Thorn and others, 1993	Screen length from Bexfield and others, 1999.
WA-3	350931106315501	9,650	729	13	–	–	13	Thorn and others, 1993	Formerly named Ponderosa-9.
WB-1	351029106332001	42,080	725	58	–	–	58	Thorn and others, 1993	
WB-2	351013106333501	19,970	726	28	–	–	28	Thorn and others, 1993	
YA-1	350426106372601	15,280	624	24	–	–	24	Thorn and others, 1993	
YA-2	350358106372901	19,560	828	24	–	–	24	Thorn and others, 1993	
YA-3	350435106380101	8,040	672	12	–	–	12	Thorn and others, 1993	

The presence of the axial-fluvial sediments, bounded to the east and west by finer-grain units, creates anisotropy with respect to horizontal hydraulic conductivity within the upper Santa Fe Group. Natural microscale layering within upper Santa Fe Group sediments and the presence of the fine-grain A1 and A2 units within the axial-fluvial sediments create anisotropy with respect to vertical hydraulic conductivity. In addition to anisotropy resulting from lithologic textures and depositional units, the generally north-south striking faults in the Middle Rio Grande Basin could impede groundwater flow across fault planes primarily by juxtaposition of finer-grain units on one side of the fault plane against coarser-grain units on the other side of the fault plane (McAda and Barroll, 2002). Impedance of east-west groundwater flow would enhance the general north-south anisotropy in the aquifer. Linear trends in land-surface subsidence and rebound detected by Heywood and others (2002, fig. 2*B*) and by Driscoll and Brandt (2017) may indicate that faults influence groundwater flow in eastern Albuquerque. Aside from estimates for groundwater-flow models, little work has been published regarding horizontal anisotropy in the Middle Rio Grande Basin. Data from an upper Santa Fe Group aquifer test in Albuquerque near the Rio Grande indicated a vertical anisotropy (horizontal hydraulic conductivity divided by vertical hydraulic conductivity) of 82:1 (McAda, 2001).

While horizontal groundwater flow along the corridor of axial-fluvial sediments is relatively unimpeded, vertical groundwater flow is generally impeded by lower vertical hydraulic conductivities of Santa Fe Group sediments (McAda and Barroll, 2002) and, as shown by groundwater hydrographs (fig. 6), is substantially impeded by the A1 and A2 units. Groundwater-level data from the TR-1A, TR-1B, and TR-1C wells (fig. 6) in the Trumbull well cluster (fig. 2) with water-intake screens above the A2 unit (TR-1A, shallow), between the A1 and A2 units (TR-1B, middle), and below the A1 unit (TR-1C, deep) show substantial differences in both water levels and the character of water-level response (fig. 6*A*) to aquifer stresses such as water-supply well pumping. Nearby water-supply wells obtain water from above, below, and between the A1 and A2 units. Water-level differences between these wells show that, at this location, water levels in the deep (TR-1C) well are always higher than those in the middle (TR-1B) and shallow (TR-1A) wells (fig. 6*B*). Water levels in the middle well usually are higher than in the shallow well, indicating an upward vertical groundwater gradient, but there are periods when water levels reverse and water levels in the middle well drop below those in the shallow well (fig. 6*A*). During periods when the water levels are reversed, the vertical groundwater gradient is oriented downward, and groundwater would flow downward were it not impeded by the fine-grain A2 unit. The differences in groundwater levels above, between, and below the A1 and A2 units provide evidence that the vertical hydraulic conductivities of the A1 and A2 units are substantially lower than for the axial-fluvial sediments and that below the A2 unit the aquifer is confined or semiconfined.

Groundwater Recharge and Discharge

Components of recharge to and discharge from the Santa Fe Group aquifer in relation to Middle Rio Grande Basin groundwater-flow models have been discussed comprehensively by McAda and Barroll (2002) and Bexfield and others (2011). The following discussion summarizes components of recharge and discharge; for detailed discussions the reader is referred to McAda and Barroll (2002), Bexfield and others (2011), and Heywood (2013).

Recharge

Although precipitation in arid environments rarely infiltrates more than about 6 ft below land surface before evaporating or being used by plants (Walvoord and Phillips, 2004), focused recharge may occur where water collects in stream channels (tributary recharge) or along mountain fronts (mountain-front recharge) where the less permeable montane rocks meet the more permeable basin-fill sediments (Bartolino and Cole, 2002). Recharge also may occur as seepage from rivers and canals, from irrigated agriculture areas, from septic fields, from water-distribution and sewage-collection systems leakage (Heywood, 2013), and from subsurface inflow of groundwater at basin margins.

Persistent flow in minor streams issuing from the west side of the Sandia and Manzanita Mountains generally does not extend more than a few hundred meters beyond the mountain front (Niswonger and Constantz, 2001) and is considered a component of mountain-front recharge (Anderholm, 2001). Within the Middle Rio Grande Basin, flow in the larger drainages, such as the Bear Canyon and Tijeras Arroyos (fig. 2), can extend a substantial distance into the basin (U.S. Geological Survey, 2017) and has been treated separately in groundwater-flow model development as tributary recharge (McAda and Barroll, 2002; Bexfield and others, 2011). Bear Canyon Arroyo also is the site of the Bear Canyon Recharge Project, which is authorized to recharge up to 3,000 acre-ft per year (Albuquerque Bernalillo County Water Utility Authority, 2016) but currently recharges about 600 acre-ft per year only during winter months (Katherine Yuhas, Albuquerque Bernalillo County Water Utility Authority, written commun., 2018).

Within the Middle Rio Grande Basin, recharge and discharge relations among the Rio Grande, its associated irrigation canals and drains, and groundwater are complex, but there is a net loss of water from this system of water conveyances in the Albuquerque reach of the river to the Santa Fe Group aquifer (Veenhuis, 2002; Bexfield and others, 2011; Rankin and others, 2013, 2016). Increased sediment input, channel modifications, construction of dams upstream, and decreased peak streamflows have caused the Rio Grande channel to aggrade (Swanson and others, 2011), resulting in a river channel and river water levels through Albuquerque that are higher than the water table on either side of the river (Rankin and others, 2013). Drains on either

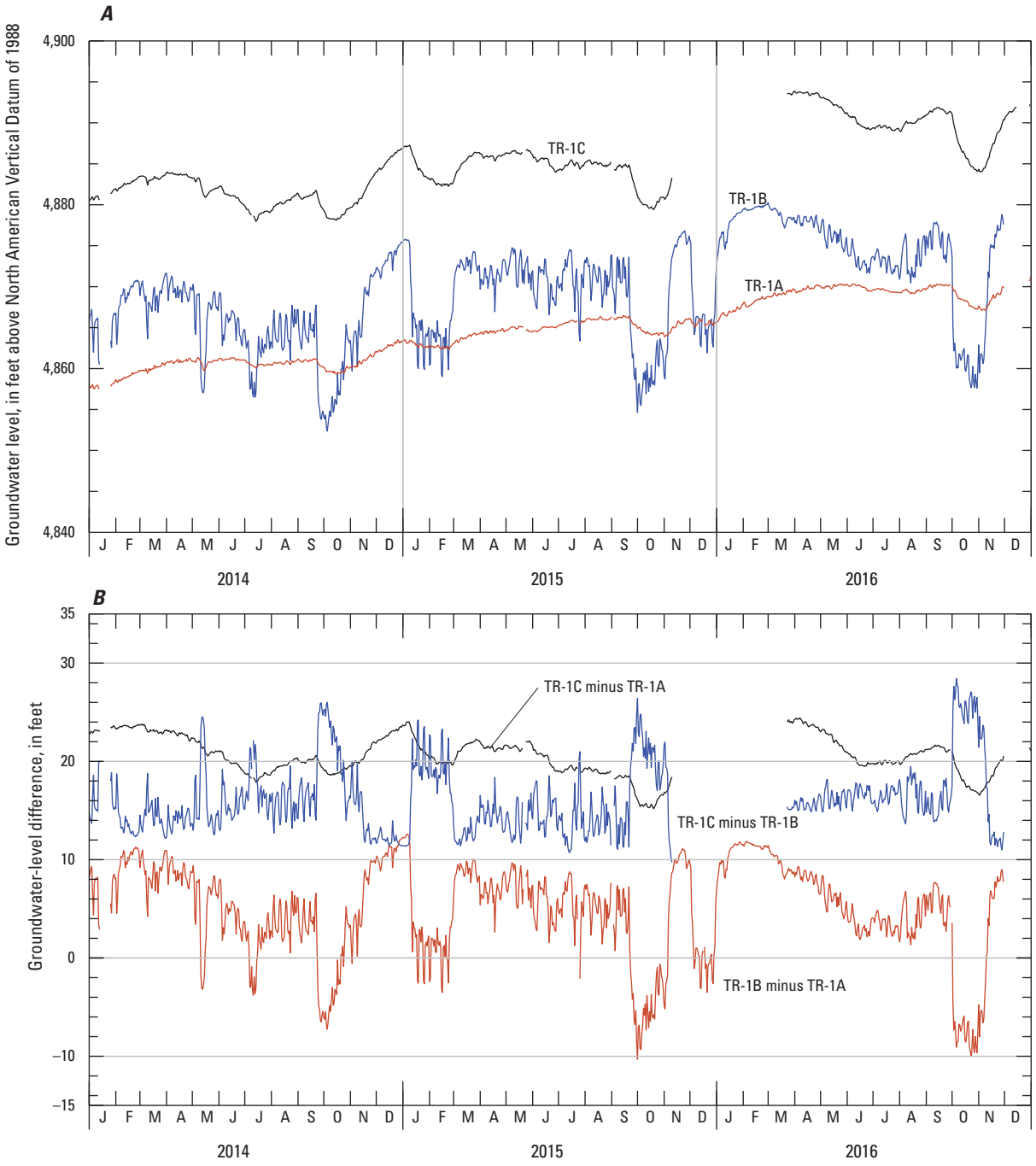

Figure 6. Groundwater-level hydrographs for Trumbull wells TR-1A, TR-1B, and TR-1C, January 2014 through December 2016 (U.S. Geological Survey, 2017). The well screen for TR-1A is above the A2 unit, the well screen for TR-1B is between the A1 and A2 units, and the well screen for TR-1C is below the A1 unit (fig. 3). Location of Trumbull well cluster shown on figure 2. *A*, Groundwater levels. *B*, Groundwater-level differences. Gaps in the hydrographs indicate periods of missing data.

side of the Rio Grande are designed to capture and convey shallow groundwater back to the river, but seepage from canals outside the drains probably contributes substantial amounts of recharge to the aquifer (McAda and Barroll, 2002). In addition, the drains only influence shallow groundwater (Rankin and others, 2013) and probably do not greatly affect deep groundwater flow. While the Rio Grande channel bed and surface-water elevations have risen, widespread groundwater pumping from the Santa Fe Group aquifer has caused groundwater levels to decline (Bexfield and Anderholm, 2002; Falk and others, 2011), thus enhancing the loss of water from the river to the aquifer.

Irrigated agriculture areas are present, or were present in the past, within the Middle Rio Grande Basin along the Rio Grande and Jemez River Valleys and in Tijeras Arroyo (McAda and Barroll, 2002). A portion of the water applied to agriculture areas is assumed to infiltrate below the root zone and recharge the aquifer (McAda and Barroll, 2002; Bexfield and others, 2011). Application of water to parks, golf courses, and other green space in the Albuquerque-Rio Rancho metropolitan area may also contribute recharge to the aquifer (Heywood, 2013).

Seepage of water from septic fields may be a source of recharge in populated areas of the Middle Rio Grande Basin without municipal sewers. Rates of recharge from septic fields have been estimated on the basis of population density and per-person nonconsumptive water use in areas without municipal sewers (McAda and Barroll, 2002; Bexfield and others, 2011).

Leakage from municipal water-distribution and sewage-collection systems is another potential source of recharge. Areas that have the potential for pipe leakage were determined by the extent of Albuquerque and the water and sewer pipes as the developed areas expanded through the 20th century (Bexfield and others, 2011).

Another source of water to the Middle Rio Grande Basin groundwater-flow model is subsurface inflow that occurs from adjacent basins or from water-bearing rock underlying Santa Fe Group sediments. Adjacent basins include the San Juan and Española Basins (fig. 1). The bordering Sandia, Manzanita, and Manzano Mountains (fig. 1) also may contribute subsurface inflow to the Middle Rio Grande Basin (Bartolino and Cole, 2002; McAda and Barroll, 2002).

Discharge

Currently (2019), discharge from the aquifer in the Albuquerque area occurs primarily by seepage to irrigation drains and by groundwater pumping (McAda and Barroll, 2002). Other sources of discharge from the Santa Fe Group aquifer include riparian evapotranspiration along the Rio Grande and groundwater subsurface outflow from the Middle Rio Grande Basin at the southern end of the basin (McAda and Barroll, 2002; Bexfield and others, 2011). Prior to the beginning of widespread groundwater withdrawals in the 1960s, however, discharge from the aquifer was primarily by evapotranspiration from shallow groundwater along the Rio Grande (McAda and Barroll, 2002). Groundwater-level data compiled by Bloodgood (1930) between 1918 and 1922 for the Albuquerque area and analyzed by Theis (1938) indicate very small groundwater gradients away from the Rio Grande and a small loss of water from the river to the aquifer. This small loss of water likely was a result of evapotranspiration uptake of groundwater near the river (Theis, 1938; Bartolino and Cole, 2002). After construction of the Middle Rio Grande irrigation system in the 1930s, the Albuquerque reach of the Rio Grande continued to lose water to the aquifer (Theis, 1938, pl. 6; Bexfield and Anderholm, 2000). Currently (2019) the Albuquerque reach of the Rio Grande loses water to the aquifer; some of this water is captured by irrigation drains, and some moves farther into the aquifer in response to groundwater pumping (McAda and Barroll, 2002). Subsurface outflow of groundwater occurs at the southern end of the Middle Rio Grande Basin but is a relatively minor component of discharge from the aquifer (Kernodle and Scott, 1986; Sanford and others, 2004; Bexfield and others, 2011).

Hydrochemical Zones

Hydrochemical zones, areas of groundwater with distinct chemical and isotopic characteristics defined by Plummer and others (2004), provide insight into likely sources of recharge and general groundwater-flow paths within the Middle Rio Grande Basin. Three hydrochemical zones are present in the local-scale model area (fig. 7) including the central, eastern mountain-front, and Tijeras Arroyo zones. The eastern mountain-front zone borders the Sandia and Manzanita Mountains on the east and the central zone on the west. In the local-scale model area, the eastern mountain-front zone is split by the Tijeras Arroyo zone where it extends west from the mountains into the Middle Rio Grande Basin. The central zone borders the eastern mountain-front zone on the east and extends west of the Rio Grande (fig. 1) in the Albuquerque area. The Tijeras Arroyo zone extends west from the mountains to the central zone boundary. The boundary between the central and eastern mountain-front zones extends from the southwest to the northeast in the local-scale model, passing just east of the EDB plume and near the Trumbull, Cesar Chavez, and Southern observation well clusters and the K-3, K-16, LV-8, RC-5, RC-4, and other water-supply wells (fig. 7).

Plummer and others (2004) stated that recharge to the eastern mountain-front zone most likely is from water recharged along the mountain fronts and from subsurface groundwater inflow from the east. Recharge to the Tijeras Arroyo zone most likely is from infiltration of surface water from Tijeras Arroyo, subsurface groundwater inflow from the Tijeras Arroyo watershed, and mountain-front recharge (Plummer and others, 2004). Recharge to the central zone most likely is from the Rio Grande (Plummer and others, 2004).

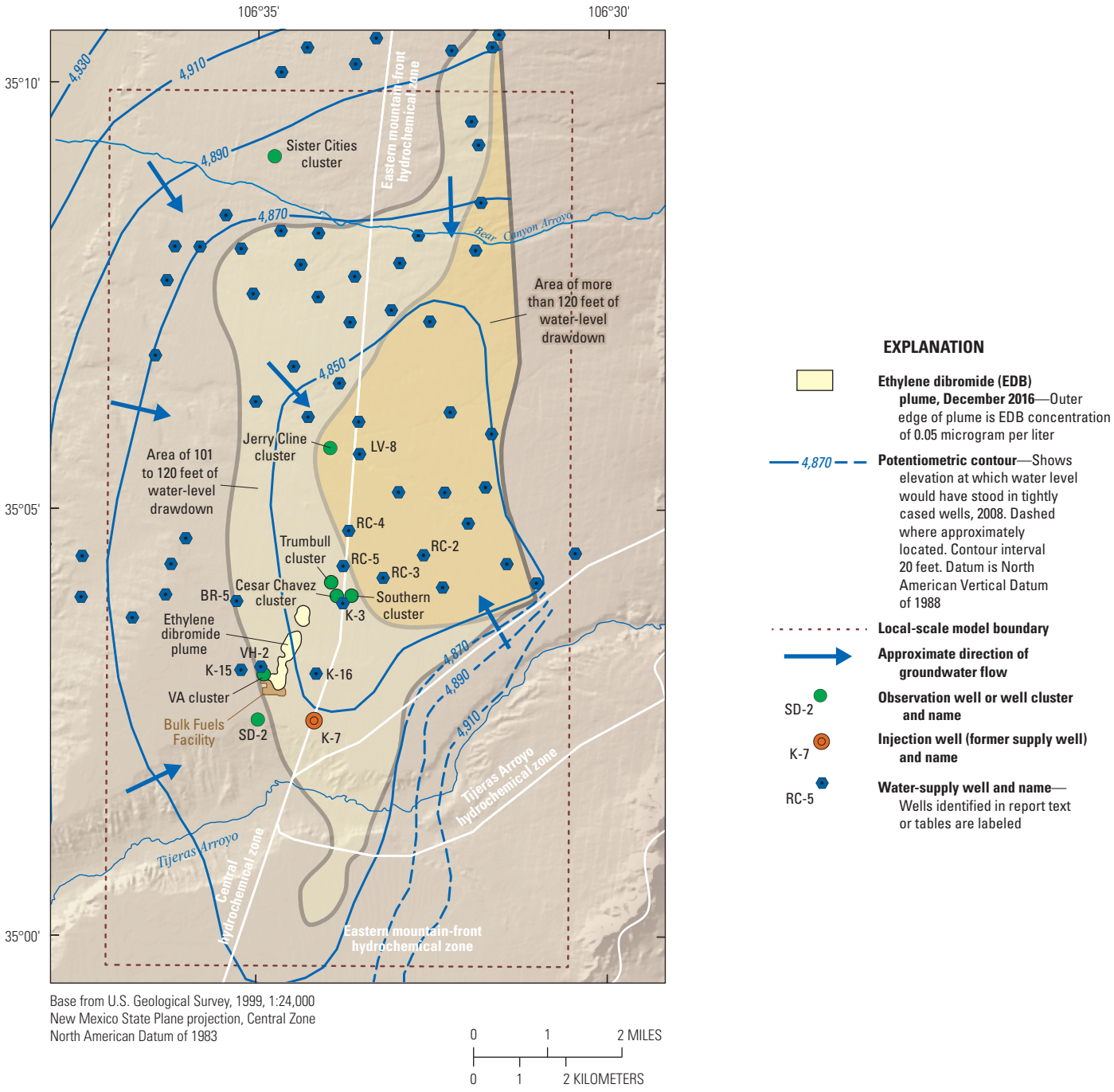

Figure 7. Hydrochemical zones (Plummer and others, 2004), potentiometric contours and areas of water-level drawdown in 2008 (Falk and others, 2011), and ethylene dibromide (EDB) plume (U.S. Army Corps of Engineers, 2017b) in the local-scale model area.

Water-Level and Groundwater-Flow Changes

Because of groundwater pumping in the Middle Rio Grande Basin, water levels in many areas have declined and groundwater-flow directions have changed since the beginning of widespread development of groundwater resources in the 1960s. Prior to widespread development of groundwater resources, groundwater in the basin flowed away from recharge sources in adjacent upland and mountainous areas to the west and east, moved generally south along the river valley, and ultimately discharged to the river south of Albuquerque (Bexfield and Anderholm, 2000). After widespread groundwater development and pumping, groundwater levels have declined over much of the basin, but especially in the Albuquerque-Rio Rancho metropolitan area. By 2008, groundwater levels had declined more than 100 ft in southeastern Albuquerque within the local-scale model area (Falk and others, 2011) (fig. 7). The drawdown in southeastern Albuquerque caused groundwater flow in areas southwest of the area of drawdown to reverse direction from southwesterly to northeasterly (McAda and Barroll, 2002; Falk and others, 2011; Rice and others, 2014). Changes of groundwater-flow direction occurred first near clusters of water-supply wells and then propagated outward over time such that the reversal of groundwater-flow direction occurred in the BFF area in about 1980 (Rice and others, 2014).

In late 2008, the Water Authority began utilizing SJC surface water for public supply (Powell and McKean, 2014). By 2014 groundwater pumping from Water Authority water-supply wells was less than half of what it was in 2008 (Albuquerque Bernalillo County Water Utility Authority, 2016, fig. 4.5). As a result of decreased pumping, water levels in southeastern Albuquerque began to rise in early 2009 (fig. 8) and were still rising at the end of 2016 (Galanter and Curry, 2019).

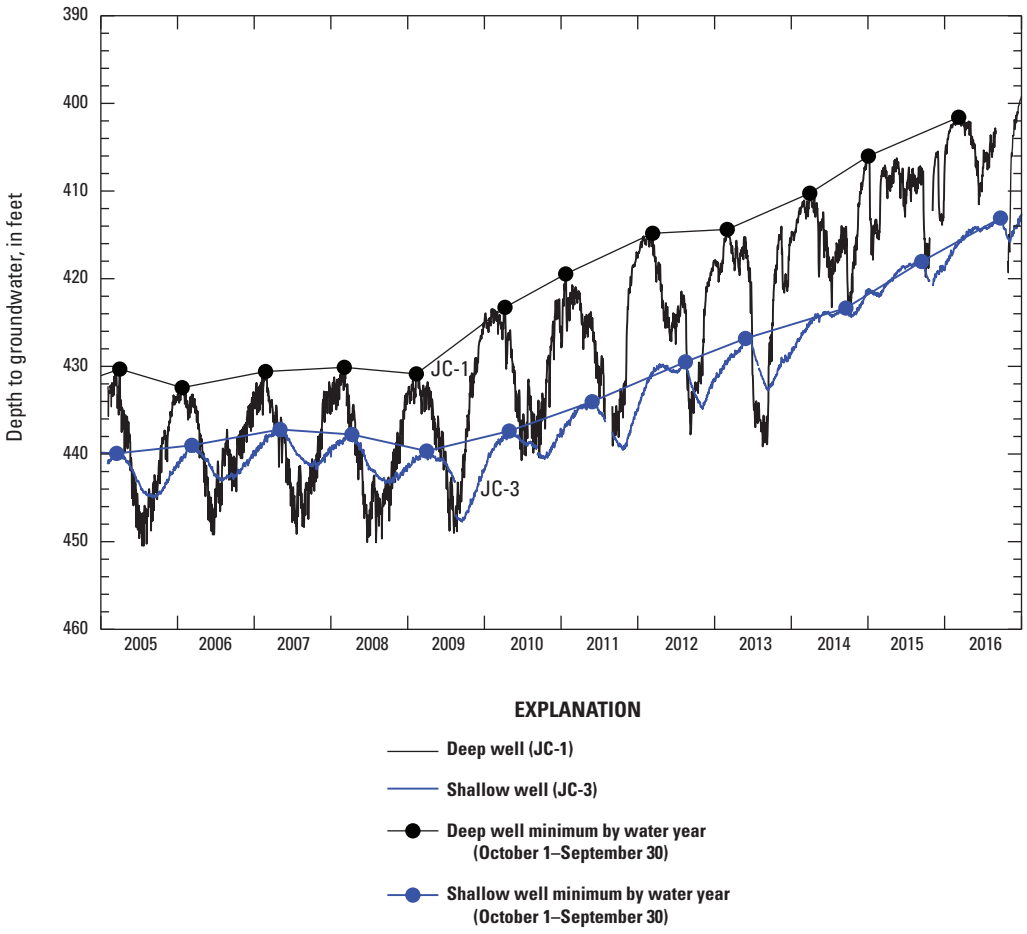

Figure 8. Daily mean and annual (water year) depth to groundwater in the deep and shallow Jerry Cline wells (JC-1 and JC-3, respectively; location of well cluster shown on fig. 2), January 1, 2005–December 31, 2016 (U.S. Geological Survey, 2017), an example of water-level rise in southeastern Albuquerque after the Albuquerque Bernalillo County Water Utility Authority began using surface water for part of the municipal supply.

Aquifer Properties

Properties affecting groundwater flow and storage in the upper Santa Fe Group aquifer include hydraulic conductivity, specific storage, specific yield, horizontal and vertical anisotropy, and effective porosity. Santa Fe Group aquifer properties for the Middle Rio Grande Basin have been compiled by McAda and Barroll (2002) and refined by Bexfield and others (2011) and Heywood (2013) for groundwater-flow models of the basin. Ranges of aquifer properties are summarized in table 4. For detailed descriptions of aquifer properties the reader is referred to McAda and Barroll (2002), Bexfield and others (2011), and Heywood (2013). The application of aquifer properties in the local-scale model is described in the "Hydraulic Parameters" section of this report.

Formation of the EDB Plume

Although the extent of the EDB plume may not be fully characterized, certain logical constraints can be placed on EDB plume development. Because groundwater did not begin to flow northeast at the BFF until about 1980 and because the movement of EDB dissolved in groundwater is largely controlled by advective groundwater flow (U.S. Army Corps of Engineers, 2017a), the extent of the plume as mapped in December 2016 could not have developed prior to 1980. Although the date when fuel with EDB reached the water table is unknown, BFF storage of fuel with EDB was discontinued after 1975 (U.S. Army Corps of Engineers, 2017a), so the fuel leak had to have started prior to 1975. For this report, we assume that fuel with EDB reached the water table prior to 1980 and that the 5,800-ft extent of the plume northeast of the BFF (fig. 2), as mapped in December 2016 (U.S. Army Corps of Engineers, 2017b), has formed since about 1980.

Numerical Groundwater-Flow Model Development and Calibration

The regional groundwater-flow model for the Middle Rio Grande Basin, first developed by McAda and Barroll (2002) and modified by Bexfield and others (2011), was updated for this study. The updated regional groundwater-flow model used for this study will hereinafter be referred to as the "updated regional model." The smaller child model developed for this study will hereinafter be referred to as the "local-scale model." Groundwater levels and flows were simulated in the fine-gridded local-scale model and the surrounding coarse-gridded regional model by using a three-dimensional finite-difference numerical program, MODFLOW–LGR2 (Mehl and Hill, 2013). Similar to the Bexfield and others (2011) model, grid cell size in the updated regional model was 500 meters (m) (about 1,640 ft) on each side. Grid cell size in the local-scale model was 125 m (about 410 ft) on each side. Input and output files for the updated regional and local-scale models are provided in an associated USGS data release (Friesz and Myers, 2019). MODFLOW–LGR2 is a version of MODFLOW-2005 that enables two-way iterative coupling of separate MODFLOW–2005 (Harbaugh, 2005) models for accurate heads and fluxes along the interface between the models. Hydraulic properties and stresses representing the groundwater system in the local-scale model in some cases differ from those used to represent the aquifer in the updated regional model. Two-way coupling provided by MODFLOW–LGR2 ensures that both models have consistent heads and fluxes along their adjoining interfaces. This coupling of the two models also is important because the updated regional model extends to natural features that serve as hydrologic boundaries. After model calibration by nonlinear regression, the local-scale model can be run independently of the updated regional model with specified transient heads around the perimeter of the local-scale model. Head distributions and groundwater flows between model cells can be used to simulate and visualize advective groundwater-flow paths by using the particle-tracking program MODPATH (Pollock, 1994). In addition to using groundwater-level observations to constrain the model solution during calibration, an advective-transport observation of the conservative EDB plume was incorporated into the calibration by comparison of particle-track distance and direction to the December 2015 plume migration distance and direction (U.S. Army Corps of Engineers, 2016c). Areas contributing recharge (ACRs) and zones of contribution (ZOCs) to selected water-supply wells for historical pumping conditions and for potential future pumping scenarios were then simulated by using the calibrated model and particle-tracking simulations. The ACR to a water-supply well is defined as the surface area at the water table where water entering the groundwater system eventually flows to the well (Reilly and Pollock, 1993). The ZOC is the three-dimensional volumetric part of the aquifer through which groundwater flows to the well from the ACR (Morrissey, 1989)

Description and Modification of the Updated Regional Model

The updated regional groundwater-flow model used in this study to simulate groundwater flow in Santa Fe Group sediments of the Middle Rio Grande Basin was first developed by McAda and Barroll (2002) and later modified by Bexfield and others (2011) to include simulation of 8.8 additional years of groundwater withdrawal data, smaller grid cells, leakage from water-distribution and sewage-collection systems in the Albuquerque area, and the use of the Multi-Node Well version 1 (MNW1) package (Halford and Hanson, 2002). The McAda and Barroll (2002) model used MODFLOW–2000 software (Harbaugh and others, 2000), whereas the Bexfield and others (2011) model used MODFLOW–2005 software (Harbaugh, 2005). The following overview of the 2,346-mi^2 Bexfield and others (2011) model provides background information

Table 4. Ranges of aquifer properties in the Middle Rio Grande Basin, New Mexico.

Geologic unit	Range of reported values	Source
Hydraulic conductivity (feet per day)		
Rio Grande alluvium	0.5–40	Kernodle and others, 1995; Kernodle, 1998.
Upper Santa Fe Group, piedmont-slope facies	4–15	Thorn and others, 1993; Connell and others, 1998; McAda, 2001.
Upper Santa Fe Group	1.3–150	Thorn and others, 1993; Kernodle and others, 1995; Kernodle, 1998; Ellinger, 2013; U.S. Army Corps of Engineers, 2016a.
Middle Santa Fe Group	4–11	Kernodle and others, 1995; Kernodle, 1998; McAda, 2001.
Lower Santa Fe Group	2–10	Kernodle and others, 1995; Kernodle, 1998.
Specific storage (per foot)		
Santa Fe Group	$1.2 \times 10^{-6} – 2 \times 10^{-6}$	Heywood, 1998, 2001; McAda, 2001.
Specific yield (dimensionless)		
Santa Fe Group	0.15–0.20	Kernodle and others, 1995; Tiedeman and others, 1998; Barroll, 2001.
East-west to north-south anisotropy ratio (dimensionless)		
Santa Fe Group	1:1–5:1	McAda and Barroll, 2002.
Horizontal to vertical anisotropy ratio (dimensionless)		
Santa Fe Group	82:1–3,500:1	Kernodle and others, 1995; Tiedeman and others, 1998; McAda, 2001.
Total porosity		
Santa Fe Group	0.30–0.40	Bexfield and others, 2011; Ellinger, 2013.
Effective porosity		
Santa Fe Group	0.27	Ellinger, 2013.

for this study's updated regional model and the design of the embedded local-scale model.

The Bexfield and others (2011) regional model simulated groundwater flow in the basin-fill sediments by using nine model layers (fig. 9*A*) with uniformly spaced horizontal model cells of 500 by 500 m. In the vertical dimension, the nine-layer model extended from land surface to the consolidated pre-Santa Fe Group bedrock surface; the total thickness of the model in some areas was greater than 2.5 miles (mi). The Bexfield and others (2011) regional model included a predevelopment steady-state simulation of average hydrologic conditions prior to 1900 followed by a transient simulation of changing hydrologic conditions from 1900 through 2008. Mean annual conditions were simulated for 5-year periods from 1900 through 1974 and 1-year periods from 1975 through 1989. Seasonal conditions (winter and irrigation seasons) were simulated from 1990 through 2008. Aquifer hydraulic properties were adjusted during model calibration by use of 1,818 groundwater levels, which helped to constrain the model solution. Hydrologic boundaries, which represent sources of recharge and discharge to the aquifer, were specified in the model and were not adjusted during calibration.

Hydrologic processes of recharge, evapotranspiration from the water table, well withdrawals, and the interaction between the aquifer and surface water were simulated in the Bexfield and others (2011) regional model. Simulated water inflow to the model included recharge from mountain fronts and associated tributaries, canals and surface application of irrigation, septic-field infiltration, and water-distribution and sewage-collection systems leakage. Inflow to the model also included subsurface flow from adjacent basins along the perimeter of the model. Simulated water outflow from the model included evapotranspiration along the Rio Grande and pumping by domestic, municipal, commercial, and industrial supply wells. Aquifer and surface-water interaction was simulated for rivers, lakes, reservoirs, and drains. The model net inflow and outflow rates (Bexfield and others, 2011) for the steady-state and selected transient simulations are shown in table 5. Discharge from the aquifer to streams and to aquifer storage was small and was accounted for in the model inflow terms (Bexfield and others, 2011). Of the 169 cubic feet per second (ft^3/s) total net inflow for steady-state pre-1900 conditions, 58.5 percent was from rivers, lakes, and reservoirs, 24.3 percent was from subsurface inflow, and 17.2 percent was from mountain-front and tributary recharge (table 5). Simulated mean net outflow (170 ft^3/s) in the steady-state model was all from riparian evapotranspiration. Of the 652 ft^3/s total net inflow for the selected transient simulation (November 1, 1998, to October 31, 1999—winter and irrigation stress periods), 67.8 percent was from river, lake, reservoir, and canal seepage, 10.7 percent was from subsurface inflow and mountain-front and tributary recharge, 10.0 percent was from irrigated agriculture and septic-field seepage and water-distribution and sewage-collection systems leakage, and 11.5 percent was from release of water from aquifer storage (table 5). Of the mean net outflow (653 ft^3/s) for the selected transient simulation 48.1 percent was from discharge to drains, 32.8 percent was from groundwater withdrawal by wells, and 19.1 percent was from riparian evapotranspiration.

For the Bexfield and others (2011) model, simulated horizontal hydraulic conductivity in the Santa Fe Group sediments ranged from 0.05 to 51 feet per day (ft/d) along model rows. Horizontal anisotropy, expressed as the ratio of model column to model row hydraulic conductivity, ranged from 1 to 5, and the anisotropic ratio of horizontal to vertical hydraulic conductivity ranged from 1.1 to 132 in the model. Uniform values of specific yield and specific storage of 0.20 and 2×10^{-6} ft^{-1}, respectively, represented the aquifer.

The updated regional model used in this study is based on the Bexfield and others (2011) model. For this study, the simulation period was extended from December 2008 to October 31, 2013 (adding five winter and five irrigation seasons). The MNW1 package (Halford and Hanson, 2002), used in the Bexfield and others (2011) model to simulate the generally high-capacity municipal, commercial, and industrial wells, was replaced in the updated regional model with the revised Multi-Node Well MNW2 (MNW2) package (Konikow and others, 2009). Lastly, subsurface recharge from adjacent basins at the perimeter of the updated regional model, simulated in the Bexfield and others (2011) model by using the original MODFLOW Well package, was simulated by using the MNW2 package to inject water along the model boundary. The boundary fluxes from the last two stress periods of the Bexfield and others (2011) model were extended through the December 2008 simulation period to October 31, 2013. To ensure that the conversion from the MNW1 package to the MNW2 package was accurate, simulations were conducted by using both the Bexfield and others (2011) model and this study's updated regional model. Water budgets extracted from both models for the January–December 1989 stress period showed that total MNW1 package inflows and outflows for the Bexfield and others (2011) model were 44.14 and 202.84 ft^3/s, respectively. In comparison, total MNW2 package inflows and outflows for the updated regional model were 44.16 and 202.81 ft^3/s, respectively. The differences between MNW1 and MNW2 inflows and MNW1 and MNW2 outflows, 0.02 and 0.03 ft^3/s, respectively, are less than the combined model budget closure error calculated by using Taylor's (1997, p. 60) equation for cumulative uncertainty:

$$CU = \sqrt{u_1^2 + u_2^2 + \ldots + u_n^2}\ , \qquad (1)$$

where

CU is the cumulative uncertainty, in cubic feet per second; and

u_n is the model budget closure error for each model, in cubic feet per second.

With equation 1 and model budget closure errors of 0.34 ft^3/s for the Bexfield and others (2011) model and 8.8×10^{-5} ft^3/s for the updated regional model, the combined model budget closure error is about 0.34 ft^3/s.

A

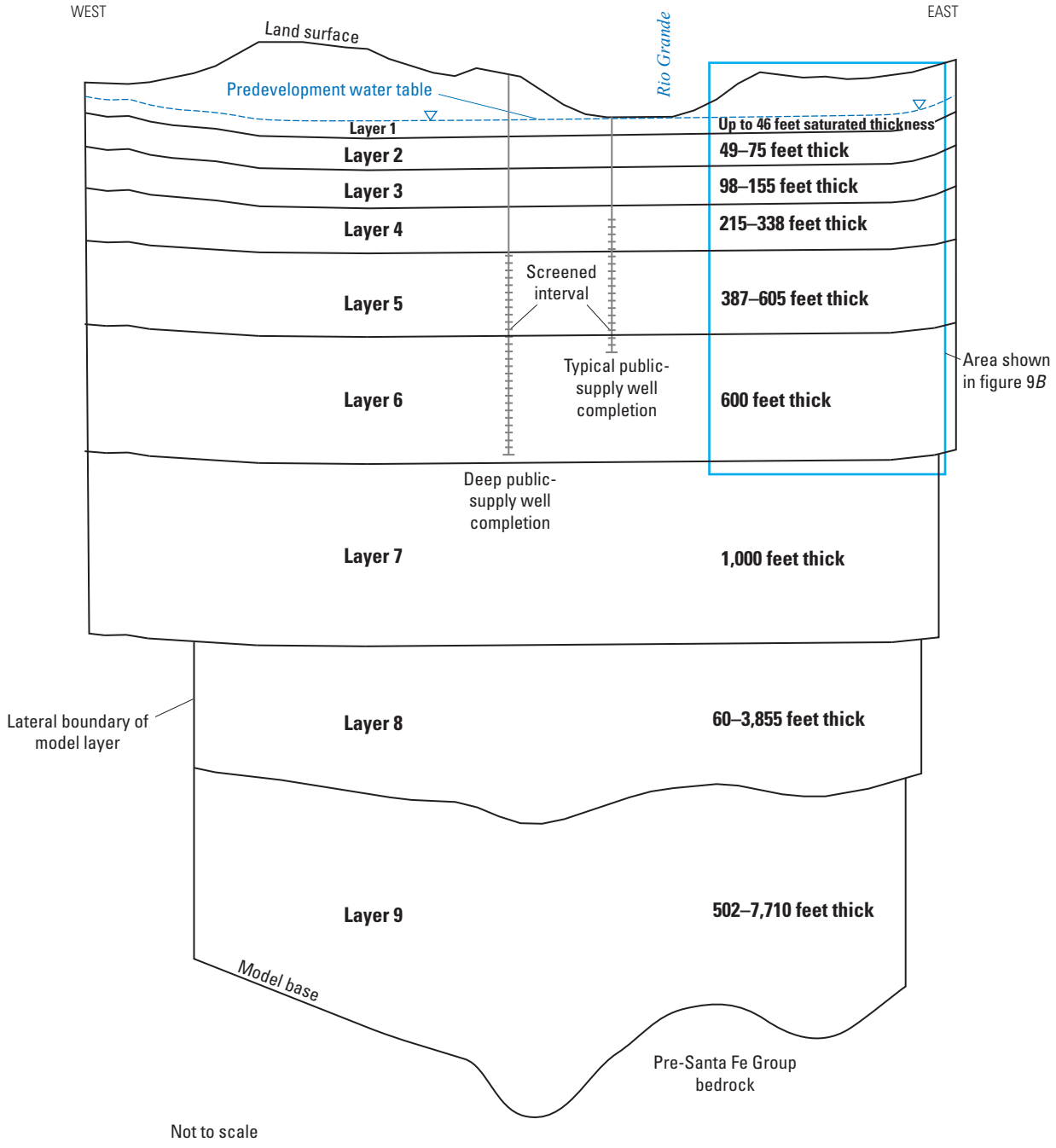

Figure 9. Layer thicknesses in *A*, the updated regional model (modified from Bexfield and others, 2011, fig. 2.13) and *B*, the local-scale model.

B

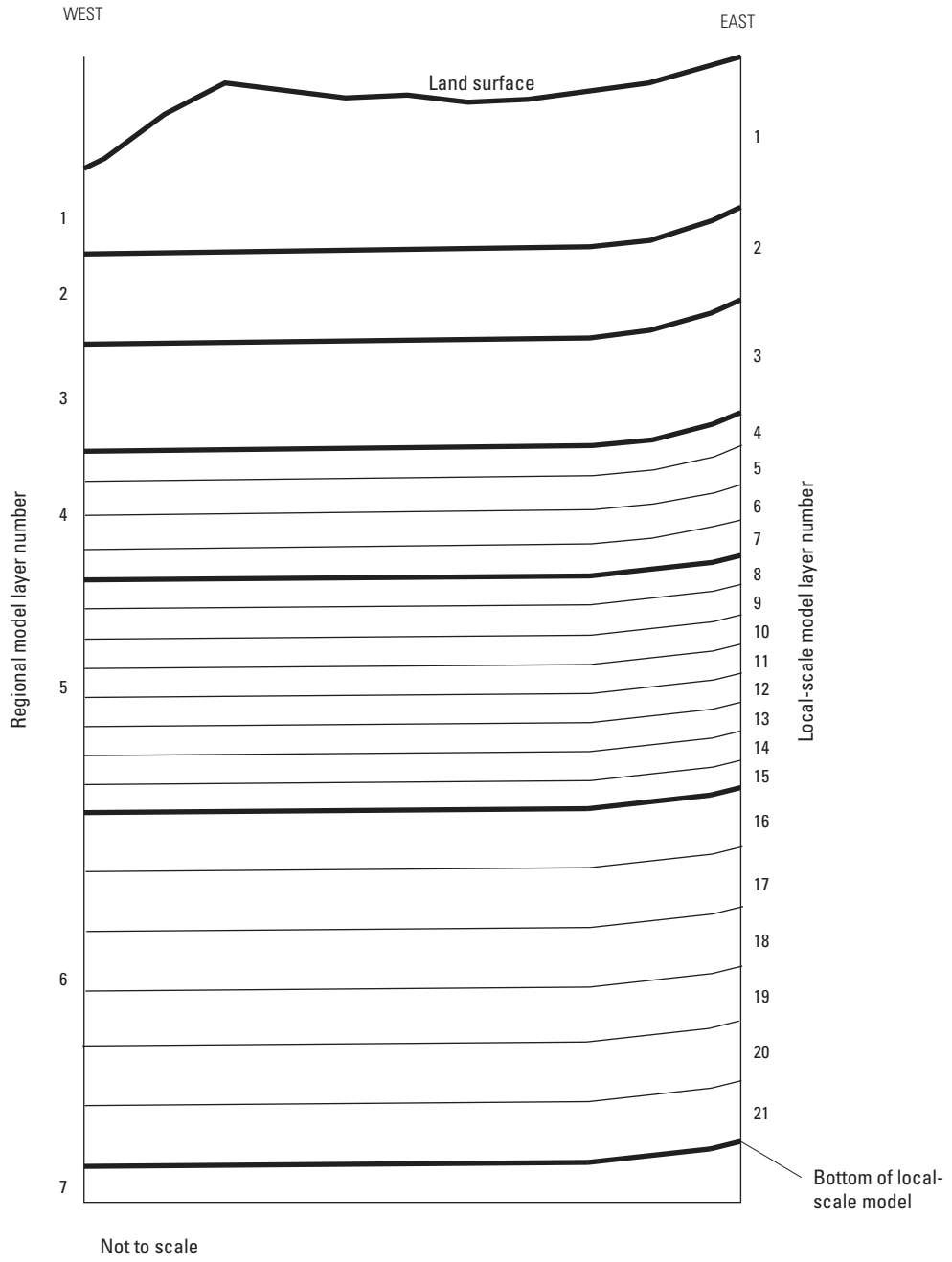

Figure 9. Layer thicknesses in *A*, the updated regional model (modified from Bexfield and others, 2011, fig. 2.13) and *B*, the local-scale model.—Continued

Table 5. Net water budget values for the regional and local-scale models.

[–, not applicable; <, less than; NP, inflow or outflow feature not present in local-scale model]

	Regional model (Bexfield and others, 2011)						Local-scale model, November 1, 1998–October 31, 1999 (winter and irrigation stress periods)	
	Steady-state model (pre-1900)			Transient model, November 1, 1998–October 31, 1999 (winter and irrigation stress periods)				
				Selected transient				
	Net flow (million cubic meters per year)	Net flow (cubic feet per second)	Percent of net inflow or outflow	Mean net flow (million cubic meters per year)	Mean net flow (cubic feet per second)	Percent of mean net inflow or outflow	Mean net flow (cubic feet per second)	Percent of mean net inflow or outflow
Model inflow								
Mountain-front recharge	15	17	10.1	15	17	2.6	0.16	0.17
Tributary recharge	11	12	7.1	11	12	1.8	0.68	0.72
Water-distribution and sewage-collection systems leakage	0	0	0	14	16	2.4	2.5	2.65
Irrigated agricultural seepage	0	0	0	41	46	7.1	0.00035	<0.01
Septic-field seepage	0	0	0	3	3	0.5	0.034	0.04
Aquifer storage	–	–	–	67	75	11.5	14	14.83
Subsurface inflow	37	41	24.3	37	41	6.3	[1]77	81.59
Canal seepage	0	0	0	115	129	19.8	NP	NP
Rio Grande and Cochiti Lake seepage	74	83	49.1	264	295	45.2	NP	NP
Jemez River and Jemez Canyon Reservoir seepage	14	16	9.4	16	18	2.8	NP	NP
Total inflow[2]	**151**	**169**	**100**	**583**	**652**	**100**	**94.37**	**100**
Model outflow								
Groundwater withdrawal	0	0	0	191	214	32.8	94.35	99.49
Subsurface outflow	0	0	0	0	0	0	[1]0.48	0.51
Riverside drains	0	0	0	148	166	25.4	NP	NP
Interior drains	0	0	0	132	148	22.7	NP	NP
Riparian evapotranspiration	152	170	100	112	125	19.1	NP	NP
Total outflow[2]	**152**	**170**	**100**	**583**	**653**	**100**	**94.83**	**100**

[1]Subsurface inflow to and outflow from the local-scale model is flow exchanged between the updated regional model and the local-scale model.

[2]Discrepancies between inflow and outflow values resulted from flow-rate rounding and model volumetric budget discrepancies.

Local-Scale Model Design

The local-scale model encompasses 190 square kilometers (73.2 mi^2)—10 kilometers (about 6.2 mi) from west to east and 19 kilometers (about 11.8 mi) from north to south in southeastern Albuquerque (figs. 1 and 2). The spatial distribution of natural and anthropogenic sources of vertical recharge in the local-scale model was inherited from the updated regional model. Most of the distribution of hydraulic properties was also inherited from the updated regional model, except for horizontal hydraulic conductivity which was a model calibration parameter. As discussed in the "Estimation of Parameters" section of this report, selected hydraulic properties were represented by model parameters for calibration by nonlinear regression.

Spatial and Temporal Discretization

The local-scale model replaced the top six layers of a 38 row by 20 column block (blue box on fig. 9*A*) of the nine-layer updated regional model in southeastern Albuquerque (figs. 1 and 2). Only the top six layers of the updated regional model were refined because the large-capacity water-supply wells are screened in these layers and because the bottom three layers of the updated regional model, in conformity to the shape of the bedrock surface, do not extend as far to the east as the upper six layers (fig. 9). The numerical code of the local grid refinement requires each local-scale model layer to have the same quantity of rows and columns. Of the six layers, the top three layers were refined horizontally, and the bottom three layers were refined both horizontally and vertically. In comparison to the updated regional model grid, the local-scale model had a 4 to 1 horizontal refinement ratio, resulting in a grid of 152 rows and 80 columns, with each cell 125 m (about 410 ft) on a side. The top 3 layers were not vertically refined, whereas the bottom 3 layers were vertically refined into 18 local-scale model layers (table 6, figs. 9*B* and 10). With vertical refinement ratios ranging from 1 to 1 and 8 to 1 (table 6), the horizontal and vertical refinements resulted in a local-scale model with 255,360 cells instead of the 4,560 cells of the updated regional model within the boundary of the local-scale model.

As required by the local grid refinement code, the local-scale model and updated regional model had the same temporal discretization. The initial steady-state stress period representing predevelopment conditions was followed by 78 transient stress periods from 1900 to October 31, 2013, which covers the historical development of the aquifer. Fifteen 5-year stress periods simulated 1900 through 1974, and 15 annual stress periods simulated 1975 through 1989. Following a short stress period for January 1–March 15, 1990, stress periods represented 24 irrigation seasons and 23 winter seasons. The irrigation seasons represent March 16–October 31, and the winter seasons represent November 1–March 15.

Table 6. Vertical refinement of local-scale model layers with respect to the updated regional model.

Regional model layer number	Vertical refinement ratio	Local-scale model layer numbers	Local-scale model layer thickness, in feet
1	1:1	1	61.3–830
2	1:1	2	49.7–54.3
3	1:1	3	99.4–109
4	4:1	4–7	54.7–59.7
5	8:1	8–15	49.7–54.3
6	6:1	16–21	100

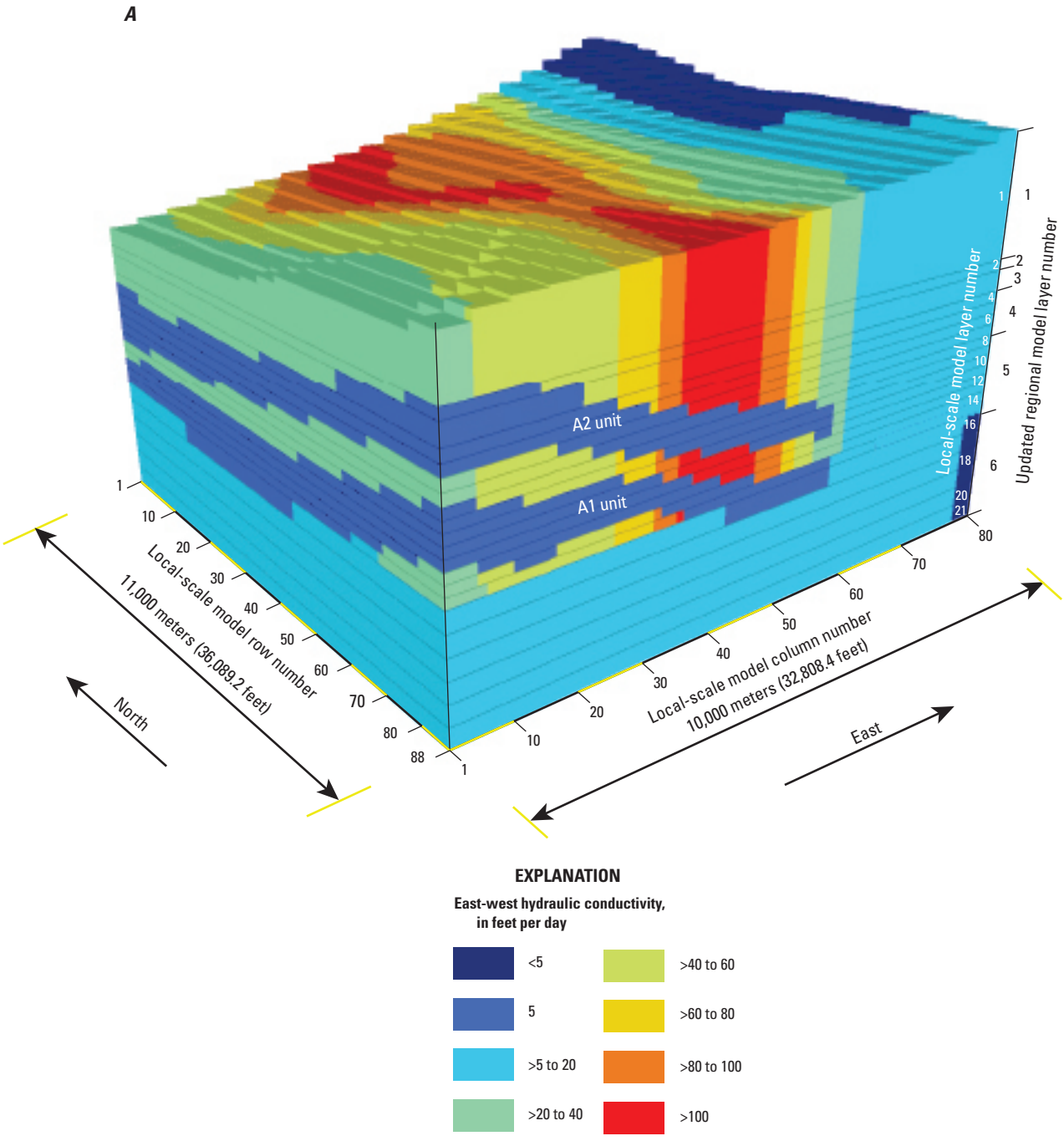

Figure 10. *A*, East-west hydraulic conductivity and *B*, the distribution of hydraulic parameters for local-scale model rows 1–88, columns 1–80, and layers 1–21. The A1 and A2 units are represented in the local-scale model by zones of lower hydraulic conductivity and by the Ka2a1 parameter. Vertical exaggeration is 10 times horizontal.

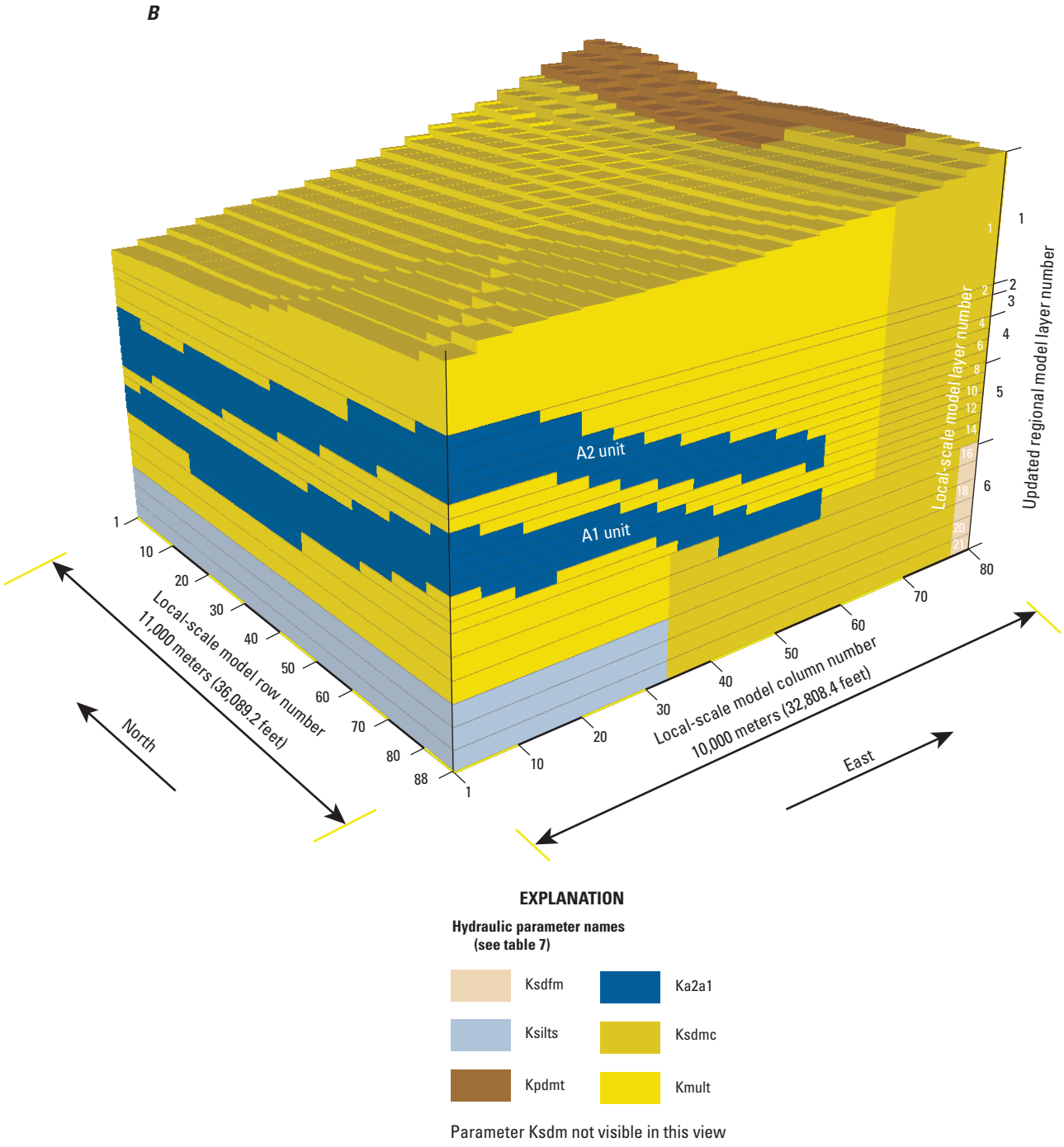

Figure 10. *A*, East-west hydraulic conductivity and *B*, the distribution of hydraulic parameters for local-scale model rows 1–88, columns 1–80, and layers 1–21. The A1 and A2 units are represented in the local-scale model by zones of lower hydraulic conductivity and by the Ka2a1 parameter. Vertical exaggeration is 10 times horizontal.—Continued

Local-Scale Model Inflow and Outflow

In the local-scale model area, simulated inflow to the model is from recharge (mountain-front recharge, tributary recharge, leakage from water-distribution and sewage-collection systems, irrigated agriculture seepage, septic-field seepage), from aquifer storage, and from subsurface inflow of groundwater from the updated regional model (table 5). Canals, lakes, rivers, and reservoirs are not present within the local-scale model area. Outflow from the local-scale model is from groundwater withdrawals by water-supply wells and from subsurface outflow of groundwater to the updated regional model (table 5). Riverside and interior drains and riparian evapotranspiration are not present within the local-scale model. Recharge to the model was simulated by using specified fluxes, whereas the groundwater withdrawals were simulated by using a head-dependent flux boundary. The spatial distribution of recharge fluxes in the local-scale model was not adjusted for the smaller grid size and so is spatially identical to recharge fluxes in the updated regional model. The vertical locations of groundwater withdrawals were adjusted on the basis of well-screen locations and the vertical refinement of the local-scale model layers. Domestic well pumping was not included in the local-scale model because only a small amount of pumping would have been present in the northeast corner of the model.

Runoff from the Sandia Mountains, providing both mountain-front and tributary recharge, is the only natural recharge in the local-scale model area and thus is the only inflow simulated during the steady-state predevelopment stress period. For the transient simulation representing 1900–2013, urban and agricultural land uses have the potential to recharge the aquifer. Although there are multiple sources of recharge to the local-scale model area, most simulated groundwater originates in the updated regional model before entering the local-scale model through the regional- and local-scale model boundary as subsurface inflow (table 5). Simulated outflow from the local-scale model is almost entirely from groundwater withdrawals. Additional details of the methods to determine the location and quantity of recharge and discharge beyond what is included in the subsequent sections are available in McAda and Barroll (2002) and Bexfield and others (2011).

Model Inflow

Mountain-Front and Tributary Recharge

Recharge originating from the Sandia Mountains east of the local-scale model enters the aquifer through two processes, mountain-front recharge and tributary recharge. Mountain-front recharge results from groundwater and surface-water runoff from the Sandia Mountains that infiltrates along the boundary between the Middle Rio Grande Basin and adjacent mountains. Tributary recharge along Tijeras Arroyo (fig. 11) results from infiltration of streamflow along the arroyo channel. Infiltration occurs because of transmissive sediments in the arroyo and because groundwater levels are lower than the channel bed of the arroyo.

Inflow from mountain-front recharge occurs in the southeastern part of the local-scale model (fig. 11*A*), where the extents of the local-scale model and updated regional model coincide (fig. 1). Simulated mean net inflow from mountain-front recharge was 0.16 ft^3/s for the November 1, 1998, to October 31, 1999 (winter and irrigation), stress periods or about 0.17 percent of the total simulated mean net inflow to the local-scale model (table 5). Simulated mean net inflow from tributary recharge was 0.68 ft^3/s for the November 1, 1998, to October 31, 1999, stress periods, or about 0.72 percent of the total simulated inflow to the local-scale model (table 5).

Leakage From Water-Distribution and Sewage-Collection Systems

Areas in the local-scale model that have the potential for leakage from water-distribution and sewage-collection systems were the same as simulated in the Bexfield and others (2011) model. As the developed parts of Albuquerque expanded, the area of simulated leakage from these systems generally spread from southwest to northeast in the local-scale model (fig. 11). Similar to the Bexfield and others (2011) model, inflow (leakage) from the expanding water-distribution and sewage-collection systems was simulated in the updated regional and local-scale models for four time periods: 1900–49, 1950–69, 1970–90, and 1991–2013 (fig. 11). Inflow from leakage was distributed homogenously over the area of the expanding water-distribution and sewage-collection systems and not at discrete points. Water not accounted for in the water-distribution system (for example, pipe leakage, meter inaccuracies, unauthorized use) has been estimated to range from 4.8 to 15.4 percent (New Mexico Environmental Finance Center, 2006). Heywood (2013) arrived at a water-distribution and sewage-collection systems leakage of 3.3 percent of Water Authority groundwater withdrawals by model calibration for an area between the Rio Grande and this study's local-scale model area. More recently the Water Authority estimated real water losses (leakage from pipes, leakage and overflow at storage tanks, and leaks at service connections) for the water-distribution system to be 5 percent (Albuquerque Bernalillo County Water Utility Authority, 2016, chapter 2, p. 13). Based on the New Mexico Environmental Finance Center (2006) report, leakage in the regional model of Bexfield and others (2011) for both the water-distribution and sewage-collection systems was specified as 10 percent of Water Authority groundwater withdrawals for each stress period. The 10 percent value was retained in the updated regional model for this study. But, based on the Heywood (2013) value of 3.3 percent and the Albuquerque Bernalillo County Water Utility Authority (2016) value of 5 percent, a leakage value of 5 percent of Water Authority groundwater withdrawals was used in the local-scale model to simulate the combined water-distribution and sewage-collection systems leakage and

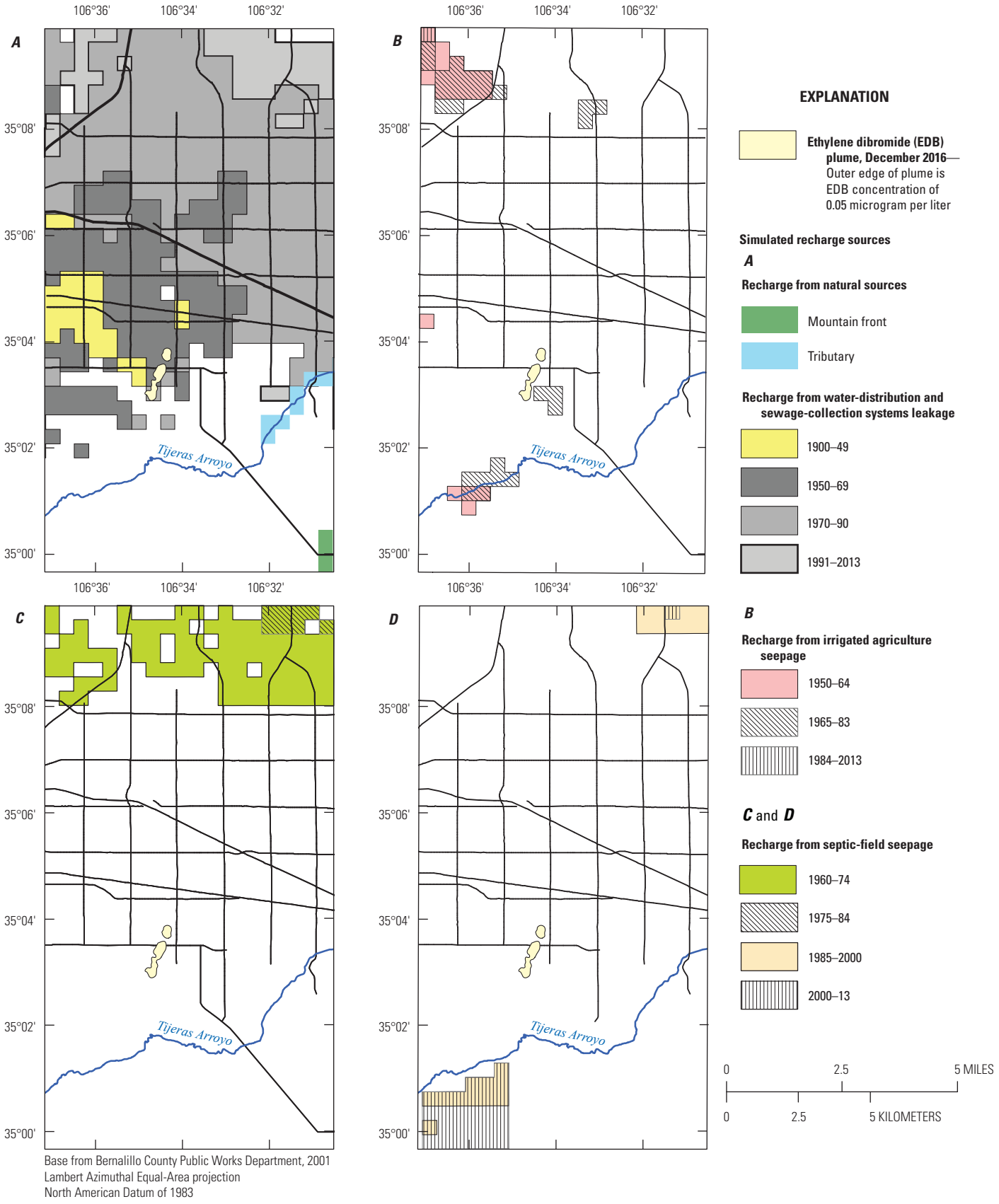

Figure 11. Spatial and temporal distribution of simulated recharge sources from *A*, mountain-front and tributary recharge and water-distribution and sewage-collection systems leakage; *B*, irrigated agriculture seepage; and *C* and *D*, septic-field seepage in the local-scale model. Ethylene dibromide plume from U.S. Army Corps of Engineers (2017b).

resulting aquifer recharge. No attempt was made to estimate the amount of leakage separately attributable to the water-distribution or sewage-collection systems. Simulated mean net inflow from water-distribution and sewage-collection systems leakage was 2.5 ft^3/s for the November 1, 1998, to October 31, 1999, model stress periods, or 2.65 percent of the total simulated mean net inflow to the local-scale model for this time period (table 5). The leakage value of 2.5 ft^3/s is less than 5 percent of groundwater withdrawals because the groundwater withdrawals term in table 5 includes industrial, domestic, and other withdrawals in addition to Water Authority withdrawals.

Irrigated Agriculture Seepage

Recharge from irrigated agriculture seepage occurs where water is applied to land surface for the purpose of irrigating crops. The spatial distribution of irrigated agriculture areas for three time periods (1950–64, 1965–83, and 1984–2013) (fig. 11*B*) indicates that most simulated recharge was in the northwest and southwest parts of the local-scale model area during 1950–83. For 1990 and later, recharge from irrigated agriculture seepage was only simulated during the stress periods representing the irrigation seasons. An average recharge rate of 5.9 in/yr from irrigated agriculture seepage was calculated by McAda and Barroll (2002). Bexfield and others (2011) used the McAda and Barroll (2002) irrigated agriculture seepage recharge rate of 5.9 in/yr and the percentage of a model cell with agriculture for selected periods to calculate the inflow to their model. Simulated recharge from irrigated agriculture seepage in the local-scale model was 0.00035 ft^3/s (less than 0.01 percent of mean net inflow) from November 1, 1998, to October 31, 1999 (table 5).

Septic-Field Seepage

Similar to the updated regional model, inflow to the local-scale model from septic fields was simulated in populated areas without sewage-collection systems. The spatial distribution of septic-field seepage for four periods (1960–74, 1975–84, 1985–2000, and 2000–13) (fig. 11*C* and *D*) indicates that most inflow is in the north and southwest parts of the local-scale model. Simulated mean net inflow from septic-field seepage was 0.034 ft^3/s for the November 1, 1998, to October 31, 1999, stress periods or about 0.04 percent of the mean net inflow to the local-scale model (table 5).

Aquifer Storage and Subsurface Inflow

As groundwater levels rise in an aquifer, the amount of water in storage increases. Conversely, as groundwater levels fall, the amount of water in storage decreases. Because less groundwater is pumped during the winter than summer, groundwater levels in the local-scale model area rise during the winter and fall during summer. From November 1, 1998, to October 31, 1999, groundwater levels fell more than they rose, so although there was a small increase in aquifer storage when water levels rose during winter, the cumulative changes resulted in decreased storage. The net decrease in aquifer storage was accounted as a mean net inflow to the local-scale model of 14 ft^3/s or 14.83 percent of the mean net inflow to the model (table 5).

Subsurface inflow to the local-scale model by far accounted for the majority of inflow to the local-scale model. All of the subsurface inflow was water exchanged between the regional and local-scale models. Subsurface inflow was 77 ft^3/s or about 81.59 percent of the mean net inflow to the model (table 5).

Model Outflow

Most of the simulated groundwater withdrawals for public-supply and commercial uses were for long-screen, high-capacity water-supply wells. The head-dependent MNW2 package (Konikow and others, 2009) allows for withdrawals from wells screened through multiple model cells. Total withdrawal from a well is specified in the model, but the contribution of pumped water from each layer is dependent on aquifer hydraulic conductivity and the hydraulic gradient between the aquifer and the well. A total of 95 water-supply wells were simulated in the local-scale model area (fig. 12), beginning with 5 wells in the 1945–49 stress period. Simulated groundwater withdrawals from water-supply wells in the local-scale model ranged from 0.85 million gallons per day (1.3 ft^3/s) in 1945–49 to 83 million gallons per day (128 ft^3/s) in the 1993 irrigation season (Friesz and Myers, 2019). The groundwater withdrawal rate was 94.35 ft^3/s for the November 1, 1998, to October 31, 1999, stress periods or 99.49 percent of the mean net outflow from the local-scale model (table 5).

As the inflow and outflow numbers show, almost all of the inflow to the local-scale model exits the model by groundwater withdrawals. Only a very small amount (0.48 ft^3/s or 0.51 percent of mean net outflow) of water exits the local-scale model by subsurface outflow to the updated regional model.

Hydraulic Parameters

Hydraulic properties of the aquifer to transmit and store water were defined by model parameters (table 7, fig. 10*B*). Hydraulic conductivity parameters were assigned on the basis of lithologic units. The spatial distribution of horizontal hydraulic conductivity parameters in the updated regional model, inherited from the McAda and Barroll (2002) and Bexfield and others (2011) models, was largely based on a three-dimensional digital geologic model of the hydrostratigraphic units developed by Cole (2001). This same distribution was used in the east and lower part of the local-scale model and generally represented fine- to medium-grain basin-fill sediments (parameters Ksilts, Ksdfm, Ksdm, Ksdmc, and Kpdmt; table 7, fig. 10*B*). Two additional parameters, Kmult and Ka2a1 (table 7, fig. 10*B*), represented horizontal hydraulic conductivity for the coarser- and finer-grain

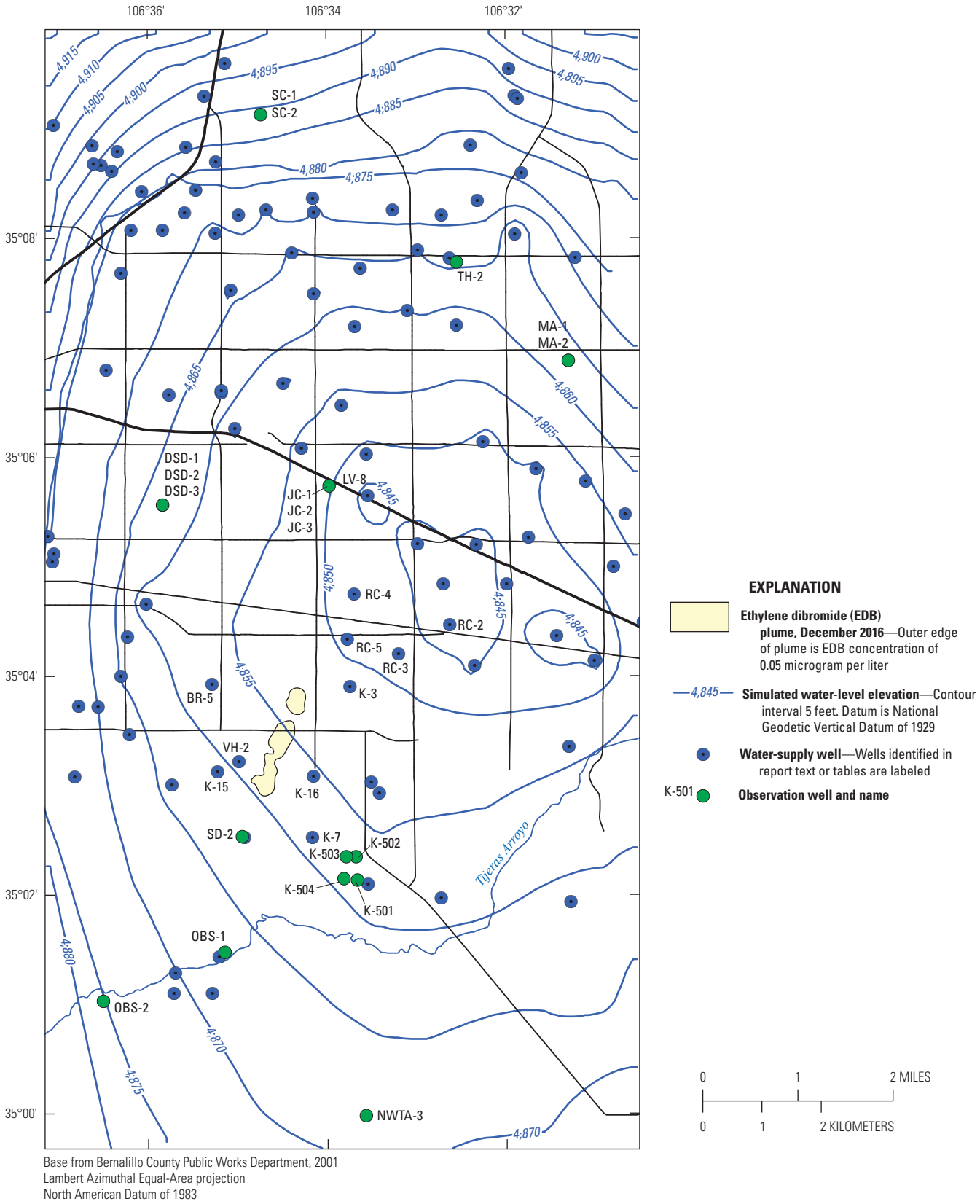

Figure 12. Locations of water-supply wells and observation wells and simulated water-level contours for October 2013 in layer 12 of the local-scale model.

axial-fluvial sediments in the local-scale model. Parameter Kmult represented the coarse- to very coarse-grain axial-fluvial sediments (figs. 3, 5, and 10), and parameter Ka2a1 represented the predominantly fine-grain A1 and A2 layers (figs. 3, 4, and 10). The Ka2a1 parameter was incorporated into the local-scale model for all of the DEM area in figure 4 and, for continuity within the model, was extended south from the southern edge of the DEM to the southern edge of the local-scale model. Parameter Kmult defined a dimensionless parameter that was used to multiply spatially varying hydraulic conductivity values that were interpolated from the hydraulic conductivity contours (fig. 5) to populate the local-scale model cells (fig. 10*A*). Uniform values of horizontal hydraulic conductivity were used in each vertical stack of cells that represent coarse-grain sediments (fig. 10*B*). A Kmult value of 1 would be equal to the hydraulic conductivity values defined by the contours. Interpolated values assigned to model cells based on the hydraulic conductivity contours (fig. 5) ranged from 14 to 115 ft/d and averaged 67 ft/d. The top end of this range is smaller than shown in figure 5 because data for the VH-1, VH-2, and KAFB-106228 wells were not available when the interpolation was done.

The seven parameters (Ksilts, Ksdfm, Ksdm, Ksdmc, Kmult, Kpdmt, and Ka2a1) were used to represent horizontal hydraulic conductivity along the east-west local-scale model rows (perpendicular to the valley axis) for various lithologic units. Because the pattern of deposition in the Middle Rio Grande Basin was generally oriented north to south, a parameter representing horizontal anisotropy (HANIyes, table 7) was assigned to most sediments. Horizontal anisotropy is defined as the ratio of hydraulic conductivity along model columns (north-south direction) to hydraulic conductivity along model rows (west-east direction). The piedmont-slope sediments near the basin margin were specified as horizontally isotropic (parameter HANIno, table 7).

Local-scale interfingering of higher and lower hydraulic conductivity sediments, as well as broader-scale stratification of sedimentary layers, can cause higher values of hydraulic conductivity in the horizontal direction compared to the vertical direction. The ratio of horizontal hydraulic conductivity along the east-west oriented rows to vertical hydraulic conductivity for the basin-fill sediments was represented by parameter VANIyes (table 7).

Water enters or leaves storage in confined model layers (specific storage) as a result of compression or expansion of the water and aquifer sediments, but in an unconfined model layer, water enters or leaves storage (specific yield) predominantly as a result of water filling or draining the pore spaces in aquifer sediments at the water table (Lohman, 1979). Parameter SY (table 7) was used to represent a uniform specific yield for the uppermost active cells, and parameter SSall was used to represent specific storage for the lower, confined local-scale model cells.

Finally, for the particle-tracking analysis, in addition to heads and fluxes from the local-scale model, a parameter for effective porosity (table 7) was used to help calibrate the model and to calculate groundwater-flow velocities. The effective porosity parameter was represented by a uniform value for the local-scale model.

Local-Scale Model Calibration

The local-scale model was calibrated with the inverse modeling program UCODE–2005 (Poeter and others, 2005; Hill and Tiedeman, 2007) by using nonlinear regression that minimizes the differences, or residuals, between field (observed) measurements and their simulated equivalents to obtain an optimal set of parameter values. Two types of observations, groundwater levels and advective transport based on the EDB plume, were used in local-scale model calibration.

The quality of this calibration was determined by the accuracy of the estimated parameter values and by analysis of the residuals. Some parameters, however, might be insensitive to the available observations, and some parameters might be highly correlated with each other and therefore cannot be estimated by nonlinear regression. Values from the updated regional model and the literature were used to specify parameter values that could not be estimated by nonlinear regression.

Observations

Hydraulic parameter values in the local-scale model were estimated by use of 295 groundwater-level observations and an advective-transport observation for the EDB plume. Observations were weighted on the basis of methods described by Hill and Tiedeman (2007) to account for the difference in the type of observations and their relative influence in nonlinear regression. Observation weights are equal to the inverse of the variance (square of the standard deviation) of the measurement uncertainty.

Local-scale model calibration included 295 water levels from 19 observation wells (fig. 12). Most water levels were from vertical clusters of observation wells at four sites that have two to three wells, generally with one well screened near the water table, one well screened in the middle part of the aquifer, and one well screened in the deep part of the aquifer. Most observation wells have short screens and are simulated in one local-scale model layer. Only one selected water-level observation from each observation well for each stress period was used in the calibration. The selected water-level observations for each observation well were judged to be representative of water-level conditions near the end of each stress period. Groundwater-level observations were available for 1949 through 2013, with most observations for 1997 and later. Groundwater-level elevations were computed using the land-surface elevation for each observation well.

Advective transport of contaminants, such as the EDB plume, can be an important observation for model calibration (Hanson and others, 2013). In contrast to a groundwater-level

Table 7. Descriptions of hydraulic parameters, optimal or specified parameter values, and parameter-estimation statistics in the local-scale model and comparison to updated regional model parameter values.

[HK, horizontal hydraulic conductivity along model rows; ft/d, foot per day; –, not determined; HANI, ratio of horizontal hydraulic conductivity along model columns to hydrualic conductivity along model rows; VANI, ratio of horizontal conductivity along rows to vertical hydraulic conductivity; SY, specific yield; SS, specific storage; ft, foot; n, effective porosity]

Parameter name	Type	Parameter description	Local-scale model			Updated regional model
			Optimal (in bold) or specified value	95-percent confidence interval range	Coefficient of variation	Specified value
Ksilts	HK	Silty deposits in layers 12–21	7.0 ft/d	–	–	7.0 ft/d
Ksdfm	HK	Fine- to medium-grain sand deposits in layers 8–21	0.05 ft/d	–	–	0.05 ft/d
Ksdm	HK	Medium-grain sand deposits in layers 13–21	1.4 ft/d	–	–	1.4 ft/d
Ksdmc	HK	Medium- to coarse-grain sand deposits in all layers	**5.8 ft/d**	3.9–8.7	0.21	7.3 ft/d
Kmult	HK	Multiplier of coarse- to very coarse-grain axial-fluvial sediments in layers 1–15	**0.97**	0.68–1.37	0.18	–
Kpdmt	HK	Piedmont sediments in all layers	**3.8 ft/d**	0.93–15.8	1.06	12.0 ft/d
Ka2a1	HK	Predominantly fine-grain deposits in layers 2–18	5.0 ft/d	–	–	–
HANIyes	HANI	All layers	**1.4**	1.1–1.9	0.16	1.5
HANIno	HANI	All layers	1.0	–	–	1.0
VANIyes	VANI	All layers	**241**	195–302	0.11	132
SY	SY	Layers 1–3	**0.14**	0.13–0.15	0.05	0.20
SSall	SS	All layers	0.000002 ft^{-1}	–	–	0.000002 ft^{-1}
Effective porosity	n	All layers	0.25	–	–	–

observation, an advective-transport observation reflects long-term groundwater-flow patterns because of the long-term scale of advective groundwater flow. Also, the intended purpose of the local-scale model is to delineate ACRs and ZOCs to selected water-supply wells, which are based on advective flow paths.

EDB has been observed to be persistent in some subsurface environments associated with releases of leaded fuel from leaking underground storage tanks (U.S. Environmental Protection Agency, 2006; Wilson and others, 2008). The biodegradation half-life of EDB in groundwater has been estimated to range from 15 to 50 days for anaerobic conditions and from 35 to 360 days for aerobic conditions (U.S. Environmental Protection Agency, 2006). The hydrolytic half-life of EDB has been estimated to range from 6 to 13.2 years at 20 degrees Celsius (Wilson and others, 2008). For the BFF EDB plume, anaerobic conditions are present in groundwater near the BFF, but aerobic conditions are present in the EDB plume northeast of the BFF (U.S. Army Corps of Engineers, 2017a). The longer potential half-life under aerobic conditions indicates that EDB northeast of the BFF could be transported by advective processes and could form a plume in the direction of groundwater flow. For this study, advective transport of EDB also was assumed predominant because of the strong groundwater gradients towards the large area of drawdown in southeastern Albuquerque (fig. 7) and the relatively large hydraulic conductivities in the plume area (fig. 5).

An observation of advective transport was created by selecting a location near the leading edge of the mapped extent of the EDB plume as known in December 2015 (U.S. Army Corps of Engineers, 2016c) (fig. 13). The dates when fuel began leaking and when contaminants reached the water table through approximately 500 ft of unsaturated sediments are unknown. However, the EDB plume is known only northeast of its source at the BFF, and simulation of groundwater flow indicated that flow in the vicinity of the EDB plume reversed direction from southwest to northeast in about 1980. For calibration purposes, a particle was released at the center of the source (fig. 13) at the water table in January 1980 and tracked forward in an approximate northeast direction along a simulated groundwater-flow path until the end of the model simulation (October 31, 2013). The distance between the particle at its final location and the advective-transport observation location is the residual. During advective transport simulations, the most recent EDB concentration and plume-outline data were for the October–December 2015 quarter (U.S. Army Corps of Engineers, 2016c). At that time, the farthest downgradient monitoring well with an EDB concentration exceeding 0.05 microgram per liter was KAFB-106225 (0.143 microgram per liter) (U.S. Army Corps of Engineers, 2016c). KAFB-106225, located near the distal end of the plume (fig. 13), was assumed to represent the location of the advective-transport observation. A standard deviation of 50 ft was used to weight the observation.

Estimation of Parameters

Thirteen hydraulic parameters were evaluated with parameter estimation: seven for horizontal hydraulic conductivity, two for horizontal anisotropy and one for vertical anisotropy, two for storage, and one for effective porosity (table 7). Parameter sensitivities, shown by their composite scaled sensitivities in figure 14, indicate whether groundwater-level and advective-transport observations provided sufficient information to permit an estimate of a given parameter. Parameters with higher sensitivities generally can be more precisely estimated through the model calibration process than can parameters with lower sensitivities. Parameters with composite scaled sensitivities that are about two orders of magnitude lower than that of the parameter with the highest value, or those with composite scaled sensitivities less than 1, indicate that nonlinear regression might not be capable of estimating the parameter (Hill and Tiedeman, 2007).

Four parameters with low sensitivities (Ksilts, Ksdfm, Ksdm, and SSall) were assigned values from the updated regional model (table 7). Parameters Ka2a1 and effective porosity were also specified (table 7). The value calculated by nonlinear regression for Ka2a1, which represented alternating silt, clay, and sand sediments, was considered unreasonably high for fine-grain material. Instead, it was given a specified value of 5.0 ft/d, similar to the value that was calculated by nonlinear regression for the fine-grain piedmont-slope sediments, Kpdmt (table 7). The effective porosity value calculated by nonlinear regression was 0.19. An estimate of effective porosity based on slug-test results and reported by Ellinger (2013) was 0.27 (table 4). Values of porosity from laboratory measurements reported by Bexfield and others (2011) and Ellinger (2013) ranged from 0.30 to 0.40 (table 4). As a compromise between values from field measurements and from the nonlinear regression, an effective porosity of 0.25 was specified in the local-scale model (table 7). A sensitivity analysis of the effects of a range in effective porosity values on simulation results is presented in the subsequent section "Delineation of Transient Areas Contributing Recharge and Zones of Contribution to Selected Water-Supply Wells."

Optimal values for the remaining six hydraulic parameters (Ksdmc, Kmult, Kpdmt, HANIyes, VANIyes, and SY) that were estimated by using nonlinear regression (table 7) are similar to values reported by other authors (table 4). The calibration results of the local-scale model and updated regional model are not directly comparable because of design changes and the difference in the number and type of observations. However, three of the five parameters that are common to both the local-scale model and the updated regional model (Ksdmc, Kpdmt, and HANIyes) have similar values. For the other two parameters common to both the local-scale model and the updated regional model, the optimal value for VANIyes increased from 132 to 241, and the optimal value for SY decreased from 0.20 to 0.14. This lower SY value is within the range of values (0.12–0.15) simulated by

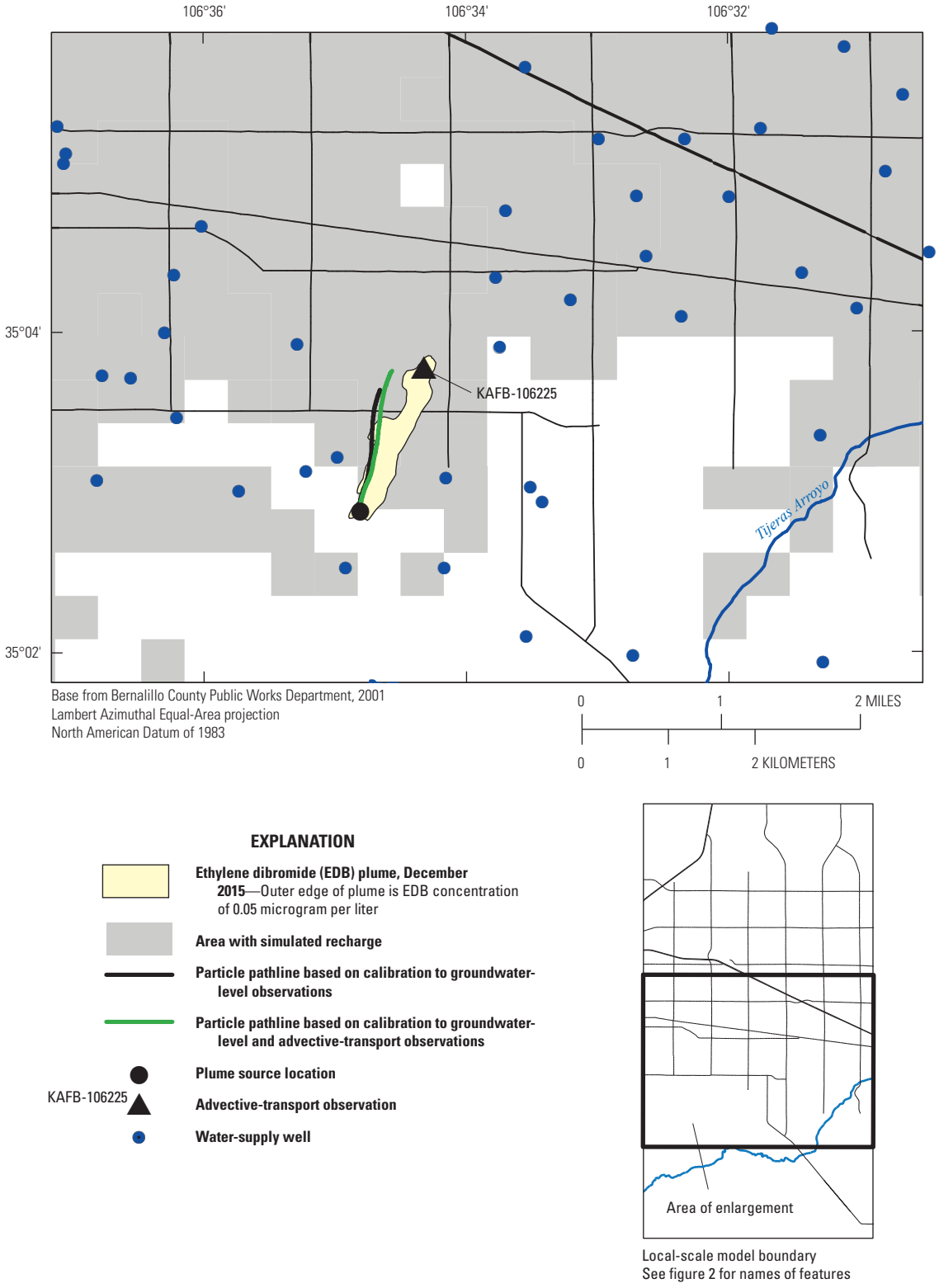

Figure 13. Plume source location and advective-transport observation for the ethylene dibromide (EDB) plume. Predicted particle pathlines are based on parameter values determined by local-scale model calibration using groundwater-level observations alone and a combination of groundwater-level and advective-transport observations. EDB plume from U.S. Army Corps of Engineers (2016c).

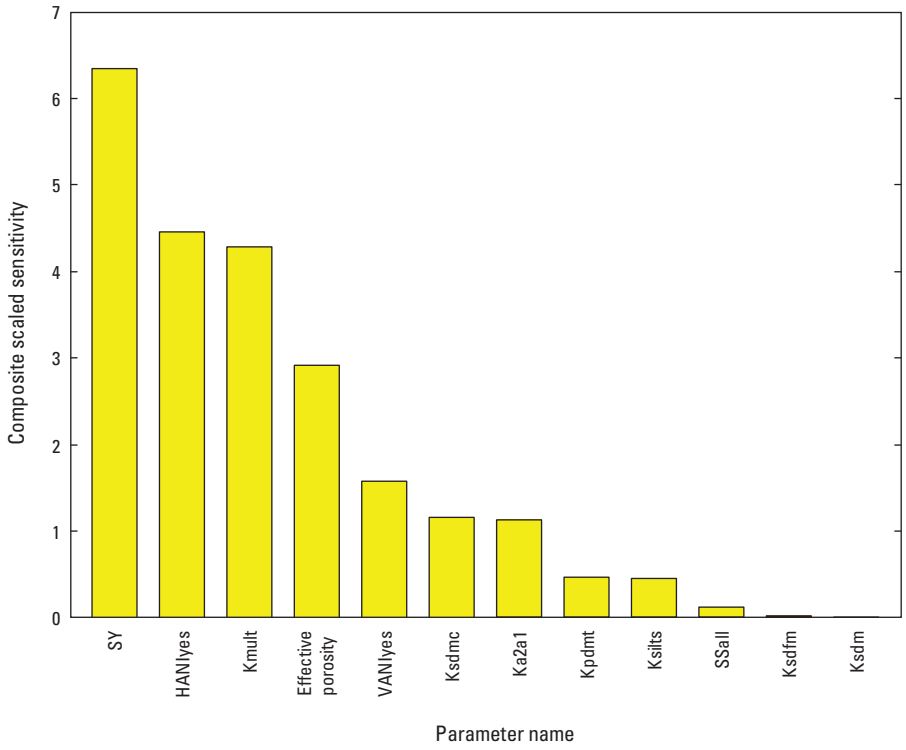

Figure 14. Composite scaled sensitivities of the hydraulic parameters for the local-scale model (table 7).

other groundwater models of the Albuquerque area (Kernodle and others, 1995; Heywood, 2013). Finally, the Kmult value is 0.97 times the interpolated values from the hydraulic conductivity contours (fig. 5).

The uncertainty of the parameter estimate is indicated by the 95-percent confidence interval for each optimal value (table 7). For these linear confidence intervals to be valid, weighted residuals should be normally distributed and the model linear near the estimated optimal values (Hill and Tiedeman, 2007). If weighted residuals are independent and normally distributed, then they plot on an approximately straight line on a normal probability graph. The correlation between weighted residuals and the normal order statistics for the calibrated model was 0.81. This value is less than the critical value for 296 observations, 0.989, at the 5-percent significance level. The degree of model linearity can be quantified by using the modified Beale's measure, calculated with the Model-Linearity program (Poeter and others, 2005). The model is considered effectively linear if the modified Beale's measure is less than 0.041 and nonlinear if it is more than 0.46. The modified Beale's measure for the model was 0.60, indicating that the model is nonlinear. The confidence intervals listed in table 7 are thus approximate values.

The 95-percent confidence intervals for the parameter estimates (table 7) are all within the ranges of reasonable values reported in the literature (table 4). A comparison of the relative precision of different parameter estimates can be made by using the coefficient of variation (standard deviation of the estimated value divided by the optimal value; table 7); a smaller coefficient of variation indicates a more precisely estimated value for the parameter. The coefficients of variation ranged from 0.05 to 1.06 (table 7). Parameter SY was the most precisely estimated, whereas parameter Kpdmt was the least precisely estimated. The order of the most to least precisely estimated parameter values generally follows the same order as that of the parameter sensitivities (fig. 14) because of the information provided by the observations in the regression.

Comparison of Observations and Simulated Equivalents

The quality of model calibration can be determined by comparison of the observations and the simulated equivalents, both numerically and graphically. Residuals should be randomly distributed and close to zero. The average weighted residual was 0.17 ft for all groundwater-level and advective-transport observations. The sum of square weighted residuals was 1,880 for the calibrated local-scale model. The calculated error variance (sum of square weighted residuals divided by the difference between the number of observations and the number of parameters estimated by nonlinear regression) was 6.48, and the standard error of the regression (square root of the calculated error variance) was 2.55. Although these measures of the overall magnitude of the weighted residuals should, theoretically, equal 1, that is not commonly the case for groundwater models (Hill and Tiedeman, 2007).

A comparison of observed and simulated groundwater-level values (fig. 15*A*) indicates a good agreement; the correlation between them was 0.99. The residuals (difference between observed and simulated values) are generally randomly distributed around zero for most simulated values (fig. 15*B*).

Hydrographs of observed water levels and their simulated equivalents from selected observation wells from different locations in the local-scale model indicate the quality of model calibration (fig. 16; locations shown in fig. 12). Observation well SD-2, in the south-central part of the local-scale model near the EDB plume, is screened over a relatively long interval from 494 to 1,000 ft below land surface. Observed and simulated water levels are generally in good agreement and show the long-term water-level decline from pumping withdrawals during the period of record from 1949 to 1988 (fig. 16*A*).

The Sister Cities (SC) observation-well cluster, in the north part of the local-scale model (figs. 2 and 12), has two wells with 5-ft-long screens with the midpoint of the screen for SC-2 at 791.5 ft below land surface and the midpoint of the screen for SC-1 at 1,300.5 ft below land surface (U.S. Geological Survey, 2015). The hydrographs show a long-term decline in water levels until about 2009, when water levels begin to rise because of decreased groundwater withdrawals (fig. 16*B*). Short-term seasonal water-level fluctuations reflect seasonal pumping demands. Simulated water levels from SC-1 adequately represent observed water levels (fig. 16*B*). Simulated water levels from SC-2 reflect the long-term trend and seasonal fluctuations of observed water levels but overestimate drawdowns in this part of the aquifer (fig. 16*C*).

The Jerry Cline (JC) observation well cluster, in the central part of the local-scale model (fig. 2), has three wells. One well, JC-3, has a 100-ft-long screen, extending from 400 to 500 ft below land surface, that intersects the water table (U.S. Geological Survey, 2015). The other two wells, JC-2 and JC-1, have 10-ft-long screens with the midpoints of the screens at 1,035 and 1,440 ft, respectively, below land surface (U.S. Geological Survey, 2015). Although other observation wells show water-level changes in southeastern Albuquerque (Galanter and Curry, 2019), the JC observation-well cluster was selected for comparison to simulated water levels because it is the closest observation well to the area of large simulated drawdowns caused by groundwater withdrawals (figs. 7 and 12). Observed and simulated water levels at JC show the water-level rise since 2009 from decreased groundwater withdrawals (fig. 16*D–F*). Simulated water levels reflect reasonably well the long-term observed trends and magnitude of seasonal fluctuations for JC-3 (fig. 16*F*) and JC-2 (fig. 16*E*), although drawdowns in some cases are overestimated in JC-3 and underestimated in JC-2. In the deep part of the aquifer at this observation nest (JC-1), drawdowns are underestimated (fig. 16*D*) and have the largest negative water-level residuals (−12.5 to −16.3 ft) in the calibration (fig. 15*B,* points that cluster around 4,860 ft).

A simulated groundwater-flow path originating at the EDB plume source was compared to the mapped EDB plume extent for calibration of advective transport. Particle tracks resulting from calibrations for two scenarios, one with only groundwater-level observations and one with groundwater levels and the advective-transport observations, are shown in figure 13. The two calibrations resulted in similar optimal parameter values except for Kmult, which increased from 0.64 to 0.97 by incorporating the advective-transport observation in the regression. Including the advective-transport observation in the calibration decreased the distance between the observation and its simulated equivalent from 1,830 to 1,220 ft, or by 610 ft. For both calibrations, the simulated flow paths are in a more northward direction than the mapped extent of the EDB plume and the advective-transport observation, although, by incorporating this observation into the calibration, the direction of the particle flow path shows a slight improvement by tracking in a more northeastward direction. To improve the simulated EDB plume path in the regression while also preserving the quality of fit to the groundwater-level observations, a more complex aquifer representation and other design changes might be needed. For example, because of the steep hydraulic gradients caused by large nearby pumping withdrawals, shorter stress periods with pumping rates averaged over shorter periods than those used in the updated regional and local-scale models might improve simulated flow paths.

The analysis of the residuals and optimal parameter values indicated that the local-scale model is acceptable for the purposes of the study. Model-fit statistics indicated that simulated values are generally close to observed values. Optimal parameter values are realistic, and their confidence intervals include reasonable values.

Local-Scale and Updated Regional Model Modifications for a Future Pumping Scenario

To delineate future potential recharge sources and groundwater-flow paths, ACRs and ZOCs were delineated for selected wells on the basis of a future pumping scenario for Water Authority water-supply wells and KAFB extraction wells. The calibrated local-scale and updated regional models were modified to incorporate 37 additional years from November 2013 to October 2050 to simulate groundwater flow for a potential future pumping scenario. ACRs and ZOCs to selected wells were determined for water withdrawn in October 2050. This simulation incorporates existing and planned extraction-well pumping in the EDB plume that was implemented beginning in 2015.

Except for groundwater withdrawals from the Water Authority, VAH, and KAFB high-capacity water-supply wells, the same boundary conditions used to represent recharge to and discharge from the aquifer during the last two stress periods of the calibrated models were used to extend model simulations to 2050. The models were extended by 37 winter

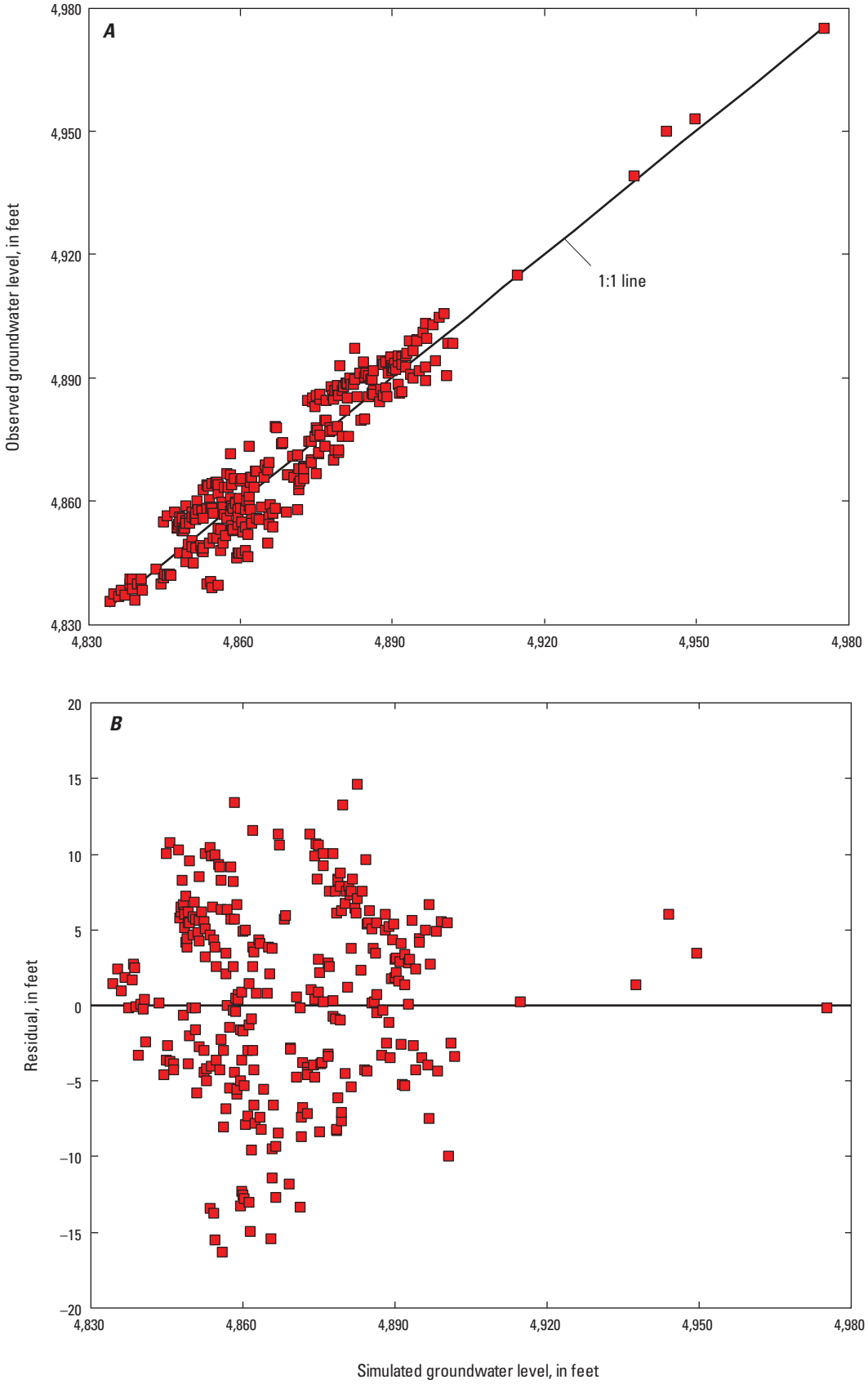

Figure 15. Relations of *A*, observed to simulated groundwater levels and *B*, residual to simulated groundwater levels.

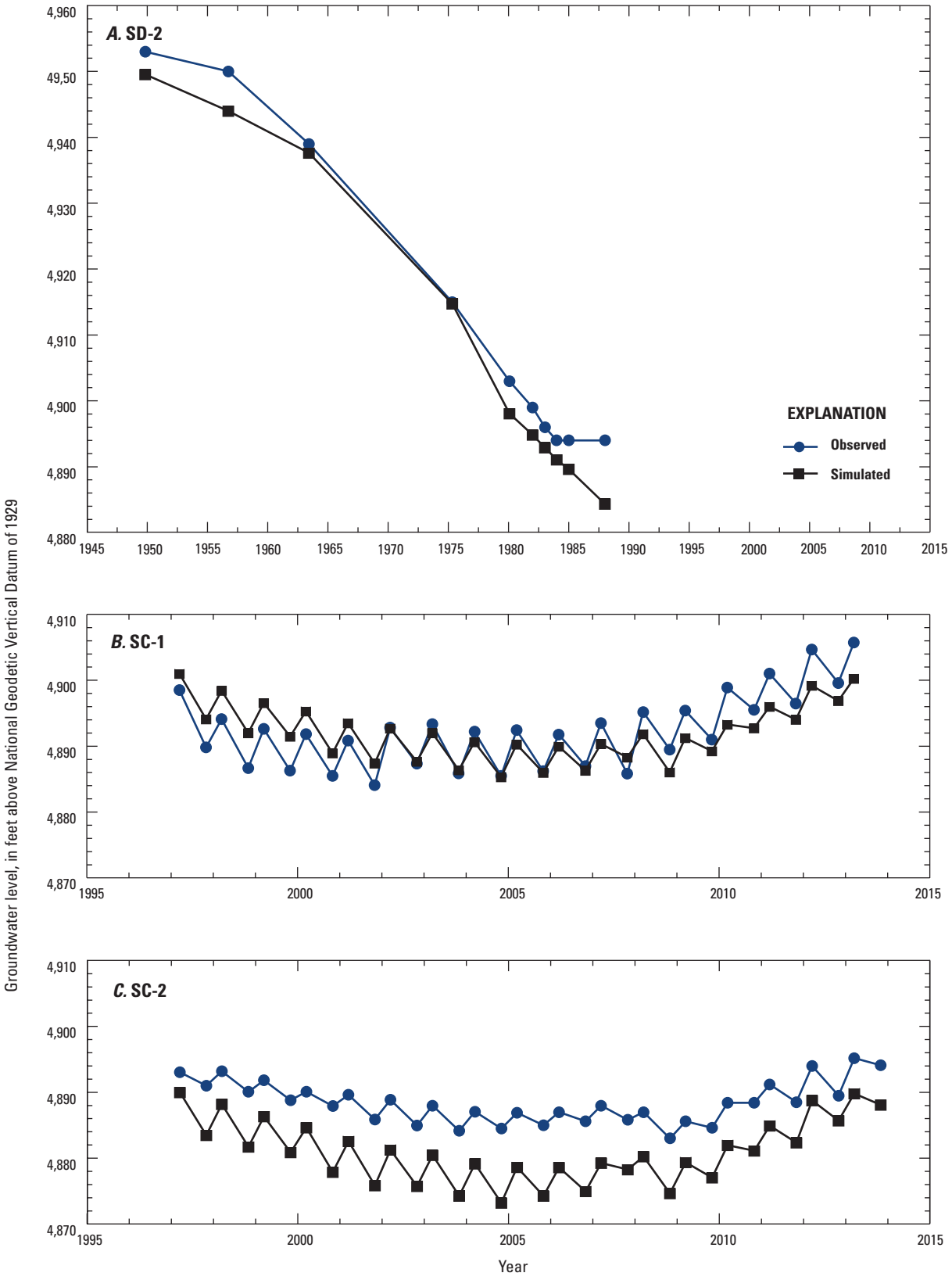

Figure 16. Observed and simulated groundwater levels for observation wells *A*, SD-2; *B*, SC-1; *C*, SC-2; *D*, JC-1; *E*, JC-2; and *F*, JC-3. Locations of observation wells shown in figure 12. Observed data from U.S. Geological Survey (2015).

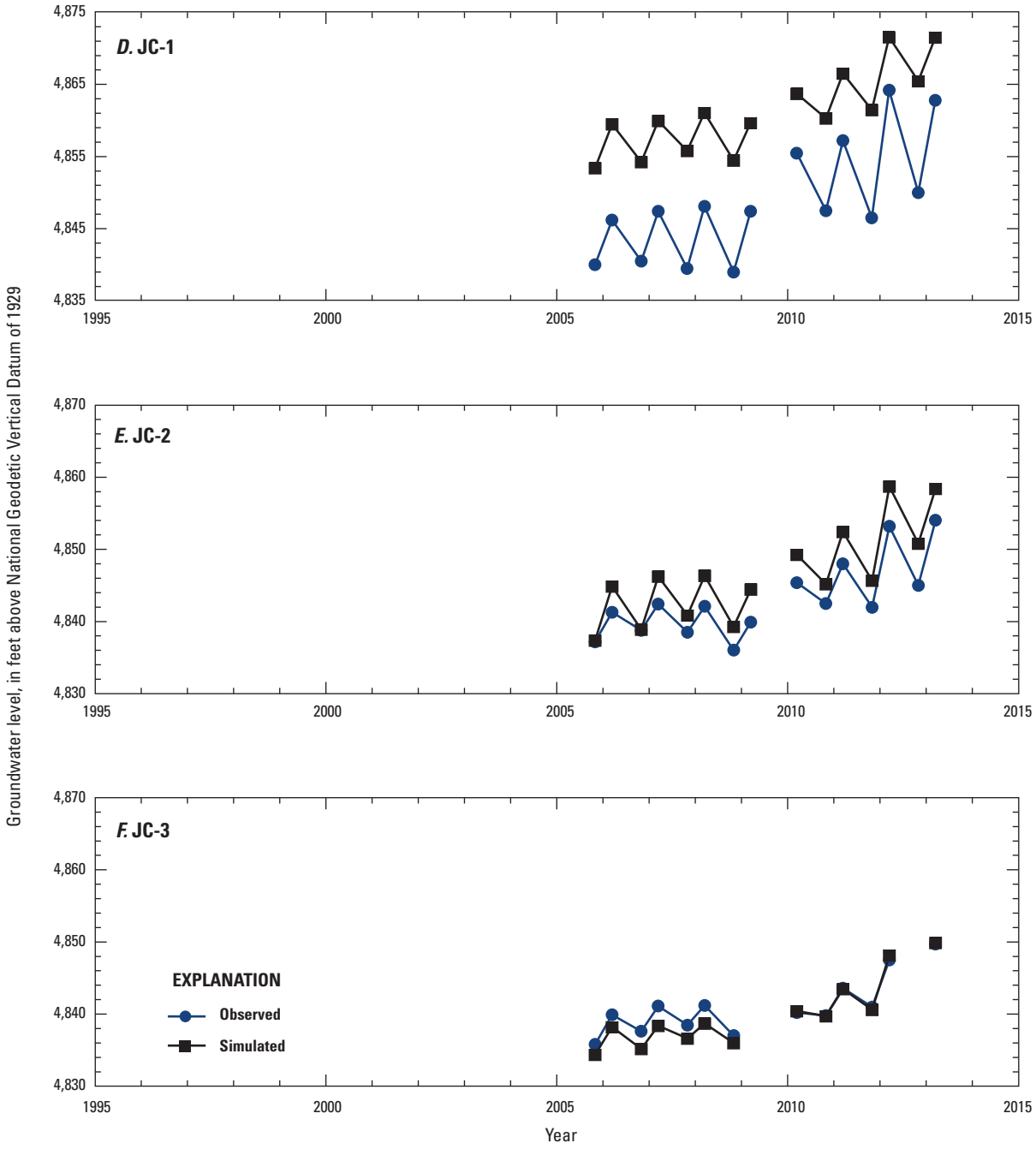

Figure 16. Observed and simulated groundwater levels for observation wells *A*, SD-2; *B*, SC-1; *C*, SC-2; *D*, JC-1; *E*, JC-2; and *F*, JC-3. Locations of observation wells shown in figure 12. Observed data from U.S. Geological Survey (2015).—Continued

seasons (November 1 to March 15) and 37 irrigation seasons (March 16 to October 31) for a total of 153 stress periods from predevelopment to 2050. The future projection assumes no changes of land use and no changes in recharge or discharge resulting from climate change.

For the Water Authority water-supply wells, projected pumping rates were based on reported winter- and irrigation-season pumping rates for November 1, 2013, to October 31, 2015, and on the Water Authority's "medium demand, medium supply" pumping scenario (Albuquerque Bernalillo County Water Utility Authority, 2016) for November 1, 2015, to October 31, 2050. Annual pumping amounts for the entire water system from the Albuquerque Bernalillo County Water Utility Authority (2016) "medium demand, medium supply" scenario were distributed to individual Water Authority water-supply wells on the basis of November 2009 through October 2010 reported monthly pumping data for each well. Monthly pumping values for November 2009 through October 2010 that were zero were replaced with reported monthly pumping values for November 2011 through October 2012. For each well, the winter-season pumping rate was determined by summing the November 1, 2009, through March 15, 2010, monthly pumping values and dividing by the number of days in the time period. Similarly, the irrigation-season pumping rate was determined by summing the March 16 through October 31, 2010, monthly pumping values and dividing by the number of days. The fraction of total Water Authority pumping that each well pumped for the November 2009 through October 2010 winter and irrigation seasons was determined by dividing each well's winter- and irrigation-season pumping rate by the total Water Authority pumping rate. Finally, the annual "medium demand, medium supply" (Albuquerque Bernalillo County Water Utility Authority, 2016) pumping amounts were divided by the number of days in the winter or irrigation seasons (to determine a pumping rate) and multiplied by the winter or irrigation fraction for each well to determine the projected winter- and irrigation-season pumping rates for each model stress period through 2050. The winter-season pumping rate was determined by using the annual pumping rate for the year when the winter season begins. For example, the 2016 winter-season pumping rate was determined by using the 2016 annual pumping rate for each well.

Projected groundwater withdrawals for a winter season and for an irrigation season were available from the VAH (Juliana Hankins, U.S. Department of Veterans Affairs hospital, written commun., 2014) for its water-supply well. Projected withdrawals for the VH-2 well were applied to all winter and irrigation seasons from November 1, 2015, to October 31, 2050.

Projections of groundwater withdrawals from the KAFB wells were not available. Instead, for most of the KAFB wells, pumping rates from the last two stress periods of the calibrated models were used to populate the winter and irrigation seasons from 2015 to 2050. For two of the KAFB wells, which had minimal pumping rates in the last two stress periods, the winter and irrigation seasons ending in 2012 were used instead to populate the projected pumping rates.

Remediation of the EDB plume includes ongoing operation of four existing extraction wells and the installation of additional extraction wells (U.S. Army Corps of Engineers, 2016b). Although the total number of extraction wells has not yet (2019) been finalized, the treatment facility to which the extracted groundwater is pumped has the capacity to treat up to 800 gallons per minute (gal/min) (New Mexico Environment Department, 2017). Extraction wells (fig. 17) are simulated as being screened in local-scale model layer 3 (containing the water table). Extraction-well pumping was simulated beginning in the 2015 irrigation season with one well withdrawing 100 gal/min, two additional wells in the subsequent winter season each withdrawing 100 gal/min, and one additional well in the 2017 irrigation season withdrawing 100 gal/min. Because the exact location and timing of future extraction wells are unknown, one additional well was simulated in the local-scale model (fig. 17) near the BFF beginning in 2018 at 100 gal/min and then increased by 100 gal/min each year until 2021 for a maximum rate of 400 gal/min from this simulated well. From 2021 through 2050, a total rate of 800 gal/min of groundwater withdrawal was simulated for five extraction wells.

After water withdrawn by the extraction wells is treated, it is pumped to well K-7 (fig. 17), which is simulated in the model as an injection well during the winter seasons. During the irrigation seasons, water from the extraction wells is used to irrigate the KAFB golf course located in the southeastern part of the local-scale model (fig. 2). It was assumed that water for irrigation at the golf course is consumed through evaporation and evapotranspiration and therefore no groundwater recharge will occur.

Limitations of Analysis

The analysis presented in this report is based on the local-scale model, which was designed to simulate the response of the groundwater system to pumping stresses and advective groundwater flow to delineate ACRs and the areal extent of ZOCs to selected water-supply wells in southeastern Albuquerque. Because no model can perfectly represent every nuance of an aquifer system, characteristics of the aquifer were necessarily simplified. Spatial resolution of simulation results was limited by the areal extent and thickness of local-scale model cells. The revised local-scale model was assumed to represent the aquifer adequately because the spatial distribution of hydraulic conductivity and other hydraulic properties was based on an understanding of the depositional history of the basin-fill sediments and field data such as aquifer-test results and geophysical and lithologic logs. Simplification included consolidating parameters that represent hydraulic properties into homogenous units and assigning these parameters to groups of local-scale model cells. Although effective porosity probably varies throughout

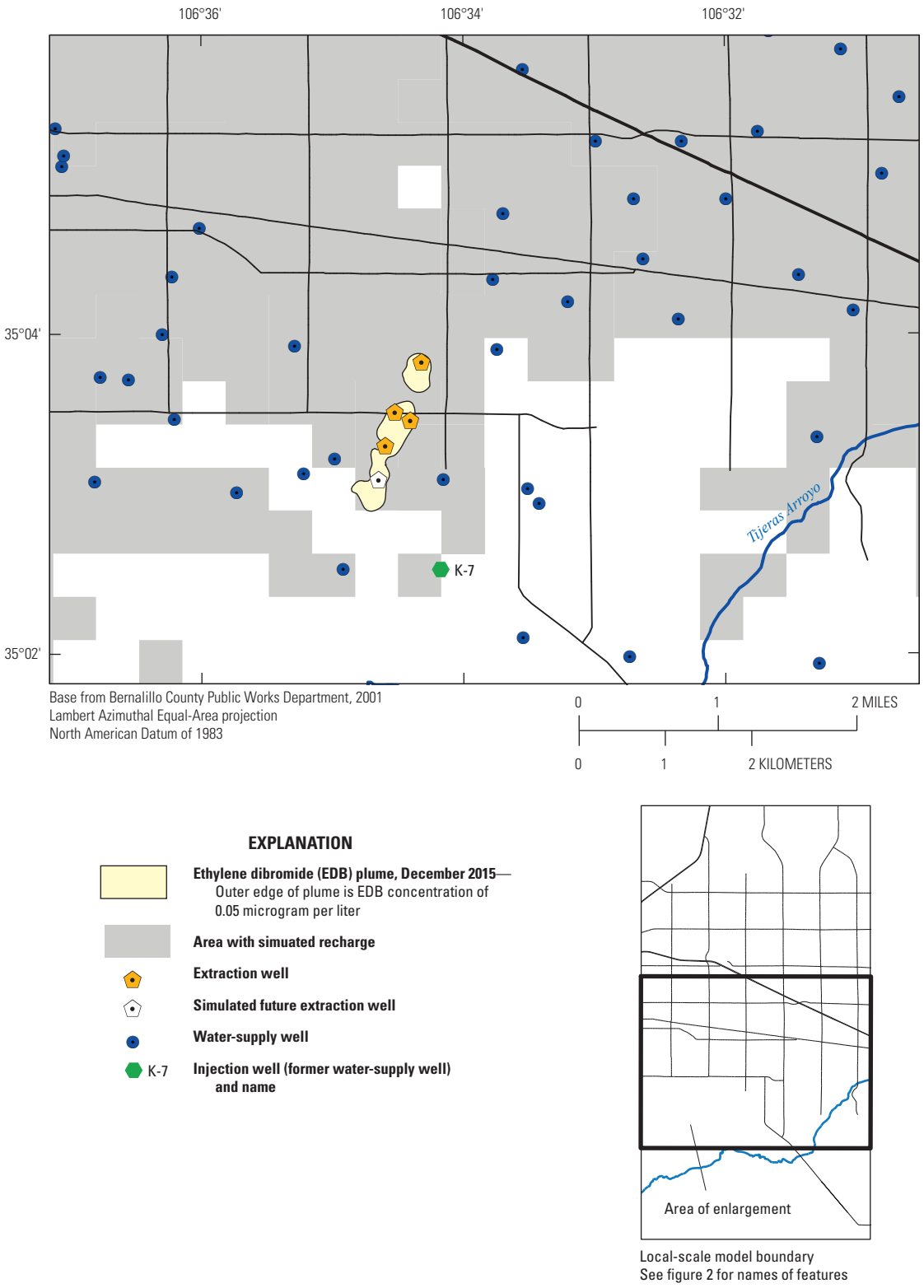

Figure 17. Locations of existing and simulated extraction, water-supply, and injection wells that were included in the historical and future pumping model scenarios. Ethylene dibromide (EDB) plume from U.S. Army Corps of Engineers (2017b).

the study area, a plausible but uniform value of effective porosity, which is important for transport, especially in this setting with the proximity of the water-supply wells to the EDB plume, was used throughout this complex aquifer. In addition, although the vertical placement of the well screens in the local-scale model was revised because of the vertical refinement of updated regional model layers, the spatial extent of other stresses, such as recharge, in the local-scale model was inherited from the grid size of the updated regional model. In particular, simulated recharge from water-distribution and sewage-collection systems may be spread over a larger area in the local-scale model than in reality because these leaks would occur along linear networks of pipes.

Calibration of the local-scale model by inverse modeling by nonlinear regression provided an optimal set of hydraulic parameter values. This optimal parameter set was estimated by minimizing the residuals between the observation dataset and simulated values. Parameter values are reasonable and consistent with previous investigations. However, calibrated values are unique to this model design, which includes boundary conditions that were specified in both the local-scale model and the updated regional model.

The volume of inflow from the updated regional model to the local-scale model along the local-scale model boundaries is a source of uncertainty. The updated regional model was calibrated by using parameter estimation by Bexfield and others (2011) using the best available information, but changes to parameters in the local-scale model were not extended into the updated regional model. If local-scale model parameter changes were extended into the updated regional model, the groundwater flow field and the flux of water at the boundary between the updated regional model and the local-scale model could be different than simulated. Uncertainty in boundary fluxes and the flow field could be simulated in future modeling work to evaluate the uncertainty in the ACRs and ZOCs presented in this report. In addition, although pumping rates were specified in model simulations, an uncertainty analysis of pumping, especially future pumping, would help evaluate the uncertainty in ACRs and ZOCs presented in this report.

ACRs and ZOCs to the water-supply wells were determined in the local-scale model, an urban area where human activities can affect the quality of water withdrawn by the wells. Because groundwater withdrawals greatly exceed available recharge from mostly anthropogenic sources in the local-scale model, most source water to the wells would be expected to originate from outside the local-scale model. Local grid refinement (Mehl and Hill, 2013) in this study uses a "ghost-node" coupling method that allows numerical solution when interface cells of the local-scale and regional models go dry, which would be the case in this setting because of the large groundwater withdrawals since the 1960s that have lowered the water table. Because of the ghost-node coupling method, the transfer of particles between the local-scale and regional models in simulations with the MODPATH particle-tracking program is not supported. Although ACRs and ZOCs to the wells outside the local-scale model were not determined through particle tracking, simulated steady-state groundwater-level contours indicated that source water to the wells from outside the local-scale model would be mostly mountain-front recharge along the eastern side of the Middle Rio Grande Basin or points farther north. Delineation of ACRs and associated ZOCs in the updated regional model to the water-supply wells from mountain-front recharge would have large uncertainties. Because of the distance from these sources to the Albuquerque-Rio Rancho metropolitan area, groundwater traveltimes can be thousands of years (Bexfield and others, 2011). To determine advective transport from recharge sources, as represented by particle pathlines, would require projecting the pre-1900 steady-state simulation, which assumes constant hydrologic conditions into the past, but we do not know how long into the past the simulated steady-state conditions accurately represent hydrologic conditions. To accurately simulate particle pathlines, transient simulations of possibly different recharge conditions over the last several thousand years would be required. This uncertainty in the ACRs and ZOCs also applies to the ZOCs analysis of the wells in the local-scale model from sources outside the local-scale model.

In addition to uncertainties related to past conditions, results of the particle-tracking analysis for future pumping scenarios have uncertainties related to future model-design assumptions. Most land-surface recharge in the local-scale model was from anthropogenic sources, and therefore any land-use changes through the mid-21st century may affect the quantity and distribution of recharge. Four future extraction wells were represented by one simulated well in the general area where they may be installed, and this may affect the groundwater system differently than withdrawals from four separately located wells. The ACR and ZOC analysis of the wells was compared to the EDB plume mapped extent only for December 2015. The size of the EDB plume has enlarged over time, most likely starting with a relatively small extent near the BFF area, from which it expanded by diffusion and advection in response to groundwater flow. Starting in about 1980, the plume probably began expanding to the northeast over time as groundwater transported EDB primarily by advection. The horizontal and vertical extent of the EDB plume over time would have to be known to determine if any particle tracks would have intersected the EDB plume in the past. Similarly, knowledge of the horizontal and vertical extent of the plume in the future would have to be estimated to determine if future particle tracks might intersect the plume. Finally, ACRs and ZOCs to the wells are unique to the simulated pumping rates used for historical pumping conditions and those selected for the future pumping scenario. Any changes in pumping rates, changes in seasonal operations, installation of new water-supply wells, or abandonment of wells most likely would affect groundwater-flow paths and the sizes and locations of the ACRs and ZOCs.

Delineation of Transient Areas Contributing Recharge and Zones of Contribution to Selected Water-Supply Wells

ACRs and ZOCs to selected water-supply wells in southeastern Albuquerque were delineated on the basis of the calibrated local-scale model under simulated historical and potential future pumping conditions by tracking groundwater-flow paths with the MODPATH particle-tracking program. Only those parts of the ACRs and ZOCs to a well within the local-scale model were delineated. Although most recharge to the Middle Rio Grande Basin is from sources outside the local-scale model, some water is recharged from sources within the basin. The quality of water withdrawn from water-supply wells within the updated regional and local-scale models would be sensitive to land uses in the recharge areas. The delineation of ACRs and ZOCs focuses on 11 water-supply wells near the EDB plume: BR-5, K-3, K-7, K-15, K-16, LV-8, RC-2, RC-3, RC-4, RC-5, and VH-2 (fig. 12, table 8).

The ACR to a water-supply well is defined as the surface area at the water table where water entering the groundwater system eventually flows to the well (Reilly and Pollock, 1993) (fig. 18). The ZOC is the three-dimensional volumetric part of the aquifer through which groundwater flows to the well from the ACR (Morrissey, 1989) (fig. 18). ACRs to the 11 water-supply wells were delineated under transient conditions because of changing groundwater-flow patterns caused by changing groundwater withdrawals in the Albuquerque-Rio Rancho metropolitan area since the mid-20th century. Only those areas that receive recharge at the water table can potentially be in the ACRs to a well; simulated sources of recharge and their spatial and temporal distribution in the local-scale model are discussed in the section "Local-Scale Model Inflow and Outflow" and shown in figure 11.

ZOCs were delineated for ACRs to the wells originating in the local-scale model and, in addition, that part of the ZOCs in the local-scale model for ACRs originating in the updated regional model. Because of the relatively long groundwater traveltimes in the aquifer, it was necessary to use simulated steady-state aquifer conditions prior to 1900 to simulate the pre-1900 portions of particle tracks between the water-supply wells and the perimeter of the local-scale model. Groundwater traveltimes from recharge locations along the basin margins to wells in the Middle Rio Grande Basin can be thousands to tens of thousands of years (Bexfield and others, 2011). The steady-state simulation, however, uses the hydrologic conditions of 1900 to simulate particle paths prior to 1900. Because hydrologic conditions hundreds to thousands of years ago likely differed from those of 1900, the simulated pathline locations and ZOCs for times prior to 1900 are uncertain, and that uncertainty increases with increasing time in the past.

In addition to ACRs and ZOCs to water-supply wells for recent withdrawals, an analysis was done for a projected "medium demand, medium supply" pumping scenario (Albuquerque Bernalillo County Water Utility Authority, 2016). Because of decreased groundwater pumping from water-supply wells resulting from increased use of surface water beginning in 2008 and, to a lesser extent, extraction-well pumping in the EDB plume, groundwater-flow patterns would be expected to continue to change and likely will affect the future size, shape, and location of the ACRs and ZOCs to the wells.

Table 8. Simulated water withdrawals from selected wells in the local-scale model.

[Well locations shown on figure 12. –, not applicable]

Well name	Model cells			Simulated pumping rates based on actuals (gallons per minute)	Simulated pumping rates based on projections (gallons per minute)
	Layers	Row	Column	March 16–October 31, 2013 (irrigation season)	March 16–October 31, 2050 (irrigation season)
BR-5	4–15	89	23	960.5	1,085.0
K-3	2–10	89	42	211.9	211.9
K-7	2–11	110	37	345.6	–
K-15	6–18	101	24	[1]142.0	142.0
K-16	6–17	102	37	[1]156.9	156.9
LV-8	6–18	64	44	1,166.3	969.5
RC-2	5–18	81	55	943.7	661.4
RC-3	4–17	85	48	344.8	782.3
RC-4	4–18	77	42	905.7	1,177.2
RC-5	5–18	83	41	1,329.4	948.3
VH-2	4–7	100	27	173.2	285.0

[1]March 16–October 31, 2012, pumping rate.

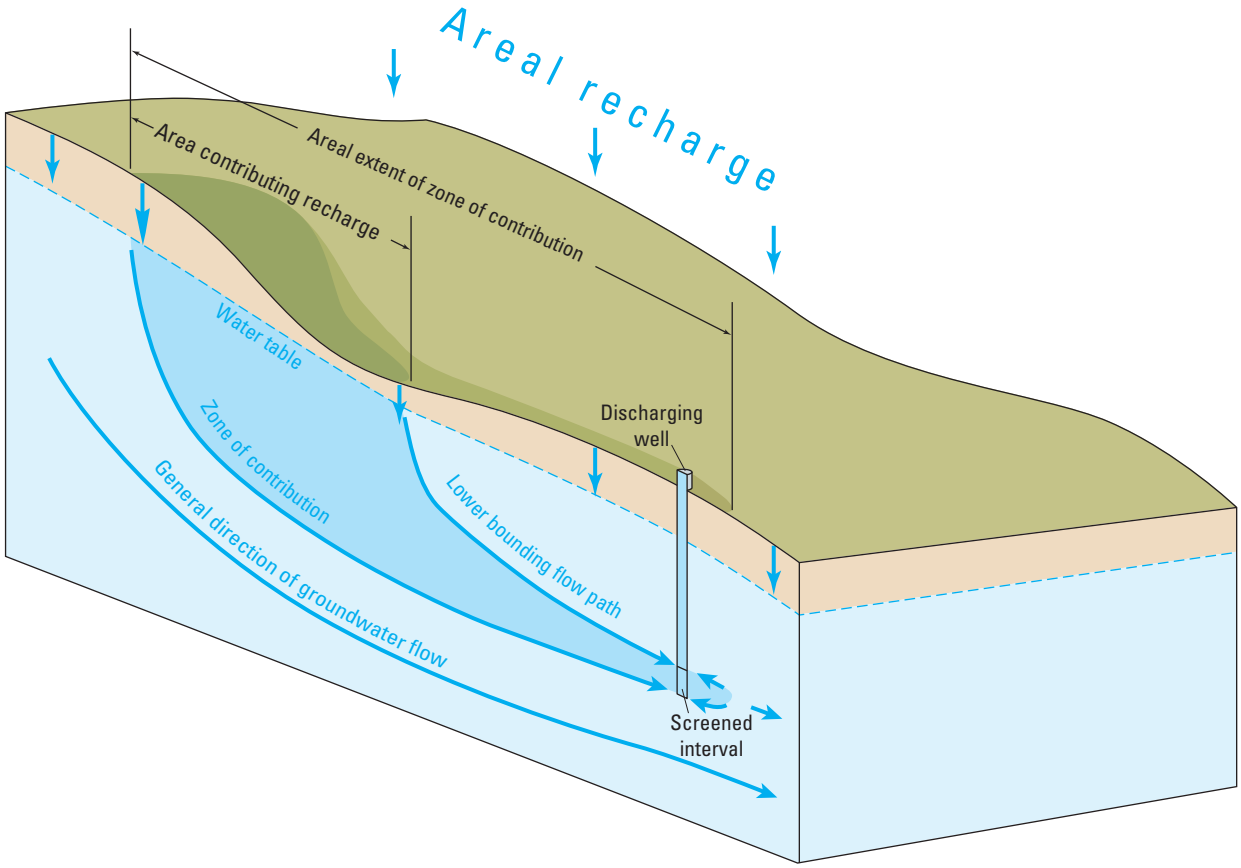

Figure 18. Area contributing recharge and zone of contribution to a single discharging well in a hypothetical groundwater system (modified from Paschke and others, 2007, fig. 1.3).

Historical Pumping Conditions

ACRs and ZOCs to the 11 water-supply wells (BR-5, K-3, K-7, K-15, K-16, LV-8, RC-2, RC-3, RC-4, RC-5, and VH-2) were delineated by tracking particles of water in the direction opposite to groundwater flow, or backwards in time starting from a specified day, from the water-supply wells towards recharge locations. Particles were tracked backwards until they reached their point of origin or until they reached the boundary between the local-scale model and the updated regional model. Figure 19 provides the reader insights into groundwater-flow patterns and traveltimes in the local-scale model. A limited number of particles were tracked backwards along groundwater-flow paths from well RC-4 (fig. 19). Particles tracked backwards from each model cell containing the RC-4 well screen (cells in local-scale model layers 4–18) represent pathlines of water withdrawn by the well on October 31, 2013 (fig. 19). Of the 61 particles used in the analysis, only one followed a path backward from the well to a point of recharge within the local-scale model (fig. 19*A, B,* and *C*, red pathline). The simulated traveltime of the red pathline particle (fig. 19) between the recharge location and the well was 32 years, meaning that the particle recharged at the water table in 1981. The remaining particles follow pathlines that originated outside the local-scale model in, or at the boundary of, the updated regional model.

Simulated particle paths between the northern perimeter of the local-scale model and RC-4 indicate traveltimes ranging from about 300 to 4,800 years with a median of 720 years (Friesz and Myers, 2019). Thus, water withdrawn from RC-4 and other wells in the local-scale model area is a mix of groundwater with a wide range of traveltimes and ages. Particles that follow pathlines in the deeper part of the aquifer, which consists of finer-grain sediments of lower hydraulic conductivity than does the shallow part of the aquifer, have the longest traveltimes. During predevelopment time and before the start of major groundwater withdrawals, particles generally travel horizontally in the aquifer and follow predevelopment flow directions (fig. 19*B* and *C*) from the basin margins toward predevelopment discharge locations along the Rio Grande. Vertical changes of particle paths prior to 1900 (fig. 19*C*) probably are caused by variations in local-scale model hydraulic properties. By the beginning of the transient period in 1900 most particles are near Interstate 40 (fig. 19*A*). Some of the particles travel south of RC-4 during the 1900–2013 transient simulation to near the northern edge of the extent

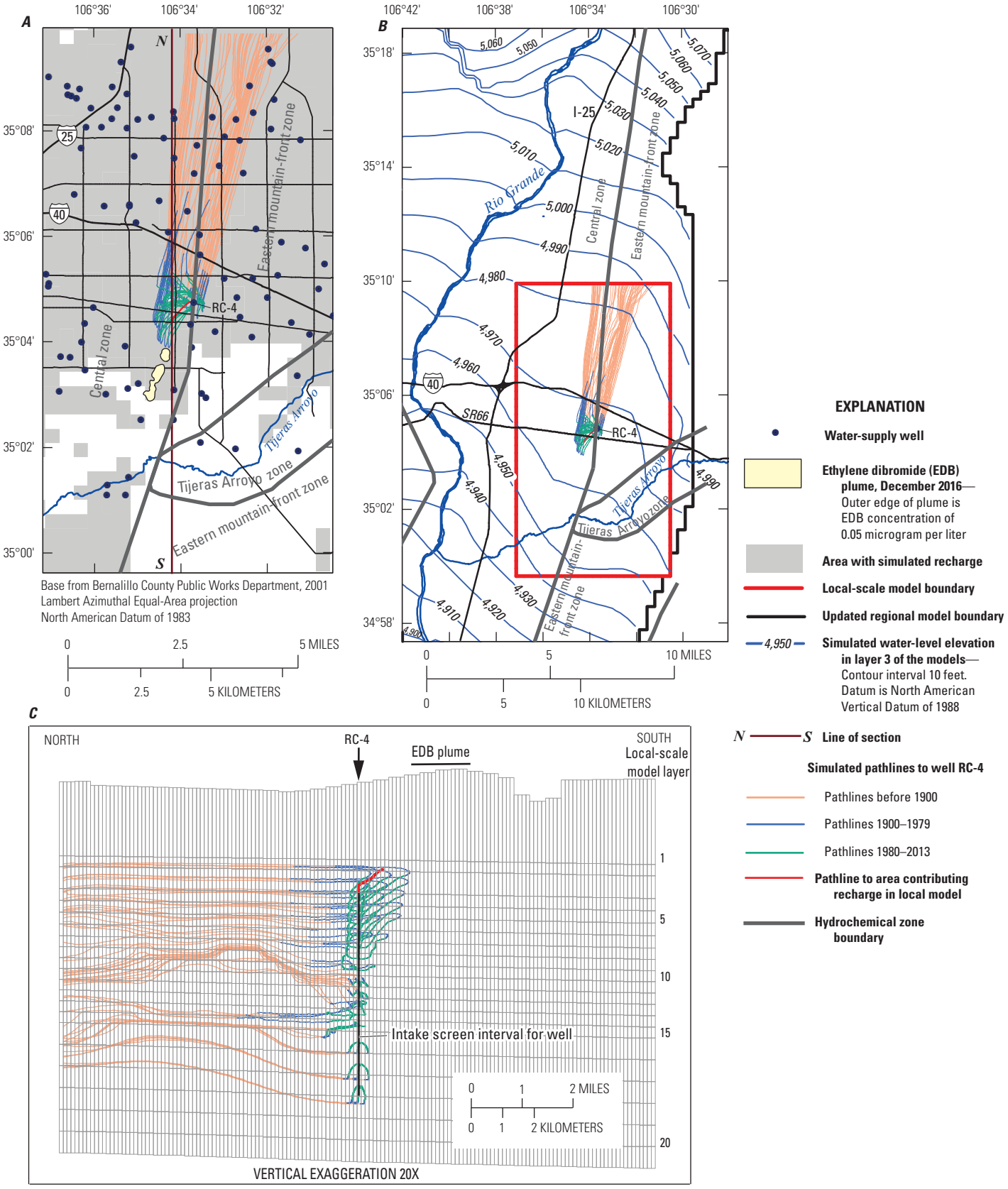

Figure 19. Simulated particle pathlines to water-supply well RC-4 for particles released on October 31, 2013, in *A*, map view, *B*, simulated particle pathlines and predevelopment steady-state water-level contours in layer 3 of the local-scale model and updated regional models, and *C*, cross-section view. Ethylene dibromide plume from U.S. Army Corps of Engineers (2017b). Hydrochemical zones from Plummer and others (2004).

of the EDB plume (as mapped in December 2016) before reversing direction in about 1980. The reversal of particle-movement direction in 1980 corresponds to the reversal of groundwater flow from southwest to northeast that was caused by pumping and development of the large area of water-level drawdown (fig. 7) northeast of the EDB plume. Because movement of EDB northeast of the BFF by groundwater advection, and the reversal in direction of particle movement that occurred at about the same time (1980), none of the particles shown in figure 19 would have interacted with the EDB plume; the particles and EDB would both have moved to the northeast at about the same rate. From about 1980 to October 2013, particles south of RC-4 travel northeasterly (fig. 19*A*), and particles in the shallower model layers move deeper in the aquifer (fig. 19*C*) in response to the declining water table.

Figure 19*B* shows particle pathlines in relation to the local-scale and updated regional models and simulated water-level contours for pre-1900 steady-state conditions. Based on these simulated water-level contours, the source of water to RC-4 originating outside the local-scale model probably is from mountain-front recharge northeast of the local-scale model or from locations farther north. The source of water to RC-4 is consistent with hydrochemical zones (fig. 19*A* and *B*) defined by Plummer and others (2004) using data from water-supply and observation wells. RC-4 is located near the boundary between the eastern mountain-front and central hydrochemical zones and could obtain water from either or both zones.

ACRs and ZOCs to 9 of the 11 water-supply wells within the local-scale model were delineated by releasing particles on October 31, 2013, using pumping rates simulated for the March 16–October 31, 2013, irrigation season (table 8). Because the March 15–October 31, 2013, pumping rates for wells K-15 and K-16 (3.1 and 0 gal/min, respectively, Friesz and Myers, 2019) were much less than for the previous irrigation season, the ACRs and ZOCs for K-15 and K-16 were delineated by releasing particles on October 31, 2012, using the March 16–October 31, 2012, pumping rates (table 8). Withdrawal rates for the 11 wells ranged from about 140 to 1,330 gal/min and averaged 610 gal/min. The ACR analysis was done with a 20 by 20 array of particles applied to each face of each model cell intersected by a well screen. The particles were then tracked backwards along transient flow paths to sources of water in the local-scale model. Of the 11 wells in this analysis, only K-3, K-7, and RC-4 derived a portion of their water from simulated sources in the local-scale model (fig. 20). The ACRs for these three wells extend generally south and southwestward of these three wells, but none overlap the BFF area or the EDB plume as delineated using December 2016 data (U.S. Army Corps of Engineers, 2017b). The southern extent of the ACRs to K-3 and K-7 are most likely affected by the location and timing of simulated recharge from irrigation or water-distribution and sewage-collection systems leakage. Recharging water from nearby sources travels along shallow-depth groundwater-flow paths and discharges to the highest active cell that contains the screens of the three wells. Two of the three wells, K-3 and K-7, which intersect the water table, have the shallowest screens of the 11 wells.

Particles defining ACRs to the three water-supply wells were placed into three groups based on their date of recharge: those that recharged the aquifer before 1980, those that recharged from 1980 to 1990, and those that recharged from 1990 to March 15, 2015 (fig. 20). Groundwater traveltimes generally depend on where recharge enters the aquifer in relation to the well, with water that recharges the aquifer near the wells being the youngest and having the shortest traveltimes. Traveltimes from recharge locations to the three wells ranged from a few months to 64 years. The median traveltimes for K-7, K-3, and RC-4, from water table to the well, were 1.2 years, 9.2 years, and 28.4 years, respectively. These relatively short median traveltimes indicate that the wells are susceptible to contaminants that may be present at the water table. Over the longer term, these traveltimes indicate that the wells could be susceptible to contaminants that may be present at land surface and that move down through the unsaturated zone to the water table. Traveltime from land surface to the water table in the local-scale model area is unknown but would depend on the thickness and properties of the soil and sediment in the unsaturated zone and on the properties of the contaminant (such as its degradation rate, affinity for soil or water, and whether it would be self-mobilizing or have to be mobilized by infiltrating water).

Under steady-state groundwater-flow conditions, effective porosities affect only groundwater velocities, but for transient flow conditions, effective porosities affect both velocities and the trajectory of groundwater-flow paths. As indicated in the "Geologic Framework" section of this report, the upper Santa Fe Group aquifer in the local-scale model area is a heterogeneous mix of fluvial sediments. Groundwater flowing through these sediments would encounter a variety of sediment types and textures having a variety of effective porosities. In general, smaller values of effective porosity correspond to smaller-diameter throats between the pore openings in aquifer material.

The variety of effective porosities presumed to be present in the aquifer was simulated in the local-scale model with the single value (0.25) that represents the average effective porosity. A sensitivity analysis was done to determine the effects of differing effective porosities (0.15 and 0.35) on the ACRs and traveltimes (fig. 21). Smaller values of effective porosity resulted in faster simulated groundwater flow and generally larger ACRs, whereas larger values of effective porosity resulted in slower simulated groundwater flow and generally smaller ACRs. Small or large values of effective porosity affect groundwater-flow velocity in the same way that small or large pipe diameters affect the velocity of water flowing through the pipe. Given the same pressure pushing water through a pipe, water will flow at a higher velocity through a small-diameter pipe than through a large-diameter pipe.

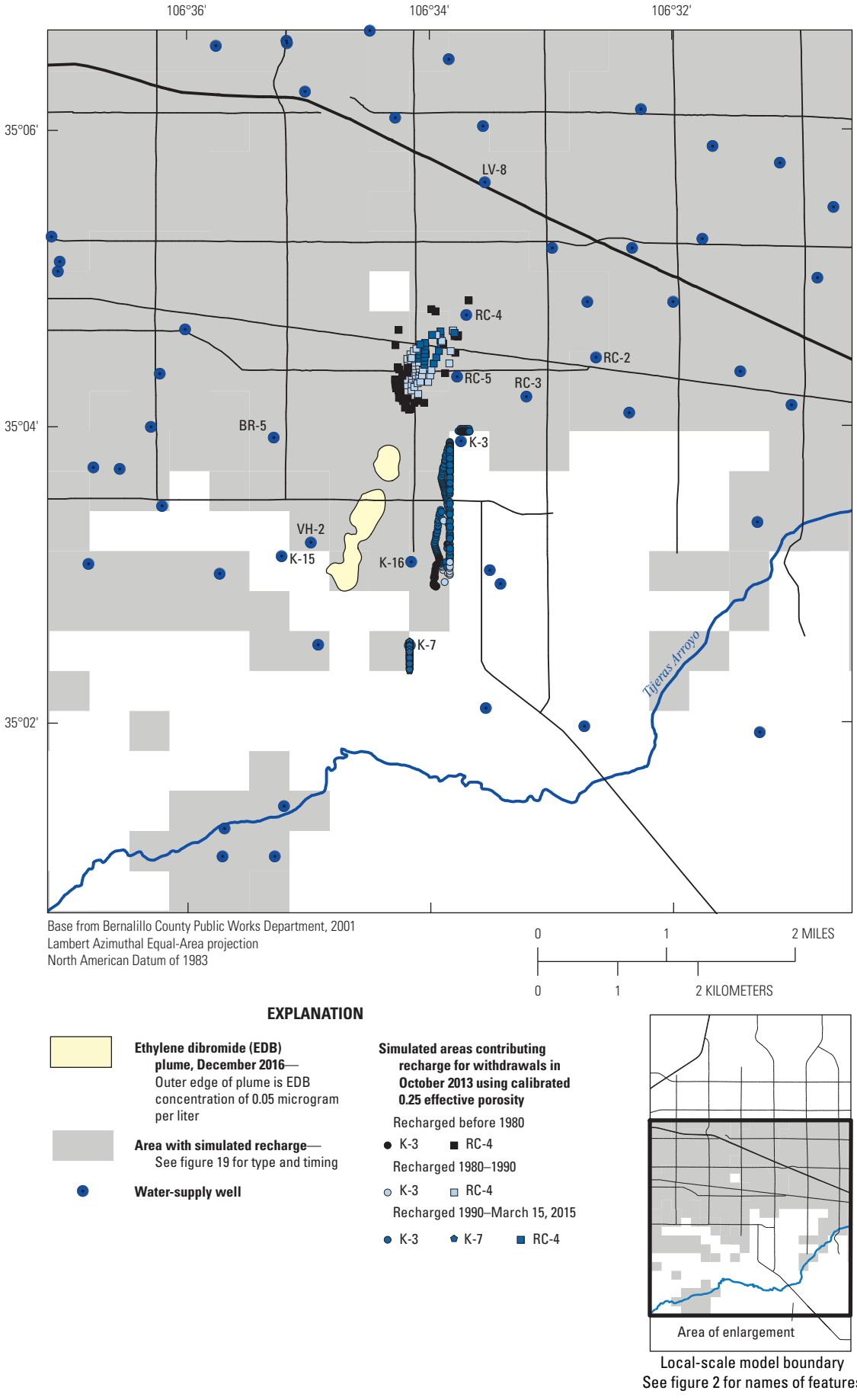

Figure 20. Areas contributing recharge to selected water-supply wells within the local-scale model area. Particles were released on October 31, 2012, for wells K-15 and K-16 and on October 31, 2013, for wells BR-5, K-3, K-7, LV-8, RC-2, RC-3, RC-4, RC-5, and VH-2. Only wells K-3, K-7, and RC-4 had areas contributing recharge within the local-scale model area. Ethylene dibromide plume from U.S. Army Corps of Engineers (2017b).

For two of the three wells (K-3 and RC-4) that have ACRs in the calibrated local-scale model area (fig. 20), an effective porosity of 0.15 increased the size of the ACRs (fig. 21*A*), whereas an effective porosity of 0.35 decreased the size of the ACRs (fig. 21*B*) as compared to an effective porosity of 0.25 in the calibrated model. For the third well, K-7, differences in the size and location of the ACR for different porosities were minimal, and the ACRs were constrained to a nearby recharge location. In the simulation using 0.15 effective porosity the pre-1980 and 1980–90 portions of the ACR for RC-4 are simulated to overlap the December 2016 plume footprint (fig. 21*A*). The footprint of the plume, which is largely unknown between 1980 and about 2007 (when the first monitoring well was drilled northeast of the BFF), would have to be determined to evaluate if the plume would interact with recharging particles in the ACRs. In the 0.15 effective porosity scenario, two additional wells (RC-3 and VH-2; fig. 21*A*) derive part of their water from sources in the local-scale model. The southern extent of the ACR to RC-3 is constrained to local recharge locations, whereas the ACR to VH-2 is a small, isolated area about 2 mi south-southeast of the VH-2 well near Tijeras Arroyo. Although the locations of ACRs are best represented in the local-scale model by using an effective porosity of 0.25, it is possible that sediments with a lower or higher effective porosity may be present along the particle flow paths used to delineate the ACRs for the selected wells.

ZOCs to the 11 water-supply wells were determined by backward tracking of pathlines through the simulated transient and steady-state groundwater-flow system by using the effective porosity of 0.25 from the calibrated local-scale model. The ZOCs analysis was done with a 5 by 5 array of particles applied to each model cell face for cells that contained the well screens. Fewer particles were used in the ZOC analysis than in the ACR analysis because of the increased computer resources required to record the pathlines. Pathlines are tracked to either recharge locations in the local-scale model or to the interface of the regional and local-scale models.

The pathlines composing the ZOCs to the 11 water-supply wells were placed into three groups on the basis of the date represented by each segment of each pathline: segments with dates prior to 1900, segments with dates from 1900 to 1979, and segments with dates from 1980 to 2013 (fig. 22). Because the ZOCs in plan view are the projection of all pathlines over the entire vertical range, the ZOCs of the pathline segment groups overlap. For better visibility, the ZOCs are plotted with the youngest and shallowest group of pathline segments (1980–2013, in green) above the 1900–79 set of pathlines (in blue), which in turn is plotted above the oldest set of pathlines (before 1900, in orange) (fig. 22). In addition, 2008–13 pathline segments with elevations above 4,800 ft are colored yellow to identify pathlines that were shallow enough to interact with EDB if they passed through the BFF area. The 4,800-ft elevation was selected on the basis of the deepest extent of the EDB plume in the BFF area as depicted in a cross section of the EDB plume in U.S. Army Corps of Engineers (2017a, fig. 6-7). The color scheme shows the maximum extent of the 1980–2013 pathlines and, in most cases, the maximum outer limit of the 1900–79 pathlines, but the most recent part of the 1900–79 pathlines is overlain by younger pathlines (fig. 22).

After determining the ZOC by backward tracking of particle pathlines from the well screen to their recharge source, then following particle pathlines forward in time, particles for all 11 wells generally moved southwest from the north and east boundaries of the local-scale model (fig. 22). Because of the southwesterly groundwater flow prior to 1980, many of the particles moved past their target well but then moved back towards their target well after 1980 when the groundwater flow direction changed to the northeast (fig. 22).

The ZOCs for each well generally are consistent with sources of water based on the hydrochemical zones defined by Plummer and others (2004) and described in the "Hydrochemical Zones" section of this report (fig. 22). Particle tracks from wells east of the boundary between the eastern mountain-front and central hydrochemical zones (K-3, RC-2, and RC-3) tended to originate more from the eastern side of the local-scale model. Particle tracks from wells located near or west of the hydrochemical boundary tended to originate from either the northern or eastern (or both) sides of the local-scale model. Particle tracks originating from the eastern side of the local-scale model would most likely have a mountain-front recharge source. Particle tracks originating from farther north might have a Rio Grande or mountain-front source or a mix of water from both sources.

The ZOCs particle-tracking analysis indicated that three of the water-supply wells (RC-5, BR-5, and VH-2) have pathlines from the 1980–2013 transient period that project in plan view with the December 2016 EDB plume footprint (fig. 22*D*, *F*, and *G*). Two wells (BR-5 and VH-2) have pathlines from the 1980–2013 transient period that project in plan view with the BFF (fig. 22*F* and *G*). The areal extent of the EDB plume to the northeast between 1980 and about 2007 is unknown, so it is difficult to determine if 1980–2013 pathlines for wells BR-5, RC-5, and VH-2 would have interacted with the EDB plume. Particles that were north of the BFF when groundwater flow reversed direction from southwest to northeast in 1980 would not have the opportunity to interact with the EDB plume because the particles and the EDB would have both been moving northwest at about the same rate by advective groundwater flow. Thus, particles traveling to RC-5 would not have had the opportunity to interact with the EDB plume. Wells BR-5, K-15, and VH-2, however, did have particles southwest of the BFF in 1980 (fig. 22*F*, *G*, and *J*). Particles traveling to BR-5 passed under the BFF area in the 1980–2013 period, but none of the 1980–2013 pathlines were shallow enough (elevation greater than 4,800 ft) to interact with EDB at the BFF (fig. 22*F*). Particles traveling to K-15 passed very near the BFF in the 1980–2013 period, but none of the 1980–2013 pathlines were shallow enough to interact with EDB at the BFF (fig. 22*J*). In contrast, some of the particles traveling

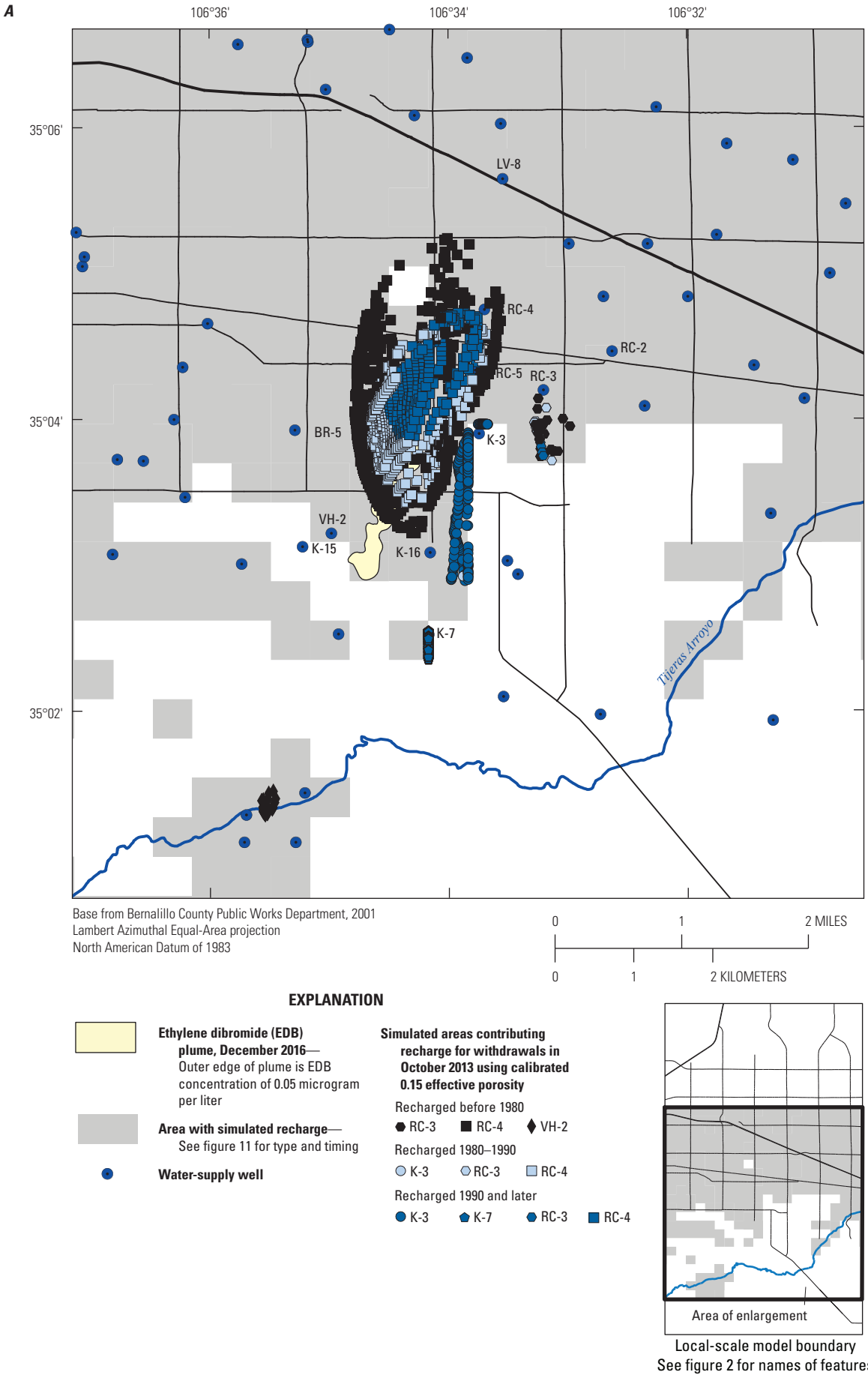

Figure 21. Sensitivity analysis of effective porosities of *A*, 0.15 and *B*, 0.35 on the areas contributing recharge to selected water-supply wells. Particles were released on October 31, 2012, for wells K-15 and K-16 and on October 31, 2013, for wells BR-5, K-3, K-7, LV-8, RC-2, RC-3, RC-4, RC-5, and VH-2. For the 0.15 effective porosity only wells K-3, K-7, RC-3, RC-4, and VH-2 had areas contributing recharge in the local-scale model area, and for the 0.35 effective porosity only wells K-3, K-7, and RC-4 had areas contributing recharge in the local-scale model area. Ethylene dibromide plume from U.S. Army Corps of Engineers (2017b).

B

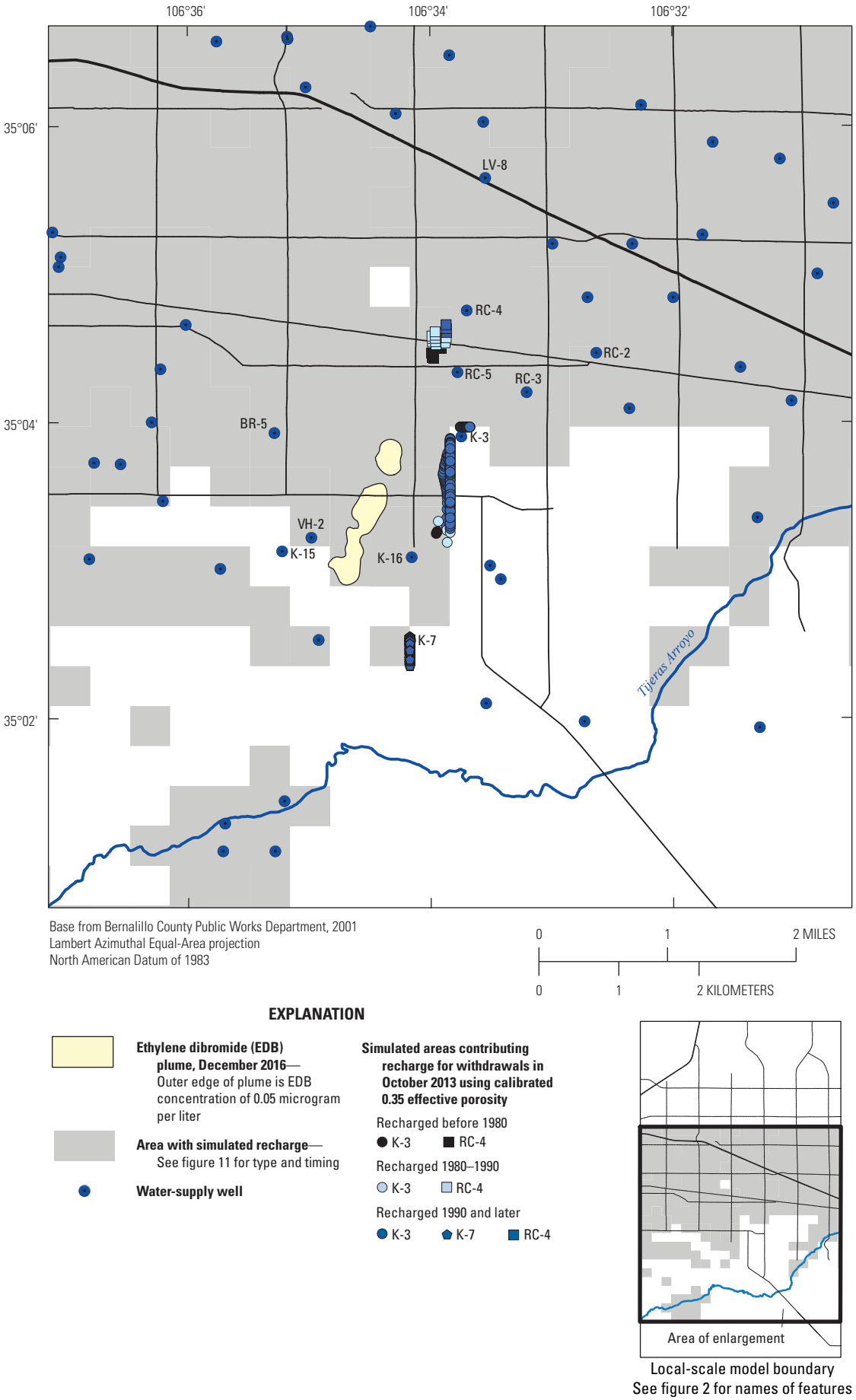

Figure 21. Sensitivity analysis of effective porosities of *A*, 0.15 and *B*, 0.35 on the areas contributing recharge to selected water-supply wells. Particles were released on October 31, 2012, for wells K-15 and K-16 and on October 31, 2013, for wells BR-5, K-3, K-7, LV-8, RC-2, RC-3, RC-4, RC-5, and VH-2. For the 0.15 effective porosity only wells K-3, K-7, RC-3, RC-4, and VH-2 had areas contributing recharge in the local-scale model area, and for the 0.35 effective porosity only wells K-3, K-7, and RC-4 had areas contributing recharge in the local-scale model area. Ethylene dibromide plume from U.S. Army Corps of Engineers (2017b).—Continued

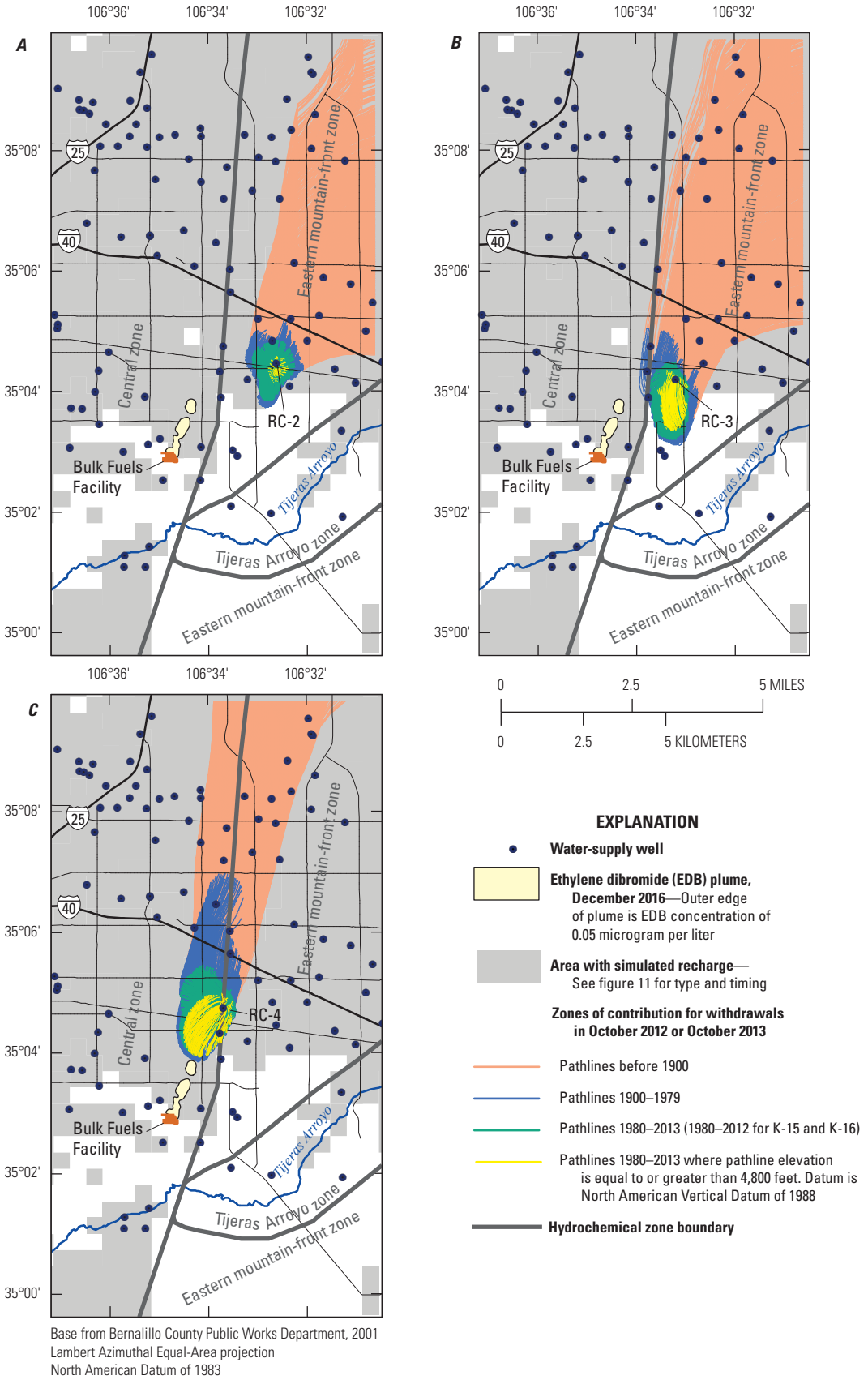

Figure 22. Zones of contribution to selected water-supply wells in the local-scale model area. Particles were released on October 31, 2012, for wells K-15 and K-16 and on October 31, 2013, for wells BR-5, K-3, K-7, LV-8, RC-2, RC-3, RC-4, RC-5, and VH-2. Ethylene dibromide plume from U.S. Army Corps of Engineers (2017b). Hydrochemical zones from Plummer and others (2004). *A*, RC-2. *B*, RC-3. *C*, RC-4. *D*, RC-5. *E*, LV-8. *F*, BR-5. *G*, VH-2. *H*, K-3. *I*, K-7. *J*, K-15. *K*, K-16.

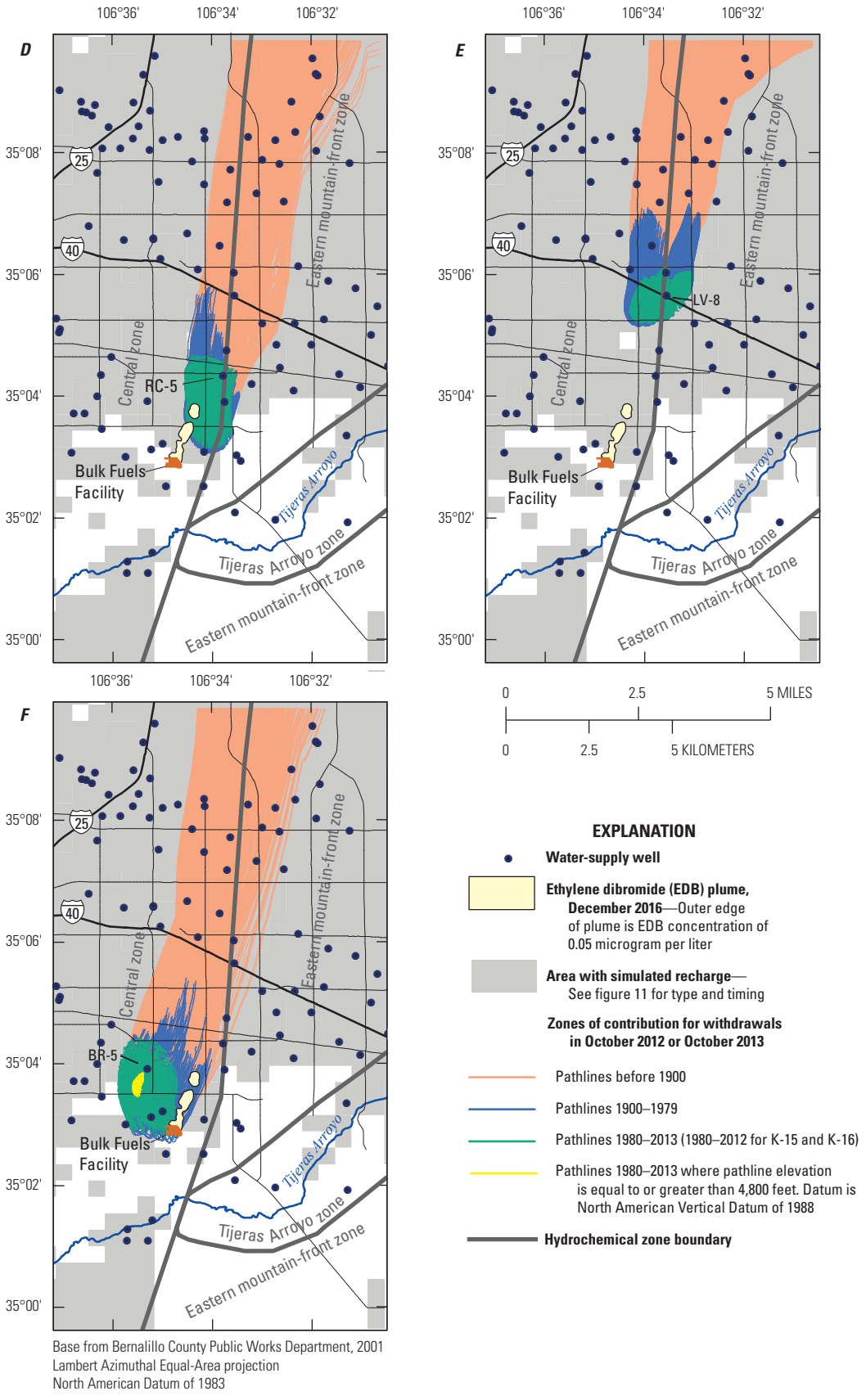

Base from Bernalillo County Public Works Department, 2001
Lambert Azimuthal Equal-Area projection
North American Datum of 1983

Figure 22. Zones of contribution to selected water-supply wells in the local-scale model area. Particles were released on October 31, 2012, for wells K-15 and K-16 and on October 31, 2013, for wells BR-5, K-3, K-7, LV-8, RC-2, RC-3, RC-4, RC-5, and VH-2. Ethylene dibromide plume from U.S. Army Corps of Engineers (2017b). Hydrochemical zones from Plummer and others (2004). *A*, RC-2. *B*, RC-3. *C*, RC-4. *D*, RC-5. *E*, LV-8. *F*, BR-5. *G*, VH-2. *H*, K-3. *I*, K-7. *J*, K-15. *K*, K-16.—Continued

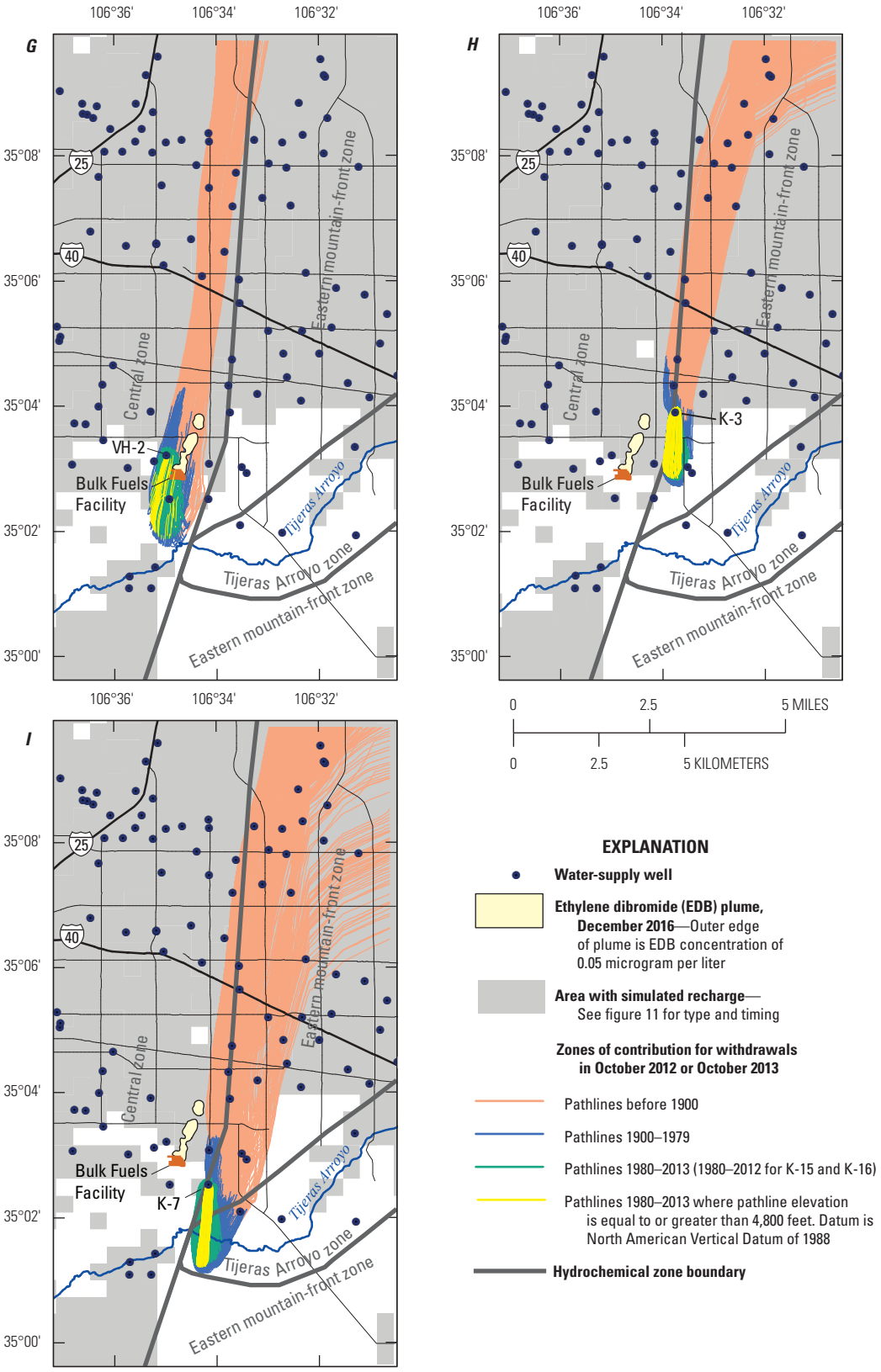

Figure 22. Zones of contribution to selected water-supply wells in the local-scale model area. Particles were released on October 31, 2012, for wells K-15 and K-16 and on October 31, 2013, for wells BR-5, K-3, K-7, LV-8, RC-2, RC-3, RC-4, RC-5, and VH-2. Ethylene dibromide plume from U.S. Army Corps of Engineers (2017b). Hydrochemical zones from Plummer and others (2004). *A*, RC-2. *B*, RC-3. *C*, RC-4. *D*, RC-5. *E*, LV-8. *F*, BR-5. *G*, VH-2. *H*, K-3. *I*, K-7. *J*, K-15. *K*, K-16.—Continued

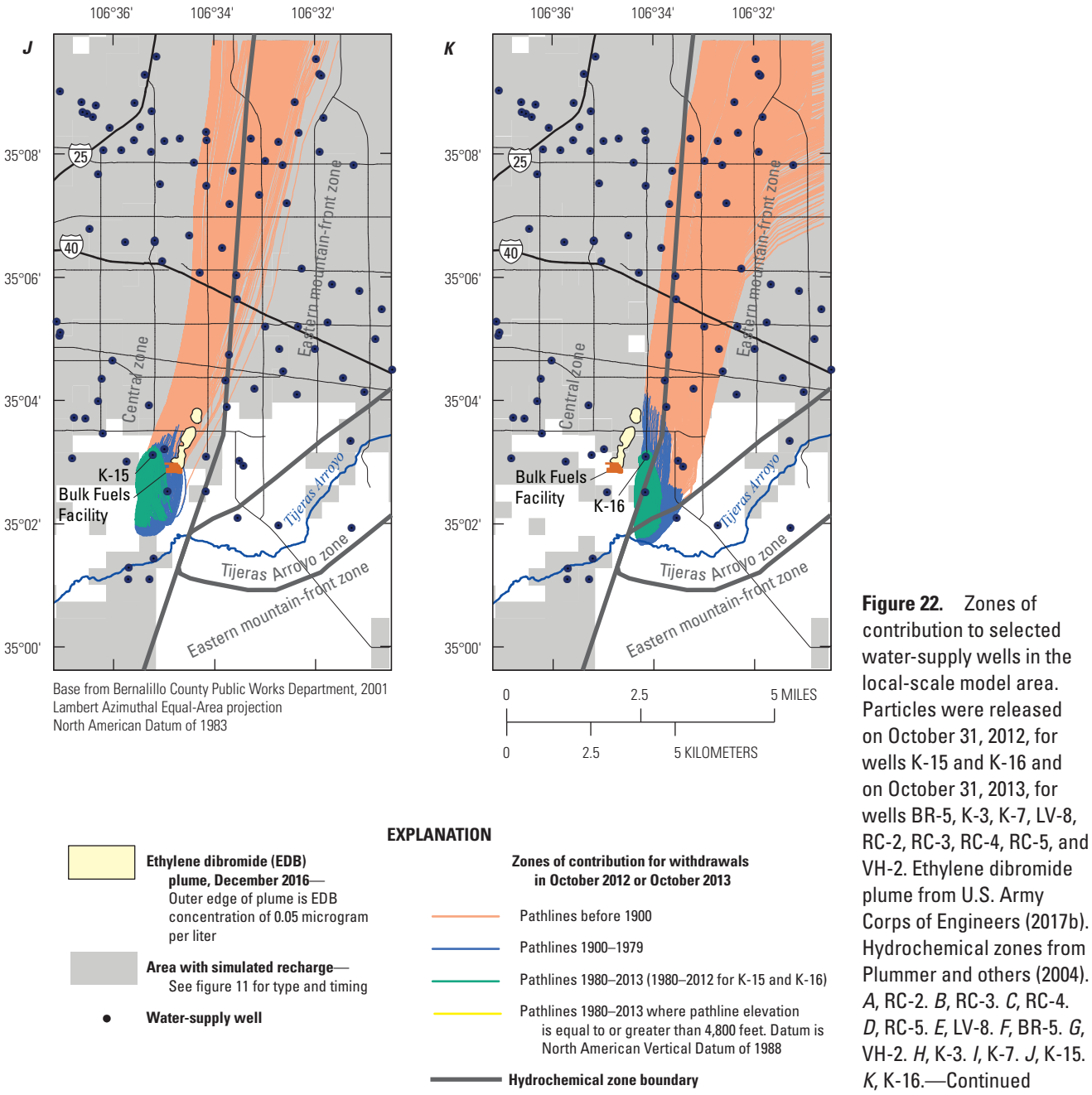

Figure 22. Zones of contribution to selected water-supply wells in the local-scale model area. Particles were released on October 31, 2012, for wells K-15 and K-16 and on October 31, 2013, for wells BR-5, K-3, K-7, LV-8, RC-2, RC-3, RC-4, RC-5, and VH-2. Ethylene dibromide plume from U.S. Army Corps of Engineers (2017b). Hydrochemical zones from Plummer and others (2004). *A*, RC-2. *B*, RC-3. *C*, RC-4. *D*, RC-5. *E*, LV-8. *F*, BR-5. *G*, VH-2. *H*, K-3. *I*, K-7. *J*, K-15. *K*, K-16.—Continued

to VH-2 passed through the BFF area at shallow enough depths to interact with EDB at the BFF in the 1980–2013 period (fig. 22*G*). A model with a smaller cell size and a more detailed aquifer representation may be needed to determine accurately if pathlines for VH-2 may have intersected the EDB plume. It is important to note that the majority of pathlines for VH-2 did not pass through the BFF area at elevations greater than 4,800 ft, indicating that the majority of water produced from the VH-2 well would not have interacted with EDB in the BFF area. EDB has not been detected in water samples collected in 2012 through 2015 from the VH-2 well (U.S. Army Corps of Engineers, 2017a, table 6-6).

The effect of effective porosity on the location and size of the ZOCs to a well was evaluated for RC-5 for simulated effective porosities of 0.15 and 0.35 (fig. 23). Although most pathlines to a well in the local-scale model are likely best represented by an effective porosity of 0.25, effective porosity may be lower and higher in parts of the aquifer. For a decreased uniform effective porosity of 0.15, the size of the areal extent of the ZOCs to RC-5 increased in comparison to the ZOCs from the calibrated local-scale model (figs. 22*D* and 23*A*), whereas the effective porosity of 0.35 had the opposite effect (figs. 22*D* and 23*B*). With the lower effective porosity and resulting higher velocity, pathlines to RC-5 include flow

farther from the well (fig. 23*A*) into the area of drawdown in southeastern Albuquerque (fig. 7). With its increased areal extent, more ZOC pathlines for the 1980–2013 period, as projected in plan view, lie within the December 2016 footprint of the EDB plume. However, as described previously for simulation using 0.25 effective porosity, all of the RC-5 particles were north of the BFF area in 1980, would have moved northeast by advective groundwater flow starting in 1980 at the same rate as the EDB, and would not have had the opportunity to interact with the EDB plume (fig. 23*A*).

Because of the increased areal extent of the ZOCs with the 0.15 effective porosity, more pathlines originate from the eastern perimeter of the local-scale model (fig. 23*A*) than in the 0.25 (fig. 22*D*) or 0.35 (fig. 23*B*) effective porosity simulations. Recharge along the eastern perimeter of the local-scale model would likely have shorter traveltimes to RC-5 than from the northern model perimeter (fig. 23*A* and fig. 1). As an independent check of groundwater-flow paths, a comparison of pathlines to the hydrochemical zone boundaries shows that the pathlines for the 0.25 and 0.35 effective porosity simulations generally are more consistent with hydrochemical zone boundaries than are the pathlines for the 0.15 effective porosity simulations (figs. 22 and 23).

Future Pumping Scenario

Future water levels were simulated in the model by using the Water Authority's "medium demand, medium supply" future pumping scenario (Albuquerque Bernalillo County Water Utility Authority, 2016). As discussed in the "Water-Level and Groundwater-Flow Changes" section of this report, water levels in southeastern Albuquerque have been rising since late 2008 because of the decrease in water-supply well pumping. Projected water levels in local-scale model layer 3 (containing the water table) for model cells near well TR-1A and at the BFF (fig. 2) show that water levels are projected to continue rising through about 2030 at both the TR-1A and BFF locations (fig. 24). After 2030, projected water levels at the TR-1A and BFF locations begin to decline (fig. 24) in response to projected increases in pumping in the Water Authority's "medium demand, medium supply" future pumping scenario (Albuquerque Bernalillo County Water Utility Authority, 2016).

ACRs and ZOCs to 10 of the 11 water-supply wells (BR-5, K-3, K-15, K-16, LV-8, RC-2, RC-3, RC-4, RC-5, and VH-2) near the EDB plume were delineated for particles released on October 31, 2050, for the future pumping scenario (table 8). Well K-7 was not included in the ACR and ZOC analyses for the future pumping scenario because K-7 currently (2019) is being operated as an injection well for treated water withdrawn by the extraction wells. Projected 2050 irrigation-season pumping rates for RC-2, RC-5, and LV-8 are less than the 2013 irrigation-season pumping rates, whereas the RC-3, RC-4, BR-5, and VH-2 projected 2050 irrigation-season pumping rates are greater than the 2013 irrigation-season pumping rates (table 8). The projected 2050 irrigation-season pumping rates for the K-3, K-15, and K-16 wells were the same as for the 2012 and 2013 irrigation seasons. The same method of ACR and ZOC analysis was used as for the historical pumping conditions except that particles were tracked backwards in time starting on October 31, 2050.

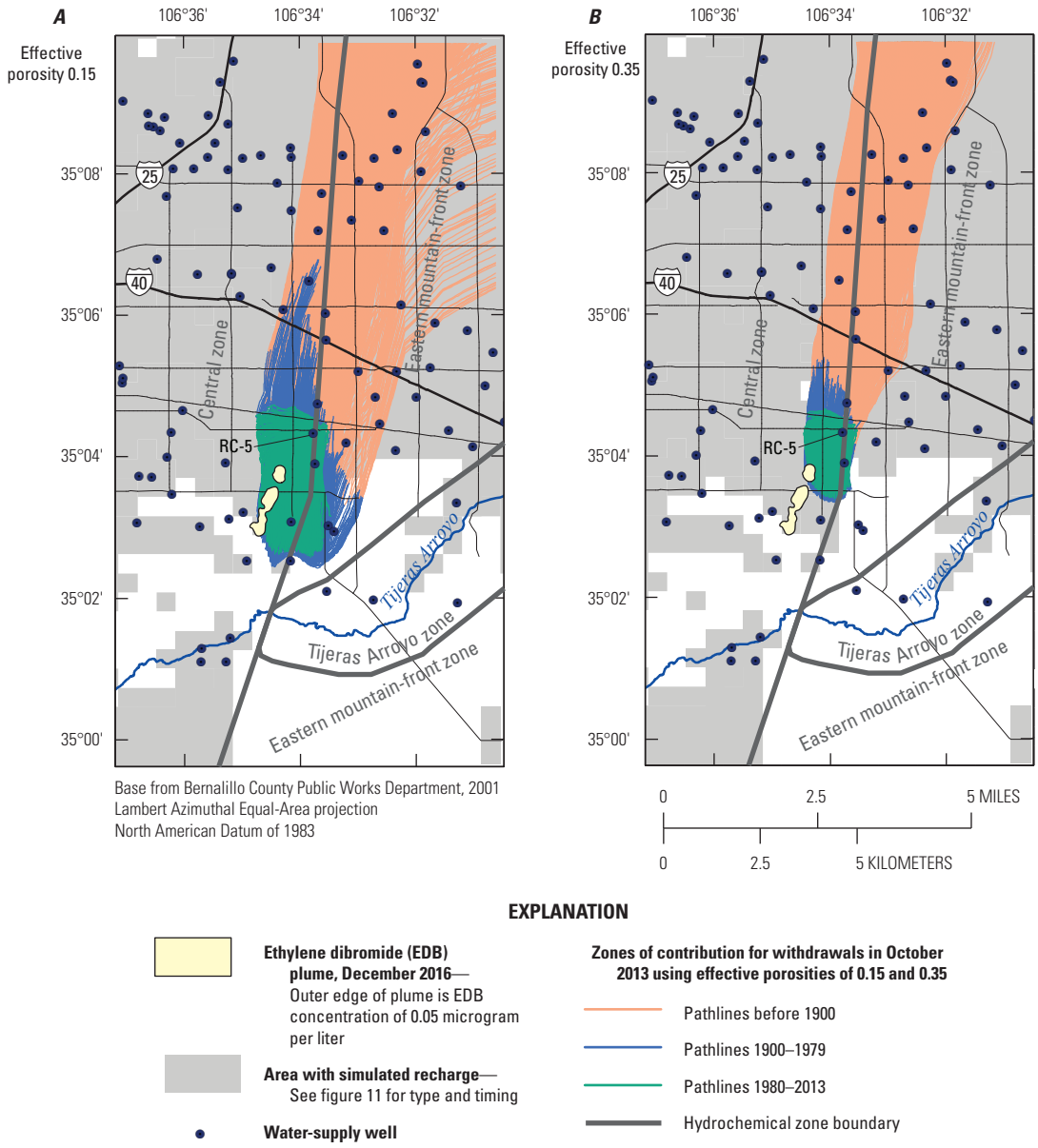

Figure 23. Sensitivity analysis of the effects of effective porosities of *A*, 0.15 and *B*, 0.35 on the zone of contribution to well RC-5 for particles released on October 31, 2013, in the local-scale model area. Ethylene dibromide plume from U.S. Army Corps of Engineers (2017b). Hydrochemical zones from Plummer and others (2004).

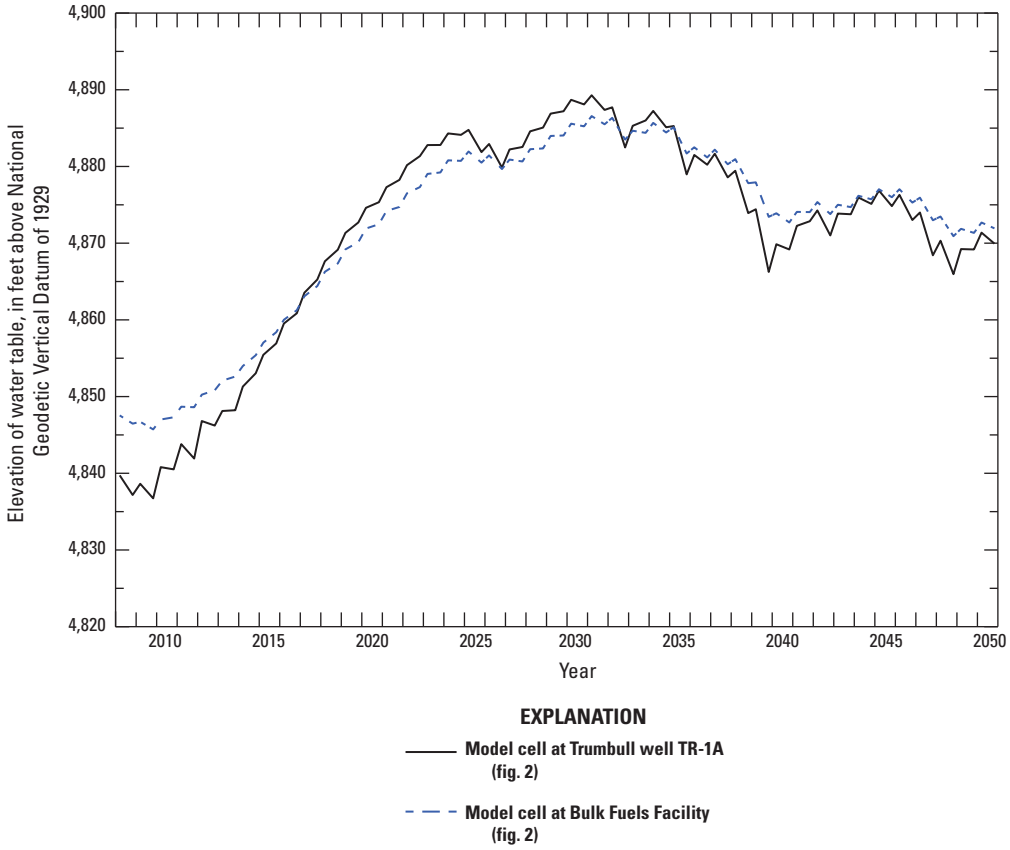

Figure 24. Projected water table elevation in local-scale model layer 3 near the Trumbull well cluster and at the Bulk Fuels Facility (fig. 2) simulated by using the "medium demand, medium supply" future pumping scenario (Albuquerque Bernalillo County Water Utility Authority, 2016). During the simulation, the water table was within local-scale model layer 3.

For the future pumping scenario (water extracted from wells on October 31, 2050), particle tracks indicated that 7 of the 10 water-supply wells (BR-5, K-15, K-16, LV-8, RC-2, RC-5, and VH-2) derived all of their water from sources outside the northern or eastern local-scale model boundary (Friesz and Myers, 2019). Only wells K-3, RC-3, and RC-4 had ACRs within the local-scale model, indicating that they derived some of their water from simulated sources within the local-scale model (fig. 25). Increased pumping rates in the future pumping scenario do not necessarily result in larger ACRs in the local model area. For example, the ACR for well RC-4 is the same size or slightly smaller for the future pumping conditions simulation (fig. 25) than for the historical pumping conditions simulation (fig. 20) despite a March 16–October 31, 2050, irrigation-season pumping rate that is 1.3 times larger than the March 16–October 31, 2013, irrigation-season pumping rate (table 8). The future pumping conditions ACR for RC-4 is located to the northwest of the well as opposed to the southwest of the well for the historical pumping conditions simulation. The RC-3 future pumping conditions ACR is south of the well, whereas in the historical pumping conditions simulation RC-3 did not have an ACR in the local-scale model. The ACRs for wells RC-3 and RC-4 do not overlap the BFF area or the December 2016 EDB plume footprint. The future pumping conditions ACR for K-3 is larger and extends farther west than in the historical pumping conditions simulation. In addition, K-3 derives part of its recharge prior to 1980 and from 1980 to 2015 from the EDB plume area.

Groundwater traveltimes from recharge locations to RC-3 and RC-4 ranged from about 50 to 101 years and had median traveltimes of about 61 years for RC-3 and 65 years for RC-4 (Friesz and Myers, 2019). Well K-3, which has a water-intake screen across the water table and is the shallowest screen of the three wells, had groundwater traveltimes ranging from a few months to about 99 years and a median traveltime of about 12 years (Friesz and Myers, 2019).

The areal extent of the ZOCs to the 10 water-supply wells was subdivided into four time periods: before 1900 (orange), 1900–79 (blue), 1980–2015 (green), and 2015–50 (brown) (fig. 26). These time periods were selected because groundwater and EDB started moving toward the northeast in 1980 and extraction-well pumping began in 2015 (fig. 26). In addition, pathlines in the 1980–2015 and 2015–50 periods with elevations higher than 4,800 ft were colored yellow (fig. 26). Similar to figure 22, the ZOCs to the wells are shown in figure 26 with younger pathlines overlying older pathlines.

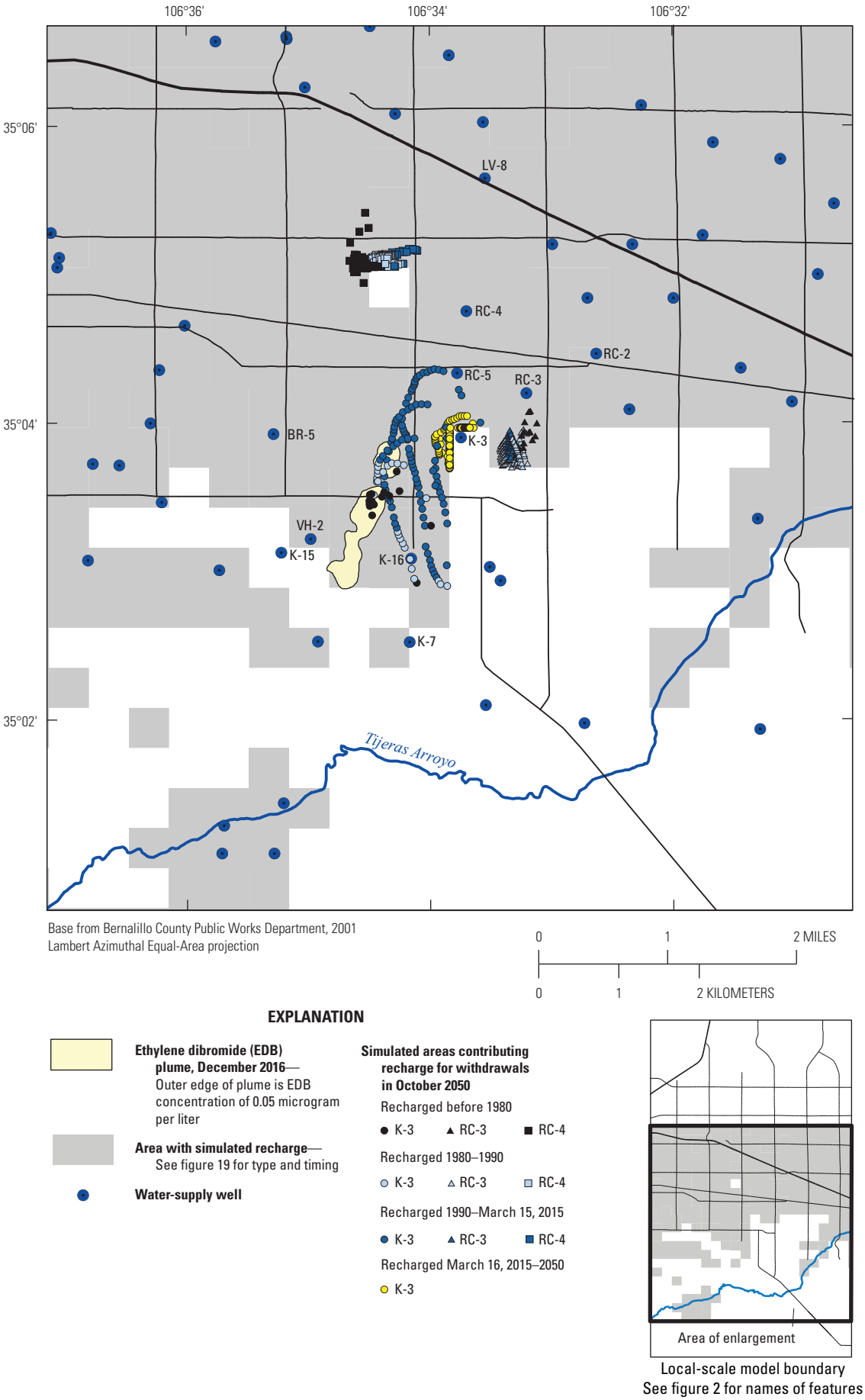

Figure 25. Areas contributing recharge to selected water-supply wells in the local-scale model area. Particles were released on October 31, 2050, for wells BR-5, K-3, K-15, K-16, LV-8, RC-2, RC-3, RC-4, RC-5, and VH-2. Only wells K-3, RC-3, and RC-4 had areas contributing recharge within the local-scale model area. Ethylene dibromide plume from U.S. Army Corps of Engineers (2017b).

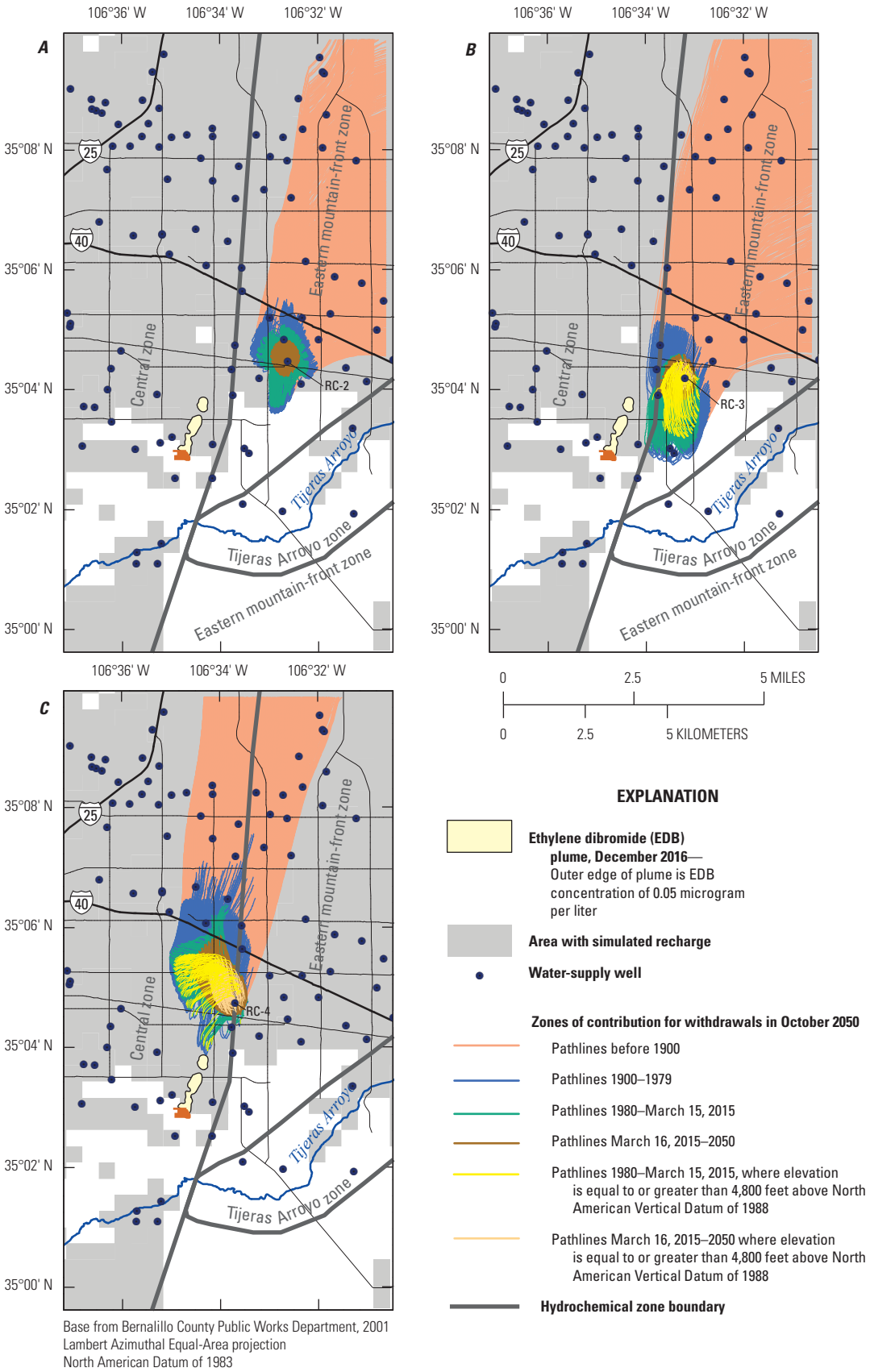

Figure 26. Zones of contribution to water-supply wells in the local-scale model area. Particles were released on October 31, 2050. Ethylene dibromide plume from U.S. Army Corps of Engineers (2017b). Hydrochemical zones from Plummer and others (2004). *A*, RC-2. *B*, RC-3. *C*, RC-4. *D*, RC-5. *E*, LV-8. *F*, BR-5. *G*, VH-2. *H*, K-3. *I*, K-15. *J*, K-16.

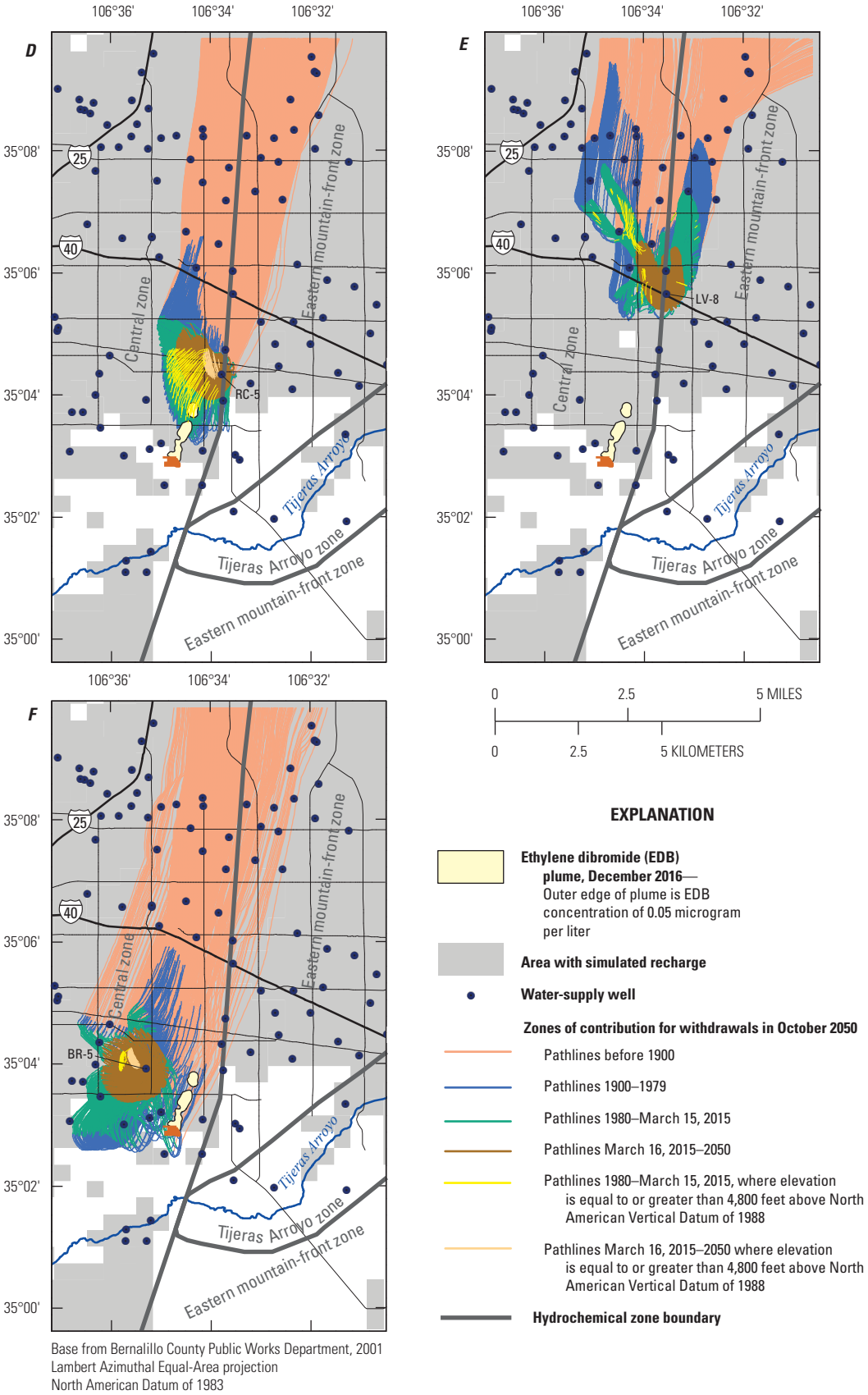

Figure 26. Zones of contribution to water-supply wells in the local-scale model area. Particles were released on October 31, 2050. Ethylene dibromide plume from U.S. Army Corps of Engineers (2017b). Hydrochemical zones from Plummer and others (2004). *A*, RC-2. *B*, RC-3. *C*, RC-4. *D*, RC-5. *E*, LV-8. *F*, BR-5. *G*, VH-2. *H*, K-3. *I*, K-15. *J*, K-16.—Continued

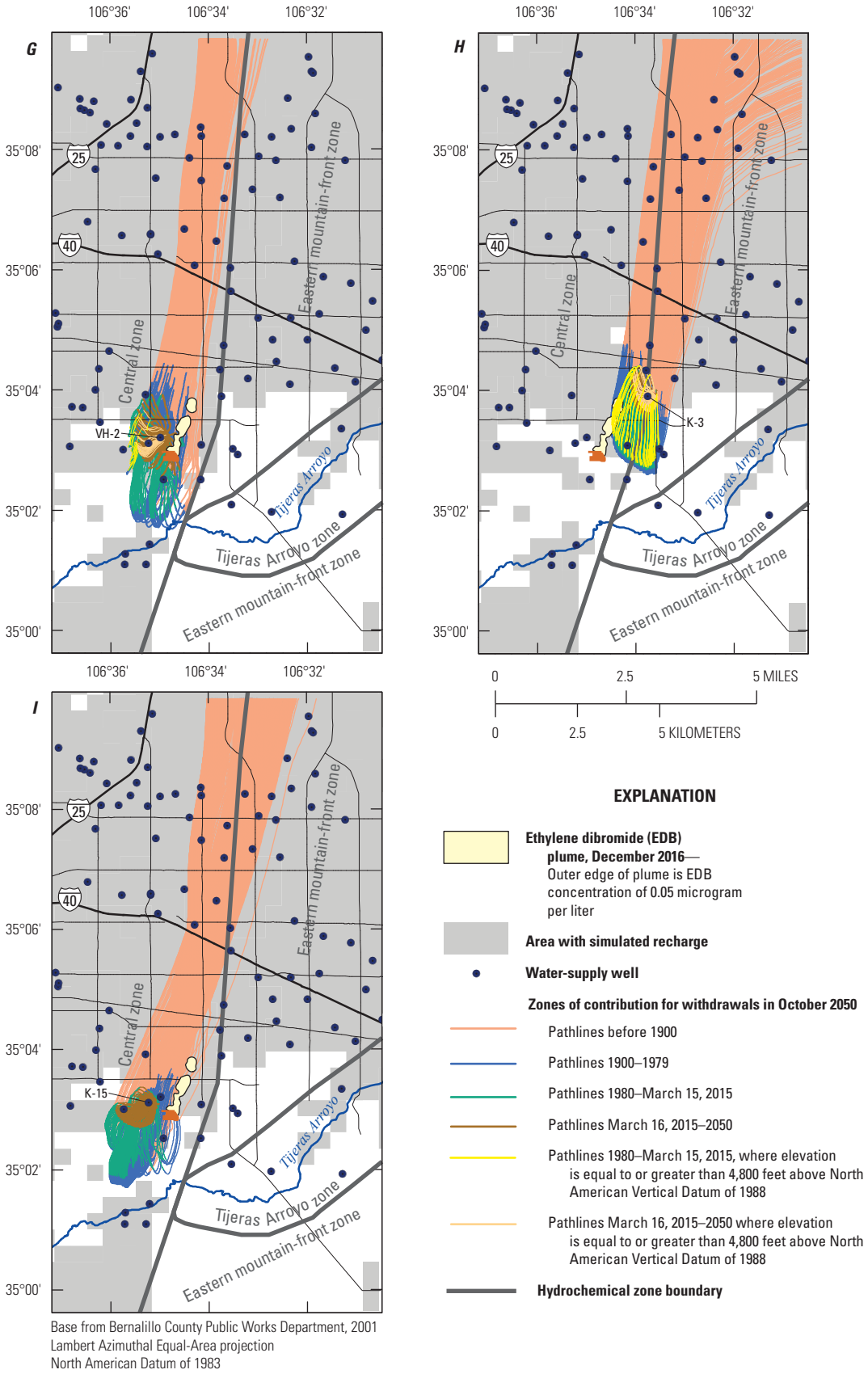

Figure 26. Zones of contribution to water-supply wells in the local-scale model area. Particles were released on October 31, 2050. Ethylene dibromide plume from U.S. Army Corps of Engineers (2017b). Hydrochemical zones from Plummer and others (2004). *A*, RC-2. *B*, RC-3. *C*, RC-4. *D*, RC-5. *E*, LV-8. *F*, BR-5. *G*, VH-2. *H*, K-3. *I*, K-15. *J*, K-16.—Continued

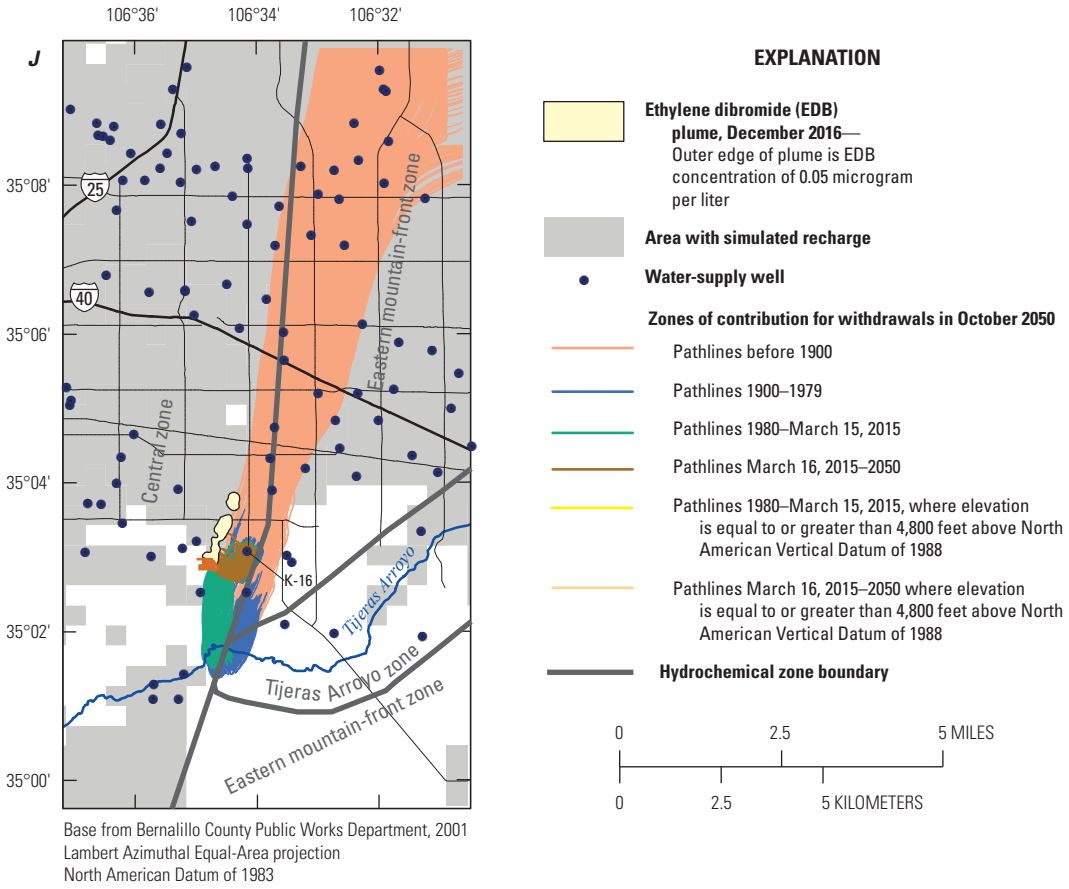

Figure 26. Zones of contribution to water-supply wells in the local-scale model area. Particles were released on October 31, 2050. Ethylene dibromide plume from U.S. Army Corps of Engineers (2017b). Hydrochemical zones from Plummer and others (2004). *A*, RC-2. *B*, RC-3. *C*, RC-4. *D*, RC-5. *E*, LV-8. *F*, BR-5. *G*, VH-2. *H*, K-3. *I*, K-15. *J*, K-16.—Continued

The future pumping scenario ZOCs analysis indicated that five of the wells, RC-5, BR-5, VH-2, K-3, and K-16, have pathlines for 1980–2015 and that two of the wells, VH-2 and K-16, have pathlines for 2015–50 that when projected in plan view overlap the December 2016 plume footprint (fig. 26*D*, *F*, *G*, *H*, and *J*). Of the five wells, only RC-5 and K-3 have pathlines for 1980–2015 that are above an elevation of 4,800 ft and could interact with the EDB plume (fig. 26*D* and *H*) if EDB was present when the particles were present. The pathlines for wells BR-5, VH-2, and K-16 that project in plan view with the December 2016 footprint of the EDB plume have elevations deeper than 4,800 ft (fig. 26*F*, *G*, and *J*) so would not have the opportunity to interact with the EDB plume, if present.

One difference of note between the historical and future pumping conditions ZOC outlines is that the future pumping conditions ZOCs appear to be wider in the east-west dimension. In particular, the future pumping conditions ZOCs for LV-8 and BR-5 have a larger footprint in map view than do the historical pumping conditions ZOCs (compare fig. 22*E* to fig. 26*E* and fig. 22*F* to fig. 26*F*). These differences may result from the changes in water levels in southeastern Albuquerque that are affecting the rate and direction of groundwater flow near the EDB plume (U.S. Army Corps of Engineers, 2017a).

Summary

The Santa Fe Group aquifer is an important source of water to communities within the Middle Rio Grande Basin, including the Albuquerque-Rio Rancho metropolitan area and Kirtland Air Force Base, New Mexico. In November 1999, Kirtland Air Force Base personnel observed fuel-stained soils at the Bulk Fuels Facility on the base. Subsequent pressure tests identified pipeline leaks. Fuels stored at the Bulk Fuels Facility have included aviation gasoline, jet propellant 4, and jet propellant 8. The exact date when the pipes began leaking and the amounts of fuels that leaked are unknown. The fuels migrated about 480 feet down to the water table. Ethylene dibromide, the constituent making up the most extensive part of the plume and a component of leaded aviation gasoline, has formed a plume that, in December 2016, was 400 to 1,300 feet wide, extended about 5,800 feet northeast from the Bulk Fuels Facility, and was about 3,700 feet from the nearest downgradient water-supply well.

Prior to widespread development of groundwater resources (1960s to 1980s) in southeastern Albuquerque, groundwater near the present-day location of the Bulk Fuels Facility flowed to the southwest. Groundwater began flowing northeast in about 1980 towards a large area of lowered water levels caused by groundwater pumping. Since the Albuquerque Bernalillo County Water Utility Authority (Water Authority) began diverting San Juan-Chama surface water from the Rio Grande in late 2008 to supplement its groundwater supply, groundwater levels in southeastern Albuquerque have been rising. In 2013 and 2014 the Water Authority, the U.S. Air Force, and the U.S. Geological Survey began a cooperative study to characterize the geology and hydrology of the Santa Fe Group aquifer in the vicinity of the ethylene dibromide plume and to develop a local-scale groundwater-flow model to delineate areas contributing recharge and zones of contribution to selected water-supply wells.

The Middle Rio Grande Basin is one of several sediment-filled structural basins associated with the north-south trending Rio Grande Rift. Mean annual precipitation at the Albuquerque International Sunport for 1981–2010 was 9.45 inches per year, of which about 55 percent fell during July through October. The principal stream in the Middle Rio Grande Basin is the north-south flowing Rio Grande, which, in the Albuquerque-Rio Rancho metropolitan area, is perennial but generally loses water to the adjacent aquifer. Within the local-scale model area, the ephemeral Tijeras Arroyo is the primary drainage. Water supplied to Albuquerque residents by the Water Authority currently (2019) is obtained from both the Santa Fe Group aquifer and from San Juan-Chama surface water. Groundwater from the Santa Fe Group aquifer was the sole source of water to Albuquerque until late 2008, when the San Juan-Chama surface-water diversion and treatment plant began supplying potable water. During 2014, water supplied to Water Authority customers was about 39 percent groundwater, 57 percent surface water, and 4 percent treated nonpotable water.

Crustal stretching and thinning along the Rio Grande Rift began 25–30 million years ago. The resulting fault-separated structural basins filled with the Oligocene- to Pleistocene-age sediments of the Santa Fe Group that are as much as about 14,500 feet thick in the central Middle Rio Grande Basin. The Santa Fe Group has been subdivided into informal lower, middle, and upper lithostratigraphic units. Within the upper Santa Fe Group, the Sierra Ladrones Formation consists of ancestral Rio Grande axial-fluvial sediments and piedmont-slope sediments derived from mountains to the east. Locally, within the axial-fluvial sediments, two lithologic units characterized by abundant silt and clay layers have informally been named the A1 and A2 units.

In general, the lithified rocks surrounding and underlying the Middle Rio Grande Basin are less permeable than the unconsolidated sediments of the Santa Fe Group. Internal hydrogeologic characteristics that influence the direction and rate of groundwater flow primarily are the hydraulic properties of geologic units and the three-dimensional stratigraphic and structural arrangement of the geologic units and faults. The presence of the axial-fluvial sediments, bounded to the east and west by finer-grain units, creates horizontal anisotropy in hydraulic conductivity and natural microscale layering, and the presence of the A1 and A2 units creates vertical anisotropy. While horizontal groundwater flow in axial-fluvial sediments is relatively unimpeded, vertical groundwater flow generally is impeded by lower vertical hydraulic conductivities.

Recharge to the Santa Fe Group aquifer in the Middle Rio Grande Basin occurs along stream channels, canals, and mountain fronts; from irrigated agriculture areas, septic fields, water-distribution and sewage-collection systems; and from subsurface inflow of groundwater at basin margins. Discharge from the Santa Fe Group aquifer in the Middle Rio Grande Basin occurs primarily by seepage to irrigation drains and by groundwater pumping but also by riparian evapotranspiration along the Rio Grande and subsurface groundwater outflow at the southern end of the basin.

Because of groundwater pumping in the Middle Rio Grande Basin, water levels in many areas have declined and groundwater-flow directions have changed. By 2008, groundwater levels had declined more than 100 ft in southeastern Albuquerque within the local-scale model area. The drawdown in southeastern Albuquerque caused groundwater flow in areas southwest of the area of drawdown to reverse direction from southwesterly to northeasterly. The reversal of groundwater-flow direction occurred in the Bulk Fuels Facility area in about 1980. In late 2008, the Water Authority began utilizing San Juan-Chama surface water for public supply, and as a result of decreased pumping, water levels in southeastern Albuquerque began to rise in early 2009 and were still rising at the end of 2016.

A previously developed Middle Rio Grande Basin regional groundwater-flow model with nine model layers and uniformly spaced horizontal model cells of 500 by 500 meters was updated, and a smaller local-scale model was developed,

for this study. Groundwater levels and flows between the updated regional and local-scale models were simulated by using MODFLOW–LGR2, which enables two-way iterative coupling of the separate MODFLOW–2005 regional and local-scale models. Advective groundwater-flow paths were simulated and visualized with the MODPATH particle-tracking program. The updated regional model, based on the previously developed regional model, includes a steady-state simulation of average hydrologic conditions prior to 1900 followed by a transient simulation of changing hydrologic conditions from 1900 to October 31, 2013.

The local-scale model had the same temporal discretization as the updated regional model. The spatial distribution of natural and anthropogenic sources of vertical recharge in the local-scale model was inherited from the updated regional model. Most of the distribution of hydraulic properties except hydraulic conductivity was also inherited from the updated regional model. The local-scale model replaced the top six layers of a 38 row by 20 column block of the updated regional model. Hydraulic properties of the aquifer, defined by model parameters Ksilts, Ksdfm, Ksdm, Ksdmc, Kpdmt, Kmult, and Ka2a1, were assigned on the basis of lithologic units. Parameter Kmult represented the coarse- to very coarse-grain axial-fluvial sediments, and Ka2a1 represented the predominantly fine-grain A1 and A2 layers. In addition, a parameter for effective porosity, applied uniformly for the local-scale model, was used to help calibrate the model and to calculate groundwater-flow velocities. The local-scale model was calibrated with the inverse modeling program UCODE–2005. Groundwater-level and advective-transport observations were used in local-scale model calibration. After calibration, the average weighted residual for all groundwater-level and advective-transport observations was 0.17 feet. A simulated groundwater-flow path originating at the ethylene dibromide plume source was compared to the mapped ethylene dibromide plume extent for calibration of advective transport. Inclusion of the advective-transport observation in the calibration decreased the distance between the observation and its simulated equivalent from 1,830 to 1,220 feet. The analysis of the residuals and optimal parameter values indicated that the local-scale model is acceptable for the purposes of the study.

For the November 1, 1998, to October 31, 1999, stress periods, mean net inflows to the local-scale model, in cubic feet per second, were mountain-front recharge, 0.16; tributary recharge, 0.68; water-distribution and sewage-collection systems leakage, 2.5; irrigated agriculture seepage, 0.00035; septic-field seepage, 0.034; release from aquifer storage, 14; and subsurface inflow, 77. For the same stress periods, mean net outflows from the local-scale model, in cubic feet per second, were groundwater withdrawals, 94.35; and subsurface outflow, 0.48.

The analysis presented in this report is based on the local-scale model which, necessarily, is a simplified representation of the aquifer system. The spatial resolution of simulation results is limited by the size of the model cells. Parameters representing hydraulic properties were consolidated and assigned to groups of model cells, and a uniform value of effective porosity was used throughout this complex aquifer. The spatial extent of recharge in the local-scale model, inherited from the updated regional model, may be spread over a larger area than in reality. Parameter values estimated through model calibration are unique to this model and its specified boundary conditions. The volume of inflow from the updated regional model to the local-scale model along the local-scale model boundaries is a source of uncertainty because changes to parameters in the local-scale model were not extended into the updated regional model.

For historical and future pumping scenarios, areas contributing recharge and zones of contribution to selected water-supply wells were delineated by tracking groundwater-flow paths with the MODPATH particle-tracking program. For the historical pumping scenario, particles were tracked backwards in time from October 31, 2013 (October 31, 2012, for wells K-15 and K-16), and for the future pumping scenario, particles were tracked backwards from October 31, 2050.

Of 11 wells included in the historical pumping analysis of areas contributing recharge, only K-3, K-7, and RC-4 derived a portion of their water from simulated recharge sources within the local-scale model. None of the areas contributing recharge overlap the Bulk Fuels Facility area or the ethylene dibromide plume footprint as delineated using December 2016 ethylene dibromide data. Traveltimes from recharge locations in the local-scale model to the three wells ranged from a few months to 64 years.

For the historical pumping analysis of zones of contribution, particles for all 11 wells generally moved southwest from the north and east boundaries of the local-scale model. Because of the southwesterly groundwater flow prior to 1980, many of the particles moved past their target well but then moved back towards their target well after 1980, when groundwater flow changed to the northeast. Of the 11 wells, only RC-5, BR-5, and VH-2 had 1980–2013 pathlines that overlapped the December 2016 ethylene dibromide plume footprint. Wells BR-5 and VH-2 had 1980–2013 pathlines that overlapped the Bulk Fuels Facility area. The areal extent of the ethylene dibromide plume between 1980 and about 2007 is unknown, so it is difficult to determine if 1980–2013 pathlines for wells BR-5, RC-5, and VH-2 would have interacted with the ethylene dibromide plume. Particles that were north of the Bulk Fuels Facility when groundwater flow reversed direction from southwest to northeast in 1980 would not have the opportunity to interact with the ethylene dibromide plume because the particles and the ethylene dibromide would have both been moving northwest at about the same rate by advective groundwater flow. Wells BR-5, VH-2, and K-15 did have particles southwest of the Bulk Fuels Facility in 1980. Particles traveling to BR-5 passed under the Bulk Fuels Facility area in the 1980–2013 period, but none of the pathlines were shallow enough to interact with ethylene dibromide at the Bulk Fuels Facility. Some of the particles traveling to VH-2 passed through the Bulk Fuels Facility area

at shallow enough depths to interact with ethylene dibromide at the Bulk Fuels Facility in the 1980–2013 period. Ethylene dibromide has not been detected in water samples collected in 2012 through 2015 from the VH-2 well. Particles traveling to K-15 passed very near the Bulk Fuels Facility in the 1980–2013 period, but none of the pathlines were shallow enough to interact with ethylene dibromide at the Bulk Fuels Facility.

Of 10 water-supply wells included in the future pumping analysis of areas contributing recharge, only wells RC-3, RC-4, and K-3 had areas contributing recharge within the local-scale model. The areas contributing recharge for wells RC-3 and RC-4 do not overlap the Bulk Fuels Facility area or the December 2016 ethylene dibromide plume footprint, but K-3 derives part of its recharge prior to 1980 and during 1980–2015 from the December 2016 plume footprint. Groundwater traveltimes from recharge locations to RC-3 and RC-4 ranged from about 50 to 101 years and from a few months to about 99 years for K-3.

The zones of contribution analysis for the future pumping scenario indicated that wells RC-5, BR-5, VH-2, K-3, and K-16 have pathlines for 1980–2015 and wells VH-2 and K-16 have pathlines for 2015–50 that when projected in plan view overlap the December 2016 plume footprint. Of these five wells, only RC-5 and K-3 have pathlines for 1980–2015 that are above an elevation of 4,800 feet and could interact with the ethylene dibromide plume if ethylene dibromide was present when the particles were present.

References Cited

Albuquerque Bernalillo County Water Utility Authority, 2016, Water 2120: Securing our water future, volume 1, main text and appendices: Albuquerque, N. Mex., Albuquerque Bernalillo County Water Utility Authority, 309 p., accessed May 9, 2017, at http://www.abcwua.org/Water_Resources_Management_Strategy.aspx.

Anderholm, S.K., 2001, Mountain-front recharge along the eastern side of the Middle Rio Grande Basin, central New Mexico: U.S. Geological Survey Water-Resources Investigations Report 00–4010, 36 p.

Barroll, Peggy, 2001, Documentation of the administrative groundwater model for the Middle Rio Grande Basin: New Mexico Office of the State Engineer, Technical Services Unit, Hydrology Bureau Report 99–3, variously paged.

Bartolino, J.R., and Cole, J.C., 2002, Groundwater resources of the Middle Rio Grande Basin, New Mexico: U.S. Geological Survey Circular 1222, 132 p.

Bexfield, L.M., and Anderholm, S.K., 2000, Predevelopment water-level map of the Santa Fe Group aquifer system in the Middle Rio Grande Basin between Cochiti Lake and San Acacia, New Mexico: U.S. Geological Survey Water-Resources Investigations Report 00–4249, 1 sheet.

Bexfield, L.M., and Anderholm, S.K., 2002, Estimated water-level declines in the Santa Fe Group aquifer system in the Albuquerque area, central New Mexico, predevelopment to 2002: U.S. Geological Survey Water-Resources Investigations Report 02–4233, 1 sheet.

Bexfield, L.M., Heywood, C.E., Kauffman, L.J., Rattray, G.W., and Vogler, E.T., 2011, Hydrogeologic setting and groundwater flow simulation of the Middle Rio Grande Basin regional study area, New Mexico, section 2 *of* Eberts, S.M., ed., Hydrologic settings and groundwater flow simulations for regional studies of the transport of anthropogenic and natural contaminants to public-supply wells—Studies begun in 2004: U.S. Geological Survey Professional Paper 1737–B, p. 2-1–2-61.

Bexfield, L.M., Lindberg, W.E., and Anderholm, S.K., 1999, Summary of water-quality data for City of Albuquerque drinking-water supply wells, 1988–97: U.S. Geological Survey Open-File Report 99–195, 138 p.

Bloodgood, D.W., 1930, The ground water of Middle Rio Grande Valley and its relation to drainage: Agricultural Experiment Station, New Mexico College of Agriculture, Bulletin 184, 60 p.

Cole, J.C., 2001, 3-D geologic modeling of regional hydrostratigraphic units in the Albuquerque segment of the Rio Grande Rift, *in* Cole, J.C., ed., U.S. Geological Survey Middle Rio Grande Basin Study—Proceedings of the Fourth Annual Workshop, Albuquerque, New Mexico, February 15–16, 2000: U.S. Geological Survey Open-File Report 00–488, p. 26–28.

Connell, S.D., 2004, Geology of the Albuquerque Basin and tectonic development of the Rio Grande Rift in north-central New Mexico, *in* Mack, G.H., and Giles, K.A., eds., The geology of New Mexico—A geologic history: New Mexico Geological Society, Special Publication 11, p. 359–388.

Connell, S.D., 2006, Preliminary geologic map of the Albuquerque-Rio Rancho metropolitan area and vicinity, Bernalillo and Sandoval Counties, New Mexico: New Mexico Bureau of Geology and Mineral Resources Open-File Report 496, 2 pls.

Connell, S.D., 2008, Refinements to the stratigraphic nomenclature of the Santa Fe Group, northwestern Albuquerque Basin, New Mexico: New Mexico Geology, v. 30, p. 14–35.

Connell, S.D., Allen, B.D., and Hawley, J.W., 1998, Subsurface stratigraphy of the Santa Fe Group from borehole geophysical logs, Albuquerque area, New Mexico: New Mexico Geology, v. 20, no. 1, p. 2–7.

Driscoll, J.M., and Brandt, J.T., 2017, Land subsidence and recovery in the Albuquerque Basin, New Mexico, 1993–2014: U.S. Geological Survey Scientific Investigations Report 2017–5057, 31 p., accessed August 14, 2017, at https://doi.org/10.3133/sir20175057.

Ellinger, Scott, 2013, Simulated mass transport of 1,2-dibromoethane in groundwater of southeastern Albuquerque, New Mexico: U.S. Environmental Protection Agency, Region 6, 79 p.

Esri, 2017, How Topo to Raster works: Accessed July 28, 2017, at http://pro.arcgis.com/en/pro-app/tool-reference/3d-analyst/how-topo-to-raster-works.htm.

Falk, S.E., Bexfield, L.M., and Anderholm, S.K., 2011, Estimated 2008 groundwater potentiometric surface and predevelopment to 2008 water-level change in the Santa Fe Group aquifer system in the Albuquerque area, central New Mexico: U.S. Geological Survey Scientific Investigations Map 3162, 1 sheet.

Friesz, P.J., and Myers, N.C., 2019, MODFLOW–LGR2 groundwater-flow model used to delineate transient areas contributing recharge and zones of contribution to selected wells in the upper Santa Fe Group aquifer, southeastern Albuquerque, New Mexico: U.S. Geological Survey data release, https://doi.org/10.5066/F79P303S.

Galanter, A.E., and Curry, L.T.S., 2019, Estimated 2016 groundwater level and drawdown from predevelopment to 2016 in the Santa Fe Group aquifer system in the Albuquerque area, central New Mexico: U.S. Geological Survey Scientific Investigations Map 3433, 1 sheet, 13-p. pamphlet.

Grauch, V.J.S., Phillips, J.D., Koning, D.J., Johnson, P.S., and Bankey, Viki, 2009, Geophysical interpretations of the southern Española Basin, New Mexico, that contribute to understanding its hydrogeologic framework: U.S. Geological Survey Professional Paper 1761, 88 p.

Halford, K.J., and Hanson, R.T., 2002, User guide for the drawdown-limited, Multi-Node Well (MNW) package for the U.S. Geological Survey's modular three-dimensional finite-difference ground-water flow model, versions MODFLOW–96 and MODFLOW–2000: U.S. Geological Survey Open-File Report 02–293, 33 p.

Hanson, R.T., Kauffman, L.K., Hill, M.C., Dickinson, J.E., and Mehl, S.W., 2013, Advective transport observations with MODPATH–OBS—Documentation of the MODPATH observation process: U.S. Geological Survey Techniques and Methods, book 6, chap. A42, 96 p.

Harbaugh, A.W., 2005, MODFLOW–2005, the U.S. Geological Survey modular ground-water model—The ground-water flow process: U.S. Geological Survey Techniques and Methods, book 6, chap. A16, variously paged.

Harbaugh, A.W., Banta, E.R., Hill, M.C., and McDonald, M.G., 2000, MODFLOW–2000, the U.S. Geological Survey modular ground-water model—User guide to modularization concepts and the ground-water flow process: U.S. Geological Survey Open-File Report 00–92, 121 p.

Hawley, J.W., 1996, Hydrogeologic framework of potential recharge areas in the Albuquerque Basin, central New Mexico, *in* Hawley, J.W., and Whitworth, T.M., comps., Hydrogeology of potential recharge areas and hydrogeochemical modeling of proposed aquifer recharge methods in basin- and valley-fill aquifer systems, Albuquerque Basin, New Mexico: New Mexico Bureau of Mines and Mineral Resources Open-File Report 402–D, p. 1–71.

Hawley, J.W., and Haase, C.S., 1992, Hydrogeologic framework of the northern Albuquerque Basin: Socorro, New Mexico Bureau of Mines and Mineral Resources Open-File Report 387, variously paged.

Hawley, J.W., Haase, C.S., and Lozinsky, R.P., 1995, An underground view of the Albuquerque Basin, *in* Ortega-Klett, C.T., ed., The water future of Albuquerque and the Middle Rio Grande Basin: Proceedings of the 39th Annual New Mexico Water Conference, November 3–4, 1994, New Mexico Water Resources Research Institute WRRI Report No. 290, p. 37–55.

Heywood, C.E., 1998, Piezometric-extensometric estimations of specific storage in the Albuquerque Basin, New Mexico, *in* Borchers, J.W., ed., Land subsidence case studies and current research: Belmont, Calif., Star Publishing Company, Proceedings of the Dr. Joseph F. Poland Symposium, Special Publication No. 8, Association of Engineering Geologists, Sacramento Section and Association of Engineering Geologists Subsidence Committee, p. 435–440.

Heywood, C.E., 2001, Piezometric-extensometric test results, *in* Thorn, C.R., Analytical results of a long-term aquifer test conducted near the Rio Grande, Albuquerque, New Mexico: U.S. Geological Survey Water-Resources Investigations Report 00–4291, p. 8–11.

Heywood, C.E., 2013, Simulations of groundwater flow, transport, and age in Albuquerque, New Mexico, for a study of transport of anthropogenic and natural contaminants [TANC] to public-supply wells: U.S. Geological Survey Scientific Investigations Report 2012–5242, 51 p.

Heywood, C.E., Galloway, D.L., and Stork, S.V., 2002, Ground displacements caused by aquifer-system water-level variations observed using interferometric synthetic aperture radar near Albuquerque, New Mexico: U.S. Geological Survey Water-Resources Investigations Report 2002–4235, 18 p.

Hill, M.C., and Tiedeman, C.R., 2007, Effective groundwater model calibration—With analysis of data, sensitivities, predictions, and uncertainty: New Jersey, John Wiley and Sons, Inc., 455 p.

Hudson, M.R., and Grauch, V.J.S., 2013, Introduction, *in* Hudson, M.R., and Grauch, V.J.S., eds., New perspectives on Rio Grande Rift Basins: From tectonics to groundwater: Geological Society of America Special Paper 494, p. 1–20, accessed September 13, 2017, at https://doi.org/10.1130/2013.2494(00).

Johnson, P.S., Connell, S.D., Allred, Barry, and Allen, B.D., 1996, Field boring log reports, City of Albuquerque piezometer nests (Sister City Park, Del Sol Dividers, Hunters Ridge Park 1, West Bluff Park, Garfield Park): New Mexico Bureau of Geology and Mineral Resources Open-File Report 426, variously paged.

Kernodle, J.M., 1996, Hydrogeology and steady-state simulation of ground-water flow in the San Juan Basin, New Mexico, Colorado, Arizona, and Utah: U.S. Geological Survey Water-Resources Investigations Report 95–4187, 117 p.

Kernodle, J.M., 1998, Simulation of ground-water flow in the Albuquerque Basin, central New Mexico, 1901–95, with projections to 2020 (supplement two to U.S. Geological Survey Water-Resources Investigations Report 94–4251): U.S. Geological Survey Open-File Report 96–209, 54 p.

Kernodle, J.M., McAda, D.P., and Thorn, C.R., 1995, Simulation of ground-water flow in the Albuquerque Basin, central New Mexico, 1901–1994, with projections to 2020: U.S. Geological Survey Water-Resources Investigations Report 94–4251, 114 p.

Kernodle, J.M., and Scott, W.B., 1986, Three-dimensional model simulation of steady-state ground-water flow in the Albuquerque-Belen Basin, New Mexico: U.S. Geological Survey Water-Resources Investigations Report 84–4353, 58 p.

Konikow, L.F., Hornberger, G.Z., Halford, K.J., and Hanson, R.T., 2009, Revised Multi-Node Well (MNW2) package for MODFLOW ground-water flow model: U.S. Geological Survey Techniques and Methods 6–A30, 67 p.

Lohman, S.W., 1979, Ground-water hydraulics: U.S. Geological Survey Professional Paper 708, 70 p.

Lozinsky, R.P., 1994, Cenozoic stratigraphy, sandstone petrology, and depositional history of the Albuquerque Basin, central New Mexico, *in* Keller, G.R., and Cather, S.M., eds., Basins of the Rio Grande Rift: Structure, stratigraphy, and tectonic setting: Geological Society of America Special Paper 291, p. 73–82.

McAda, D.P., 2001, Simulation of a long-term aquifer test conducted near the Rio Grande, Albuquerque, New Mexico: U.S. Geological Survey Water-Resources Investigations Report 99–4260, 66 p.

McAda, D.P., and Barroll, Peggy, 2002, Simulation of ground-water flow in the Middle Rio Grande Basin between Cochiti and San Acacia, New Mexico: U.S. Geological Survey Water-Resources Investigations Report 02–4200, 81 p.

Mehl, S.W., and Hill, M.C., 2013, MODFLOW–LGR—Documentation of ghost node local grid refinement (LGR2) for multiple areas and the boundary flow and head (BFH2) package: U.S. Geological Survey Techniques and Methods, book 6, chap. A44, 43 p.

Morrissey, D.J., 1989, Estimation of the recharge area contributing water to a pumped well in a glacial-drift, river-valley aquifer: U.S. Geological Survey Water-Supply Paper 2338, 41 p.

New Mexico Environment Department, 2017, 2017 strategic plan, Kirtland Air Force Base fuel leak: New Mexico Environment Department, 40 p., accessed September 12, 2017, at https://www.env.nm.gov/wp-content/uploads/2016/06/KAFB2017StrategicPlan_Version3.0_FINAL.pdf.

New Mexico Environmental Finance Center, 2006, Review of leak and repair data: Phase I report prepared for the Albuquerque Bernalillo County Water Utility Authority, 91 p.

Niswonger, Richard, and Constantz, Jim, 2001, Determination of streamflow loss to estimate mountain-front recharge at Bear Canyon, New Mexico, *in* Cole, J.C., ed., U.S. Geological Survey Middle Rio Grande Basin Study—Proceedings of the Fourth Annual Workshop, Albuquerque, New Mexico, February 15–16, 2000: U.S. Geological Survey Open-File Report 00–488, p. 38–40.

Paschke, S.S., Kauffman, L.J., Eberts, S.M., and Hinkle, S.R., 2007, Overview of regional studies of the transport of anthropogenic and natural contaminants to public-supply wells, section 1 *of* Paschke, S.S., ed., Hydrogeologic settings and ground-water flow simulations for regional studies of the transport of anthropogenic and natural contaminants to public-supply wells—Studies begun in 2001: U.S. Geological Survey Professional Paper 1737–A, p. 1-1–1-18.

Plummer, N.L., Bexfield, L.M., Anderholm, S.K., Sanford, W.E., and Busenberg, E., 2004, Geochemical characterization of ground-water flow in the Santa Fe Group aquifer system, Middle Rio Grande Basin, New Mexico: U.S. Geological Survey Water-Resources Investigations Report 03–4131, 395 p.

Poeter, E.P., Hill, M.C., Banta, E.R., Mehl, Steffen, and Christensen, Steen, 2005, UCODE_2005 and six other computer codes for universal sensitivity analysis, calibration, and uncertainty evaluation: U.S. Geological Survey Techniques and Methods, book 6, chap. A11, 283 p.

Pollock, D.W., 1994, User's guide for MODPATH/MODPATH_PLOT, version 3—A particle tracking post-processing package for MODFLOW, the U.S. Geological Survey finite-difference ground-water flow model: U.S. Geological Survey Open-File Report 94–464, 242 p.

Powell, R.I., and McKean, S.E., 2014, Estimated 2012 groundwater potentiometric surface and drawdown from predevelopment to 2012 in the Santa Fe Group aquifer system in the Albuquerque metropolitan area, central New Mexico: U.S. Geological Survey Scientific Investigations Map 3301, 1 sheet.

Rankin, D.R., McCoy, K.J., Moret, G.J.M., Worthington, J.S., and Bandy-Baldwin, K.M., 2013, Groundwater hydrology and estimation of horizontal groundwater flux from the Rio Grande at selected locations in Albuquerque, New Mexico, 2003–9: U.S. Geological Survey Scientific Investigations Report 2012–5007, 75 p.

Rankin, D.R., Oelsner, G.P., McCoy, K.J., Moret, G.J.M., Worthington, J.A., and Bandy-Baldwin, K.M., 2016, Groundwater hydrology and estimation of horizontal groundwater flux from the Rio Grande at selected locations in Albuquerque, New Mexico, 2009–10: U.S. Geological Survey Scientific Investigations Report 2016–5021, 89 p., accessed June 2, 2016, at https://doi.org/10.3133/sir20165021.

Reilly, T.E., and Pollock, D.W., 1993, Factors affecting areas contributing recharge to wells in shallow aquifers: U.S. Geological Survey Water-Supply Paper 2412, 21 p.

Rice, S., Oelsner, G., and Heywood, C., 2014, Simulated and measured water levels and estimated water-level changes in the Albuquerque area, central New Mexico, 1950–2012: U.S. Geological Survey Scientific Investigations Map 3305, 1 sheet.

Sanford, W.E., Plummer, L.N., McAda, D.P., Bexfield, L.M., and Anderholm, S.K., 2004, Use of environmental tracers to estimate parameters for a predevelopment ground-water-flow model of the Middle Rio Grande Basin, New Mexico: U.S. Geological Survey Water-Resources Investigations Report 03–4286, 102 p.

Swanson, B.J., Meyer, G.A., and Coonrod, J.E., 2011, Historical channel narrowing along the Rio Grande near Albuquerque, New Mexico in response to peak discharge reductions and engineering: Magnitude and uncertainty of change from air photo measurements: Earth Surfaces Processes and Landforms, v. 36, p. 885–900.

Taylor, J.R., 1997, An introduction to error analysis—The study of uncertainties in physical measurements (2d ed.): Sausalito, Calif., University Science Books, 332 p.

Theis, C.V., 1938, Ground water in the middle Rio Grande valley, *in* (U.S.) National Resources Committee, Regional Planning part VI—The Rio Grande joint investigation in the upper Rio Grande Basin in Colorado, New Mexico, and Texas, 1936–37: U.S. Government Printing Office, v. 1, p. 268–291.

Thorn, C.R., McAda, D.P., and Kernodle, J.M., 1993, Geohydrologic framework and hydrologic conditions in the Albuquerque Basin, central New Mexico: U.S. Geological Survey Water-Resources Investigations Report 93–4149, 106 p.

Tiedeman, C.R., Kernodle, J.M., and McAda, D.P., 1998, Application of nonlinear-regression methods to a ground-water flow model of the Albuquerque Basin, New Mexico: U.S. Geological Survey Water-Resources Investigations Report 98–4172, 90 p.

U.S. Air Force, 2011, Kirtland Air Force Base Bulk Fuel Facility spill assessment report, report to congressional committees, March 2011: U.S. House Report 111–201, 17 p.

U.S. Air Force Civil Engineer Center, 2014, Final contingency plan for groundwater production wells near the Bulk Fuels Facility spill area: Albuquerque, N. Mex., prepared by CH2MHill, variously paged.

U.S. Army Corps of Engineers, 2016a, Aquifer test report for groundwater extraction well KAFB-106228, Bulk Fuels Facility, Solid Waste Management Unit ST-106/SS-111: Albuquerque, N. Mex., prepared by CB&I Federal Services LLC, variously paged.

U.S. Army Corps of Engineers, 2016b, Updated numerical groundwater flow and contaminant transport modeling report, Bulk Fuels Facility, Solid Waste Management Unit ST-106/SS-111: Albuquerque, N. Mex., prepared by CB&I Federal Services LLC, variously paged.

U.S. Army Corps of Engineers, 2016c, Quarterly pre-remedy monitoring and site investigation report for October-December 2015 and annual report for 2015, Bulk Fuels Facility, Solid Waste Management Unit ST-106/SS-111: Albuquerque, N. Mex., Kirtland Air Force Base, variously paged.

U.S. Army Corps of Engineers, 2017a, RCRA facility investigation report, Bulk Fuels Facility release, Solid Waste Management Unit ST-106/SS-111, Kirtland Air Force Base, Albuquerque, New Mexico: Albuquerque, N. Mex., prepared by Sundance Consulting, Inc., January 2017, variously paged.

U.S. Army Corps of Engineers, 2017b, Quarterly monitoring report October-December 2016 and annual report for 2016, Bulk Fuels Facility, SWMU ST-106/SS-111: Albuquerque, N. Mex., prepared by EA Engineering, Science, and Technology, Inc., PBC, variously paged.

U.S. Department of Veterans Affairs, 1997, Construction report, Veterans hospital water well no. 2, Albuquerque, New Mexico: Albuquerque, N. Mex., prepared by Metric Corporation, variously paged.

U.S. Environmental Protection Agency, 2006, Lead scavengers compendium: Overview of properties, occurrence, and remedial technologies: U.S. Environmental Protection Agency, variously paged, accessed June 19, 2018, at https://www.epa.gov/sites/production/files/2015-03/documents/compendium-0506.pdf.

U.S. Geological Survey, 2015, USGS water data for the Nation: U.S. Geological Survey National Water Information System database, accessed March 29, 2015, at https://doi.org/10.5066/F7P55KJN.

U.S. Geological Survey, 2017, USGS water data for the Nation: U.S. Geological Survey National Water Information System database, accessed on various days during August 2017 at https://doi.org/10.5066/F7P55KJN.

U.S. Geological Survey, 2018, USGS GeoLog Locator: U.S. Geological Survey database, accessed January 15, 2018, at https://webapps.usgs.gov/GeoLogLocator/#!/.

Veenhuis, J.E., 2002, Summary of flow loss between selected cross sections on the Rio Grande in and near Albuquerque, New Mexico: U.S. Geological Survey Water-Resources Investigations Report 02–4131, 30 p.

Wahba, Grace, 1990, Spline models for observational data: Philadelphia, Society for Industrial and Applied Mathematics, CBMS-NSF Regional Conference Series in Applied Mathematics, 169 p.

Walvoord, M.A., and Phillips, F.M., 2004, Identifying areas of basin-floor recharge on the Trans-Pecos region and the link to vegetation: Journal of Hydrology, v. 292, p. 59–74.

Western Regional Climate Center, 2017, Albuquerque International Airport, New Mexico, National Climatic Data Center 1981–2010 monthly normals: Accessed May 8, 2017, at http://www.wrcc.dri.edu/cgi-bin/cliMAIN.pl?nm0234.

Wilson, J.T., Banks, K., Earle, R.C., He, Y., Kuder, T., and Adair, C.J., 2008, Natural attenuation of the lead scavengers 1,2-dibromoethane (EDB) and 1.2-dichloroethane (1,2-DCA) at motor fuel release sites and implications for risk management: Washington, D.C., U.S. Environmental Protection Agency, EPA/600/R–08/107, 58 p.

For more information about this publication, contact
Director, New Mexico Water Science Center
U.S. Geological Survey
6700 Edith Blvd. NE, Suite B
Albuquerque, NM 87113

Publishing support provided by
Lafayette Publishing Service Center

USGS

Myers and Friesz—**Hydrogeologic Framework, AOC, and ZOC, Upper Santa Fe Group Aquifer, Southeastern Albuquerque, New Mexico**—Scientific Investigations Report 2019–5052

ISSN 2328-0328 (online)
https://doi.org/10.3133/sir20195052